

**Mechanisms of C–H Bond
Activation by Platinum(II)**

Thesis by
George S. Chen

In Partial Fulfillment of the
Requirements for the Degree of
Doctor of Philosophy

Division of Chemistry and
Chemical Engineering

California Institute of Technology
Pasadena, CA

2009
(Defended November 16, 2009)

© 2009

George S. Chen

All Rights Reserved

To my parents, who throughout my life have always given me
the very best of everything.

Acknowledgements

It is hard to believe that five years have gone by so quickly. I first came to Caltech in the spring of 2004. I was a prospective student at the time, and my visit did not exactly get off to the best of starts. My luggage somehow got lost during my flight from Boston, leaving me with only what I was carrying in my pockets. To make matters worse, while leaving the hotel to come to campus the next morning, I was hit by a car while trying to cross a street when the walk sign was on. Yet, somehow, I ended up coming here for graduate school. I guess it must have been Dave Weinberg, who I first met at a poster session the first day I was here. He was clearly very drunk, but was still able to talk about his chemistry with such eloquence that I was simply blown away. After meeting Dave, I realized that there was something special about this place, and after five years here, I can say with good confidence that I had made the right choice.

I don't think I would have joined the Bercaw group if it weren't for Bolin Lin. Bolin was a TA for one of the first courses I took at Caltech, and his enthusiasm and knowledge for organometallic chemistry made my decision to enter the field an easy one. Bolin has been a great friend ever since, and I am particular glad that he took time to teach me everything from Chinese to computational chemistry. Jonathan Owen was on his way out when I joined the group. While busy writing his thesis, he helped me get started in the group. Thanks for teaching me how to use the glove box and how to activate C-H bonds! I also received a great deal of help in those early days from Theo Agapie. Thanks for showing me how to use the high vacuum line and how to not "fuck it up." Paul Elowe was another one of my former TAs. He looked mean and intimidating in

class, but turned out to be a really nice guy and a great friend. Both Sara Klamo and Jeff Byers offered a great deal of help and encouragement at the start, teaching me how to use the various instruments in lab. Endy Min was another senior student who helped me in those early days, and I really enjoyed our conversations. Steve Baldwin is one of the most knowledgeable people I have ever met, not to mention his skills when it comes to making eggnog. And then there is Dave, a fellow member of green box club, not to mention a lover of cheap Chinese food. Suzanne Golisz joined the group one year after I did. It was a great relief to no longer be the youngest member of the group! Ian Tonks and Ted Weintrob have both been great friends over the years, not to mention both love to play computer games. Ted is also one of those people who knows just about everything, and I really enjoyed our late night chats. Paul Oblad, Alex Miller, and Valerie Scott were all refuges from the third floor. It was great you guys decided to move down to the second floor instead of across the country. Rachel Klet and Ross Fu are, well, unique individuals. And to the newest and perhaps final members, Taylor Lenton, Yan Choi Lam, and Matt Winston, good luck. You guys are awesome!

I would like to thank all the postdoctoral scholars who have come and gone during my time here: Tom Driver, Parisa Mehrkhodavandi, Reto Dorta, Xingwei Li, Travis Williams, Aaron Wilson, Nilay Hazari, Ned West, Sze-Man Yu, and Melanie Zimmermann. You guys have taught me a lot of science, and it was a great experience to work with all of you. I would also like to thank Pat Anderson for her help with all the scheduling and paper work. You definitely made life in the Bercaw group easy for me.

Outside the group, I would like to thank Larry Henling and Mike Day for helping with X-ray structures, David Vander Velde and Scott Ross for NMR help, and Rich

Gerhart for glassware. And to all my other friends at Caltech, thanks! I really enjoyed my time here, be it going shopping on the weekends, going out to watch movies, eating at all sorts of restaurants, or visiting super cool places like JPL. I'll never forget my five years here in Pasadena.

I would like to wrap it up by thanking my mentors. Jay Labinger has been a great co-advisor. Extremely knowledgeable in chemistry and also a great writer, Jay has always offered key advice at important moments during my graduate career. Thanks for helping me become a better scientist and writer. I would also like the other members of my thesis committee, David Tirrell, Nathan Lewis, and Harry Gray. You guys made the process of getting a Ph.D. an enjoyable experience, and I greatly appreciated all the help and advice along the way. And last, I would like to thank John Bercaw. Thanks for taking me on five years ago and all your advice on chemistry since. I really appreciate the freedom that you have given me during my time here. After all, it is not everyday that your advisor comes into the lab to help you run an experiment using the Toepler pump.

Abstract

The rates of C–H bond activation for various alkanes by $[(N-N)Pt^{II}(CH_3)(TFE-d_3)]^+$ ($N-N = Ar-N=C(CH_3)-C(CH_3)=N-Ar$; $Ar = 3,5\text{-di-}tert\text{-butylphenyl}$; $TFE-d_3 = CF_3CD_2OD$) were studied. Both linear and cyclic alkanes give the corresponding $[(N-N)Pt^{II}(H)(alkene)]^+$ cation. Second-order rate constants for cycloalkane activation (C_nH_{2n}) are proportional to the size of the ring ($k \sim n$). For cyclohexane, the deuterium kinetic isotope effect (k_H/k_D) of 1.28(5) is consistent with the proposed rate determining alkane coordination to form a C–H σ complex. Comparing the relative rates of cyclic and linear alkanes indicates that the platinum center is relatively unselective with respect to different C–H bonds: the rate constants (per C–H bond) for the substrates examined all fall into a narrow range, and there does not appear to be any significant preference for either primary or secondary C–H bonds.

The protonolysis of platinum(II) methyl complexes was investigated by both experiment and computation. Experimental results showed that protonolysis of $(COD)Pt^{II}(CH_3)_2$ ($COD = 1,5\text{-cyclooctadiene}$) by trifluoroacetic acid gave abnormally large (greater than 10) kinetic isotope effects (k_H/k_D) at room temperature and higher. The temperature dependence of k_H/k_D for the protonolysis of $(COD)Pt^{II}(CH_3)_2$ gave Arrhenius parameters outside semi-classical limits. On the other hand, protonolysis of $(tmeda)Pt^{II}(CH_3)Cl$ ($tmeda = N,N,N',N'\text{-tetramethyl-ethylenediamine}$) by trifluoroacetic acid gave normal kinetic isotope effects and classical Arrhenius parameters. Density functional theory (DFT) was used to examine the mechanism of protonolysis of these two

systems, and the results were found to be consistent with experimental observations. Based on our experimental and computational work, we propose that protonolysis of methylplatinum(II) complexes can occur through either a concerted or stepwise pathway that is highly ligand dependent; more electron-rich ligands will favor the stepwise mechanism, while electron-deficient ligands with stronger trans influence will favor the concerted mechanism. Finally, we propose that the presence of abnormally large KIEs is an indication for a concerted pathway, and that there is a connection between the magnitude and temperature dependence of the KIE and mechanism.

In aqueous solution, $[\text{Pt}^{\text{II}}(\text{glycinato})\text{Cl}_2]^-$ catalyzes oxidation by $[\text{Pt}^{\text{IV}}\text{Cl}_6]^{2-}$ of the methyl group of *p*-toluenesulfonate to the corresponding alcohol and aldehyde, with no further oxidation to the carboxylic acid. Both rate and selectivity are improved in comparison to the original Shilov system that employs $[\text{Pt}^{\text{II}}\text{Cl}_n(\text{H}_2\text{O})_{4-n}]^{2-n}$ as the catalyst.

Table of Contents

Acknowledgments.....	iv
Abstract.....	vii
Table of Contents.....	ix
List of Figures.....	xi
List of Tables.....	xiii
Chapter 1. General Introduction.....	1
References.....	6
Chapter 2. Investigating the Mechanism of Alkane C–H Activation with Cationic Platinum(II) Complexes.....	8
Abstract.....	9
Introduction.....	10
Results and Discussion.....	12
Conclusions.....	27
Experimental.....	28
References.....	30
Chapter 3. Investigating the Temperature Dependence of the Primary Kinetic Hydrogen Isotope Effect in the Protonolysis of Platinum(II) Methyl Complexes.....	32
Abstract.....	33
Introduction.....	34
Results and Discussion.....	37

Conclusions.....	48
Experimental.....	49
References.....	51
Chapter 4. Computational Studies on the Protonolysis of Platinum(II) Methyl	
Complexes.....	55
Abstract.....	56
Introduction.....	57
Results and Discussion.....	60
Conclusions.....	71
Experimental.....	72
References.....	74
Chapter 5. Selective Oxidation of sp^3 C–H Bonds in Water Catalyzed by a	
Glycinate-Platinum(II) Complex.....	76
Abstract.....	77
Introduction.....	78
Results and Discussion.....	81
Conclusions.....	85
Experimental.....	86
References.....	88
Appendix A. X-Ray Crystallographic Data for $(COD)Pt^{II}(C_6F_5)_2$	92
Appendix B. X-Ray Crystallographic Data for $(dmpe)Pt^{II}(C_6F_5)_2$	106
Appendix C. X-Ray Crystallographic Data for the Disodium Salt of	
2,2'-Bindolyl.....	117

List of Figures

Chapter 2

Figure 1. Plot of k_{obs} versus [hydrocarbon] for C_6H_{12} and C_6D_{12} at 40 °C.....	15
Figure 2. Methane isotopologues from the reaction of 2 - $d_{0.43}$ with $\text{CD}_3\text{CH}_2\text{CH}_2\text{CD}_3$	24

Chapter 3

Figure 1. Arrhenius plots with incidence of tunneling of H and D.....	39
Figure 2. Plot of $\ln(k_{\text{H}}/k_{\text{D}})$ over $1/T$ for 1	41
Figure 3. Plot of $\ln(k_{\text{H}}/k_{\text{D}})$ over $1/T$ for 4	44

Chapter 4

Figure 1. Potential energy surface scan for the deprotonation of 8 by CF_3COO^- to give 3	61
Figure 2. Plot of calculated $\ln(k_{\text{H}}/k_{\text{D}})$ over $1/T$ (without tunneling corrections) for 3	64
Figure 3. Potential energy surface scan for the deprotonation of 11 by CF_3COO^- to give 2	66
Figure 4. Plot of calculated $\ln(k_{\text{H}}/k_{\text{D}})$ over $1/T$ (without tunneling corrections) for 2	69

Chapter 5

Figure 1. Formation of 2 and 3 using 5 as the catalyst and $\text{Pt}^{\text{IV}}\text{Cl}_6^{2-}$ as the oxidant; formation of 2 and 3 using $\text{Pt}^{\text{II}}\text{Cl}_4^{2-}$ as the catalyst and $\text{Pt}^{\text{IV}}\text{Cl}_6^{2-}$ as the oxidant.....	83
--	----

List of Tables

Chapter 2

Table 1. Rate constants for reactions of alkanes with 2 - <i>d</i> _{0,43}	18
---	----

Chapter 3

Table 1. Temperature dependence of k_H/k_D in the protonolysis of 1 by TFA.....	41
Table 2. Temperature dependence of k_H/k_D in the protonolysis of 4 by TFA.....	44

Chapter 4

Table 1. Calculated KIEs (without tunneling corrections) for the protonolysis of 3 by TFA at various temperatures.....	63
Table 2. Calculated KIEs (without tunneling corrections) for the protonolysis of 2 by TFA at various temperatures.....	69

Chapter 5

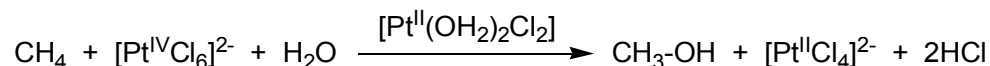
Table 1. Oxidation of 1 using 5 or Pt ^{II} Cl ₄ ²⁻ as the catalyst and Pt ^{IV} Cl ₆ ²⁻ as the oxidant at 105 °C.....	82
---	----

Chapter 1

General Introduction

The selective activation and functionalization of saturated alkane C–H bonds has far-reaching practical implications.¹ Alkanes are the main constituents of oil and natural gas, and the ability to efficiently transform them to more valuable products such as alcohols, ketones, acids, and other non-saturated molecules is highly desirable. Unfortunately, alkanes are relatively inert at ambient temperatures and pressures, due to their high homolytic bond strengths and very low acidity and basicity.² Partial oxidations of alkanes are among the few processes that could, in principle, lead to value-added products in thermodynamically favorable transformations. Although alkane oxidations at high temperatures and pressures are well known, those reactions often take place through free radical mechanisms, making it difficult to achieve both high conversion and partial-oxidation selectivity.³ In contrast, low-temperature homogeneous activations of C–H bonds need not, and often do not, involve radicals, and may lead to more selective reactions than those promoted by heterogeneous catalysts operating at high temperatures.

Over the past several decades, numerous examples of partial alkane oxidations catalyzed by homogeneous transition metal complexes, often under remarkably mild conditions and with high selectivity, have been reported in the literature.⁴ One of the first and most promising examples is the so-called Shilov system, which catalytically converts methane to methanol (and methyl chloride) by aqueous platinum salts in water (Scheme 1).⁵ Although it is not yet practical because of low reaction rates, catalyst instability and the employment of expensive oxidant, the Shilov system remains one of few examples of catalytic routes to alkane functionalization.

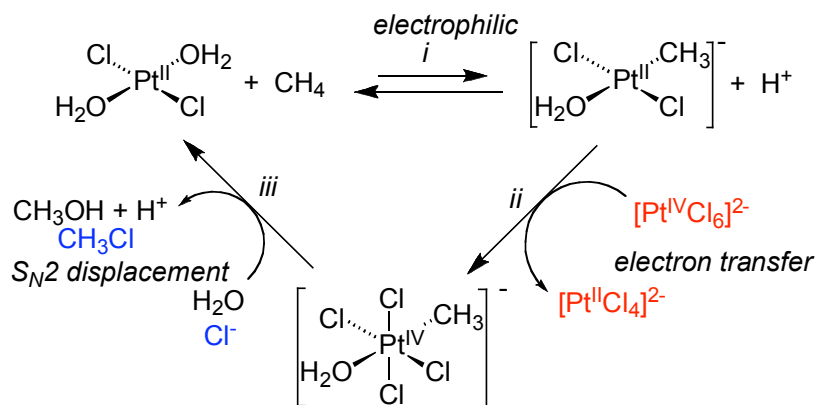
Scheme 1

Since the report of Shilov's system, a number of homogeneous catalysts based on late transition metals, especially platinum and palladium, have been shown to oxidize C–H bonds, leading to good yields of partially oxidized products. For example, [(2,2'-bipyrimidine)Pt^{II}Cl₂] catalyzes the selective oxidation of methane in fuming sulfuric acid to give methyl bisulfate in 72% one-pass yield at 81% selectivity based on methane.⁶ It has also been demonstrated that with a proper cocatalyst (CuCl₂) at elevated temperature, Shilov chemistry can be made catalytic with dioxygen as the terminal oxidant.⁷ In addition to platinum, palladium salts can also oxidize methane to methanol derivatives in strongly acidic solvents such as trifluoroacetic acid.⁸ By combining three redox couples (Pd(II)/Pd(0), quinone/hydroquinone, NO₂/NO), one-pot catalytic oxidation of methane selectively to methanol by dioxygen in CF₃COOH at a temperature as low as 80 °C can be achieved.⁹ While a great deal of progress has been made, the development of practical catalysts to transform alkanes to value-added products with milder conditions and higher catalytic turnover numbers remains an on-going challenge.

In order to find insights that can lead to further improvements of currently available catalytic systems, a great deal of effort has been devoted to understanding the mechanism of the Shilov system.¹⁰ The catalytic cycle has been shown to consist of three main steps (Scheme 2): (i) electrophilic activation of the alkane by platinum(II) to generate an alkylplatinum(II) intermediate, (ii) oxidation of alkylplatinum(II) to generate

an alkylplatinum(IV) species, and (iii) nucleophilic attack by water or chloride to liberate the product and regenerate the platinum(II) catalyst.

Scheme 2



The C–H activation step (i) governs the overall rate as well as the selectivity of the catalytic cycle shown in Scheme 2. Unfortunately, direct detailed study of the mechanism of this step is difficult in the “real” Shilov system because of its complexity and interfering side reactions. As a result, many researchers have turned to model systems in order to study in detail the elementary steps involved.¹¹

In the following chapters, we will investigate the mechanism of C–H activation by platinum(II) using several different model systems. In Chapter 2, we will examine the rates of C–H bond activation for various alkanes by $[(\text{N}-\text{N})\text{Pt}^{\text{II}}(\text{CH}_3)(\text{TFE}-d_3)]^+$ ($\text{N}-\text{N} = \text{Ar}-\text{N}=\text{C}(\text{CH}_3)-\text{C}(\text{CH}_3)=\text{N}-\text{Ar}$; $\text{Ar} = 3,5\text{-di-}t\text{-butylphenyl}$; $\text{TFE}-d_3 = \text{CF}_3\text{CD}_2\text{OD}$). In Chapters 3 and 4, we will study the microscopic reverse of the C–H activation step through protonolysis of two different alkylplatinum(II) model systems: $(\text{COD})\text{Pt}^{\text{II}}(\text{CH}_3)_2$ and $(\text{tmeda})\text{Pt}^{\text{II}}(\text{CH}_3)\text{Cl}$ ($\text{COD} = 1,5\text{-cyclooctadiene}$; $\text{tmeda} = \text{N},\text{N},\text{N}',\text{N}'\text{-tetramethyl-}$

ethylenediamine). In the last chapter, we will describe our efforts that led to the discovery of a new platinum(II) catalyst capable of selectively oxidizing sp^3 C–H bonds in water.

References

- (1) (a) Labinger, J. A.; Bercaw, J. E. *Nature* **2002**, *417*, 507–514. (b) Dyker, G. Ed. *Handbook of C–H Transformations*; Wiley-VCH: Weinheim, Germany, **2005**, and references therein.
- (2) Arndtsen, B. A.; Bergman, R. G.; Mobley, T. A.; Peterson, T. H. *Acc. Chem. Res.* **1995**, *28*, 154–162.
- (3) (a) Crabtree, R. H. *Chem. Rev.* **1995**, *95*, 987–1007. (b) Stahl, S. S.; Labinger, J. A.; Bercaw, J. E. *Angew. Chem. Int. Ed.* **1998**, *37*, 2180–2192.
- (4) (a) Sen, A. *Acc. Chem. Res.* **1998**, *31*, 550–557. (b) Jia, C.; Kitamura, T.; Fujiwara, Y. *Acc. Chem. Res.* **2001**, *34*, 633–639. (c) Lersch, M.; Tilset, M. *Chem. Rev.* **2005**, *105*, 2471–2526.
- (5) (a) Goldshlegger, N. F.; Tyabin, M. B.; Shilov, A. E.; Shteinman, A. A. *Zh. Fiz. Khim.* **1969**, *43*, 2174–2175. (b) Goldshlegger, N. F.; Eskova, V. V.; Shilov, A. E.; Shteinman, A. A. *Zh. Fiz. Khim.* **1972**, *46*, 1353–1354. (c) Shilov, A. E.; Shul'pin, G. B. *Chem. Rev.* **1997**, *97*, 2879–2932.
- (6) Periana, R. A.; Taube, D. J.; Gamble, S.; Taube, H.; Satoh, T.; Fujii, H. *Science* **1998**, *280*, 560–564.
- (7) Lin, M.; Shen, C.; Garcia-Zayas, E. A.; Sen, A. *J. Am. Chem. Soc.* **2001**, *123*, 1000–1001.
- (8) Kao, L. C.; Hutson, A. C.; Sen, A. *J. Am. Chem. Soc.* **1991**, *113*, 700–701.
- (9) An, Z.; Pan, X.; Liu, X.; Han, X.; Bao, X. *J. Am. Chem. Soc.* **2006**, *128*, 16028–16029.

- (10) (a) Luinstra, G. A.; Labinger, J. A.; Bercaw, J. E. *J. Am. Chem. Soc.* **1993**, *115*, 3004–3005. (b) Labinger, J. A.; Herring, A. M.; Lyon, D. K.; Luinstra, G. A.; Bercaw, J. E.; Horvath, I. T.; Eller, K. *Organometallics* **1993**, *12*, 895–905. (c) Luinstra, G. A.; Wang, L.; Stahl, S. S.; Labinger, J. A.; Bercaw, J. E. *Organometallics* **1994**, *13*, 755–756. (d) Hutson, A. C.; Lin, M.; Basickes, N.; Sen, A. *J. Organomet. Chem.* **1995**, *504*, 69–74.
- (11) (a) Hill, G. S.; Rendina, L. M.; Puddephatt, R. J. *Organometallics* **1995**, *14*, 4966–4968. (b) Stahl, S. S.; Labinger, J. A.; Bercaw, J. E. *J. Am. Chem. Soc.* **1995**, *117*, 9371–9372. (c) Stahl, S. S.; Labinger, J. A.; Bercaw, J. E. *J. Am. Chem. Soc.* **1996**, *118*, 5961–5976. (d) Romeo, R.; Plutino, M. R.; Elding, L. I. *Inorg. Chem.* **1997**, *36*, 5909–5916. (e) Heiberg, H.; Johansson, L.; Gropen, O.; Ryan, O. B.; Swang, O.; Tilset, M. *J. Am. Chem. Soc.* **2000**, *122*, 10831–10845. (f) Wik, B. J.; Lersch, M.; Tilset, M. *J. Am. Chem. Soc.* **2002**, *124*, 12116–12117. (g) Driver, T. G.; Day, M. W.; Labinger, J. A.; Bercaw, J. E. *Organometallics*, **2005**, *24*, 3644–3654. (h) Khaskin, E.; Zavalij, P. Y.; Vedernikov, A. N. *J. Am. Chem. Soc.* **2006**, *128*, 13054–13055. (i) Romeo, R.; D'Amico, G. *Organometallics* **2006**, *25*, 3435–3446. (j) Williams, T. J.; Labinger, J. A.; Bercaw, J. E. *Organometallics*, **2007**, *26*, 281–287. (k) Driver, T. G.; Williams, T. J.; Labinger, J. A.; Bercaw, J. E. *Organometallics*, **2007**, *26*, 294–301.

Chapter 2

Investigating the Mechanism of Alkane C–H Activation with Cationic Platinum(II) Complexes

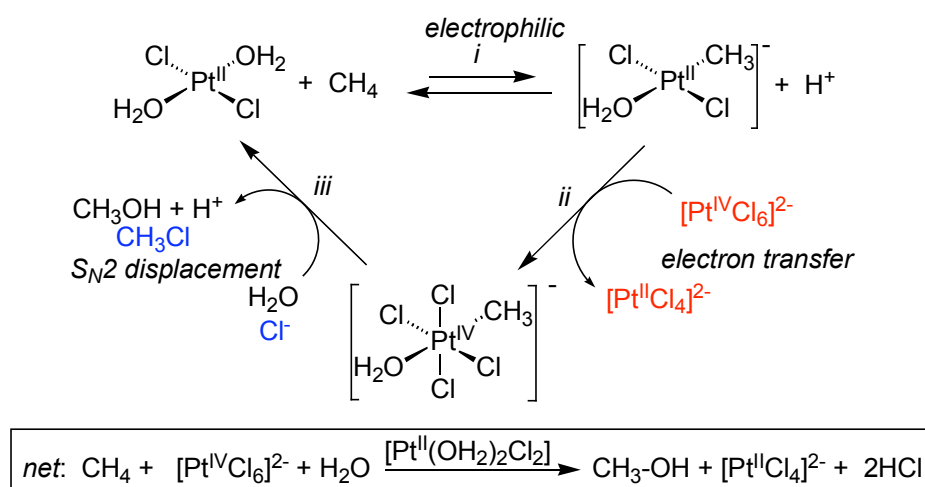
Abstract

The rates of C–H bond activation for various alkanes by $[(N-N)Pt^{II}(CH_3)(TFE-d_3)]^+$ ($N-N = Ar-N=C(CH_3)-C(CH_3)=N-Ar$; $Ar = 3,5\text{-di-}tert\text{-butylphenyl}$; $TFE-d_3 = CF_3CD_2OD$) were studied. Both linear and cyclic alkanes give the corresponding alkene-hydride cation $[(N-N)Pt^{II}(H)(alkene)]^+$ via (a) rate determining alkane coordination to form a C–H σ complex, (b) oxidative cleavage of the coordinated C–H bond to give a platinum(IV) alkyl-methyl-hydride intermediate, (c) reductive coupling to generate a methane σ complex, (d) dissociation of methane, and (e) β -H elimination to form the observed product. Second-order rate constants for cycloalkane activation (C_nH_{2n}) are proportional to the size of the ring ($k \sim n$). For cyclohexane the deuterium kinetic isotope effect (k_H/k_D) of 1.28(5) is consistent with the proposed rate determining alkane coordination to form a C–H σ complex. Statistical scrambling of the five hydrogens of the Pt-methyl and the coordinated methylene unit, via rapid, reversible steps (b) and (c), and interchange of geminal C–H bonds of the methane and cyclohexane C–H σ adducts, is observed prior to loss of methane.

Introduction

Detailed studies of the Shilov system have established the three-step mechanism and overall stoichiometry shown in Scheme 1, in which platinum(II) catalyzes the oxidation of alkanes to alcohols by platinum(IV) at 120°C.¹ Although it is currently impractical because of low reaction rates, expensive oxidant, and catalyst instability, the system does exhibit useful regioselectivity ($1^\circ > 2^\circ > 3^\circ$) and chemoselectivity.

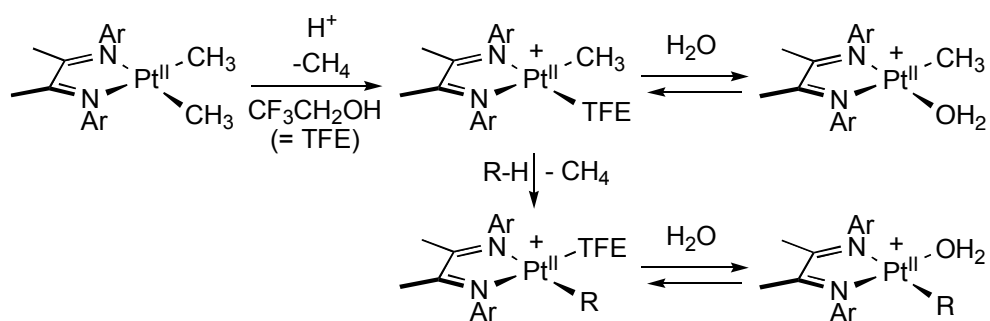
Scheme 1



The C–H activation step (step *i* in Scheme 1) is responsible for determining both activity and selectivity; but direct detailed study of its mechanism is not possible in the “real” Shilov system, because of its complexity and interfering side reactions. Accordingly, we turned to model systems, generalized in Scheme 2. The platinum methyl cations $[(\text{N}-\text{N})\text{Pt}^{\text{II}}(\text{CH}_3)(\text{solv})]^+$ ($\text{N}-\text{N} = \text{Ar}-\text{N}=\text{C}(\text{CH}_3)-\text{C}(\text{CH}_3)=\text{N}-\text{Ar}$, $\text{Ar} = 3,5\text{-di-}t\text{-butylphenyl}$; $\text{solv} = \text{TFE} = 2,2,2\text{-trifluoroethanol}$) react with a variety of R–H groups

(Ar-H, benzyl-H, indenyl-H, Me₃SiCH₂-H, etc.) to afford the corresponding organoplatinum products, and have proved to be particularly well suited for mechanistic investigations.² The relative reactivities of chemically differing C-H bonds are of particular importance for determining selectivity. We report herein on an investigation of the rate and selectivity of C-H bond activation for various linear and cyclic alkanes with this model system.

Scheme 2

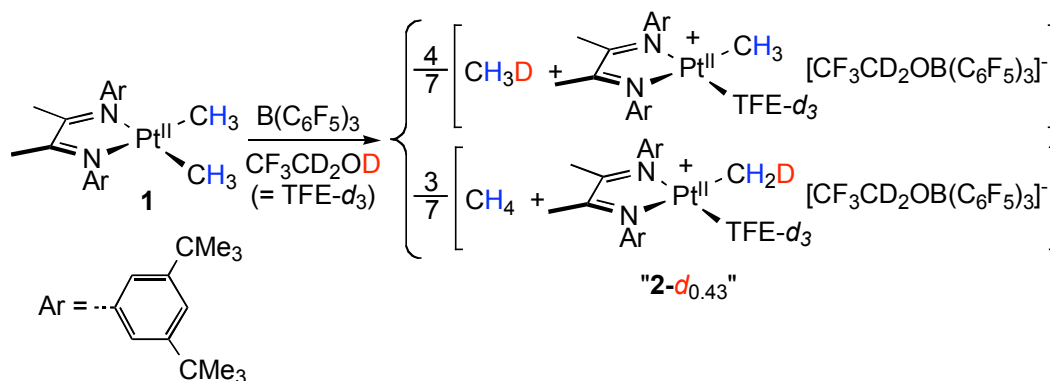


Results and Discussion

Preparation of $[(N-N)Pt^{II}(CH_3)(TFE-d_3)]^+$ and reactions with cyclic alkanes.

Protonolysis of **1** with $B(C_6F_5)_3$ in anhydrous $TFE-d_3$ gives platinum(II) monomethyl cation **2**, trifluoroethoxytris(pentafluorophenyl)borate, and methane (Scheme 3). Although only 1 equivalent of $B(C_6F_5)_3$ is required by the stoichiometry of the protonation, 2 equivalents are needed to cleanly generate **2**. Both **2** (**2-CH₃** and **2-CH₂D**) and the released methane (CH_3D and CH_4) are obtained as a statistical mixture of isotopologues, the result of fast H/D scrambling among the 7 positions of the $[(N-N)Pt^{II}(D)(CH_3)_2]^+$ intermediate prior to methane dissociation (Scheme 4).^{2f}

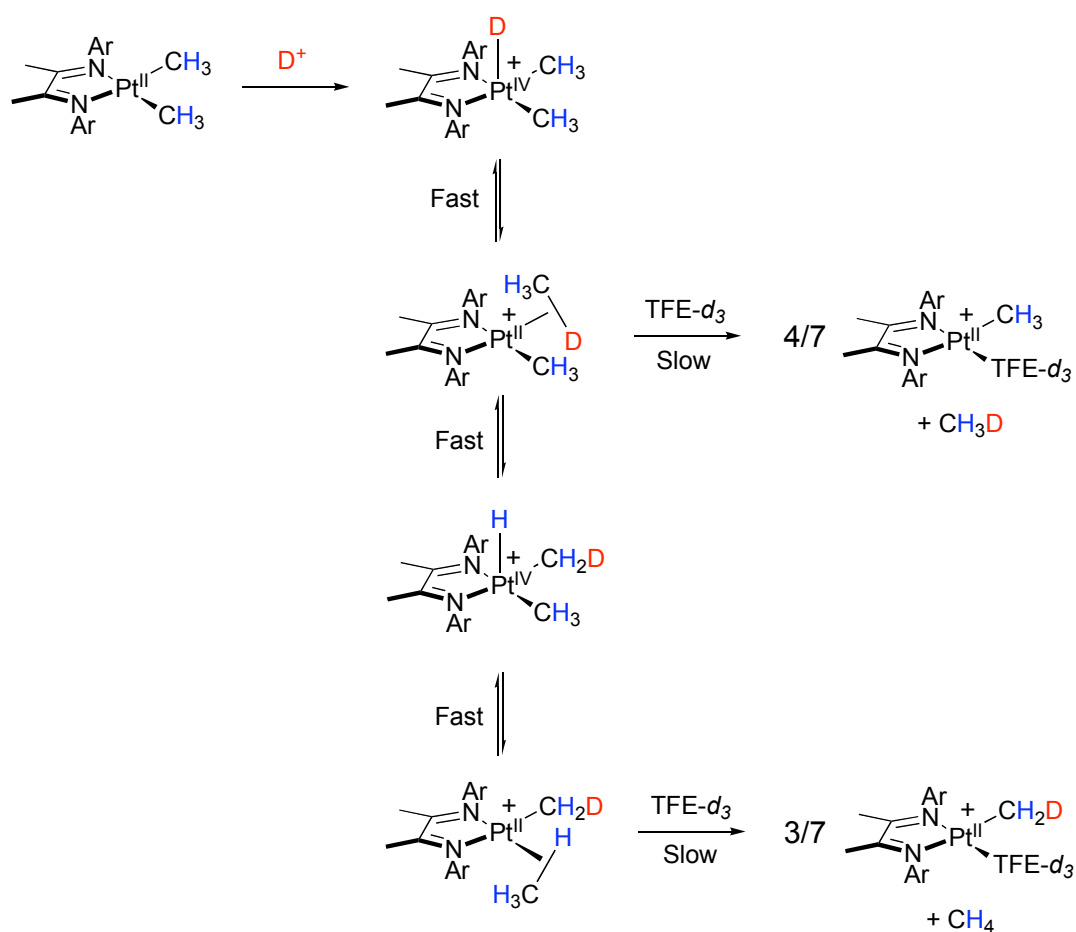
Scheme 3



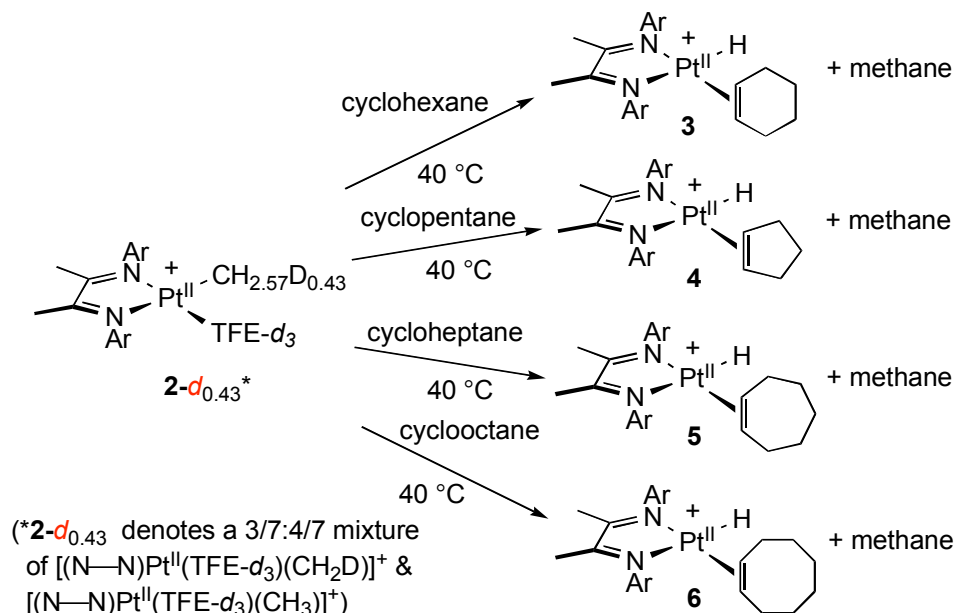
Cyclohexane, cyclopentane, cycloheptane, and cyclooctane react cleanly with the platinum methyl cation **2** at 40 °C as shown in Scheme 5. Addition of cyclohexane to a solution of **2-*d*_{0.43}** (3/7:4/7 mixture of $[(N-N)Pt^{II}(TFE-d_3)(CH_2D)]^+$ and $[(N-N)Pt^{II}(TFE-d_3)(CH_3)]^+$) in $TFE-d_3$ produces a single species **3** over the course of several hours. No intermediate platinum species are observed. 1H NMR spectra for **3** support the

proposed cyclohexene-hydride formulation, exhibiting in particular a platinum-coordinated olefin peak at $\delta = 4.9$ and a distinctive platinum hydride peak at $\delta = -22.2$ with ^{195}Pt satellites ($J_{\text{Pt-H}} = 1320$ Hz). Cyclopentane, cycloheptane, and cyclooctane all react similarly with **2** to generate the corresponding species **4**, **5**, and **6** (Scheme 5). Unfortunately, we were not successful in isolating any of these products in pure form; they decompose on concentration, or more slowly on just standing in TFE- d_3 solution.

Scheme 4



Scheme 5

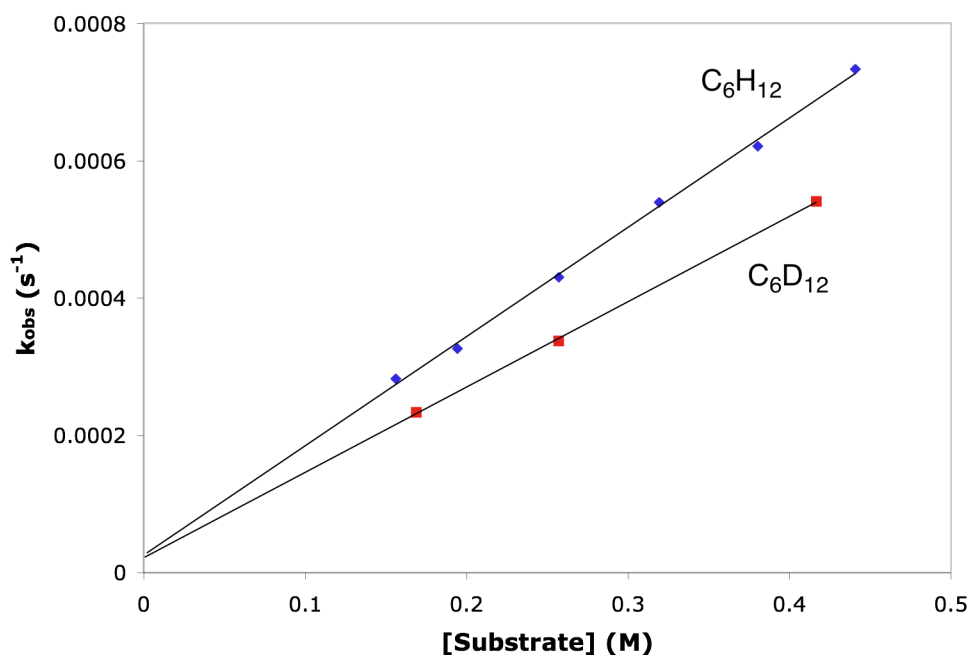


Kinetics of cycloalkane C-H activation by 2. The kinetics for reactions of **2-d_{0.43}** with C₆H₁₂ or C₆D₁₂ at 40 °C were examined by following the disappearance of **2-d_{0.43}** (methyl backbone signal at $\delta = 2.0$) and appearance of **3** by ¹H NMR. Reactions displayed clean first-order kinetics for the disappearance of [**2**] and first-order dependence on [C₆H₁₂], with $k_2 = 1.59(4) \times 10^{-3} \text{ M}^{-1} \text{ s}^{-1}$ (Figure 1). The methane isotopologues CH₃D and CH₄ were generated in the ratio of ~1:2. Formation of **3** was accompanied by a much slower background decomposition reaction,^{2f} indicated by both the appearance of additional new ¹H NMR signals and the nonzero intercept of Figure 1 ($k_{\text{decomp}} = 2.52(5) \times 10^{-5} \text{ s}^{-1}$). The rate constant for the reaction of **2-d_{0.43}** with C₆D₁₂ at 40 °C was found to be $k_2 = 1.24(4) \times 10^{-3} \text{ M}^{-1} \text{ s}^{-1}$ (with a similar non-zero intercept, $k_{\text{decomp}} = 2.14(8) \times 10^{-5} \text{ s}^{-1}$), corresponding to a kinetic deuterium isotope effect of $k_{\text{H}}/k_{\text{D}} = 1.28(5)$

(Figure 1). Methane isotopologues (CH_4 , CH_3D , CH_2D_2 , CHD_3) were observed by ^1H NMR in the latter reaction.

The kinetics of the reactions of the other cyclic alkanes (cyclopentane, cycloheptane, and cyclooctane) with $\mathbf{2-d_{0.43}}$ showed similar behavior (background decomposition rates were somewhat higher) releasing CH_3D and CH_4 in $\sim 1:2$ ratio, with second-order rate constants $k_2 = 1.34(20) \times 10^{-3} \text{ M}^{-1} \text{ s}^{-1}$ and $1.86(12) \times 10^{-3} \text{ M}^{-1} \text{ s}^{-1}$ for cyclopentane and cycloheptane, respectively. The solubility of cyclooctane in TFE is too low to attain pseudo-first-order conditions, precluding a comparably precise determination; an approximate value of $k_2 = 2.1(5) \times 10^{-3} \text{ M}^{-1} \text{ s}^{-1}$ was estimated. In contrast, cyclopropane undergoes rapid C–C bond cleavage instead of C–H activation under these conditions, presumably promoted by the strong Brønsted acidity resulting from the excess of $\text{B}(\text{C}_6\text{F}_5)_3$ in $\text{CF}_3\text{CD}_2\text{OD}$ required for clean generation of $\mathbf{2-d_{0.43}}$.³

Figure 1. Plot of k_{obs} versus [hydrocarbon] for C_6H_{12} (\blacklozenge) and C_6D_{12} (\blacksquare) at 40°C

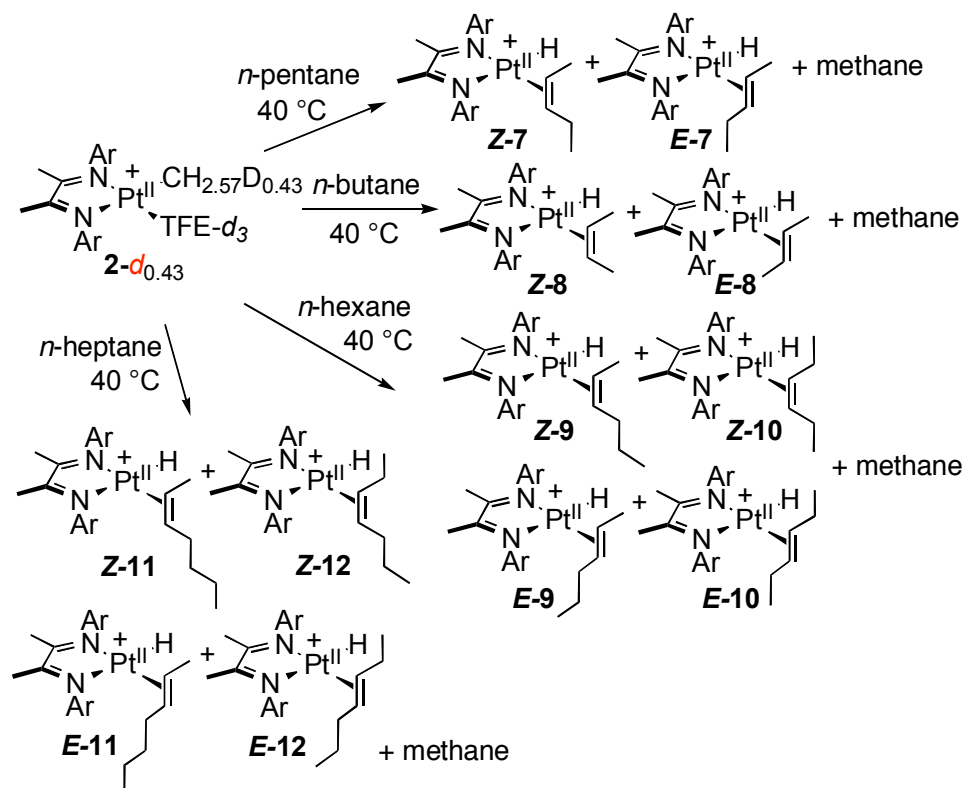


Reactions of linear alkanes with 2. The reaction of *n*-pentane with **2**-*d*_{0.43} in TFE-*d*₃ proceeds similarly to those described above: new ¹H NMR signals attributable to platinum-olefin-hydride complexes along with CH₃D and CH₄ (again in a ratio of ~ 1:2) grow in over several hours at 40 °C. However, in this case the NMR shows clear evidence for two products: platinum hydride signals at $\delta = -22.2$ and -23.3 in a ~ 2:1 ratio, respectively, along with two distinct sets of platinum-coordinated olefin peaks. As before, isolation of products was not achieved, and conclusive identification by NMR was not possible; but addition of excess PMe₃ to the reaction mixture after completion displaced coordinated olefins. These were extracted and shown to consist of *E*-2-pentene and *Z*-2-pentene in approximately 2:1 ratio (by gc); no 1-pentene was detected. We conclude therefore that the products of the reaction of *n*-pentane with **2**-*d*_{0.43} are the *E* and *Z* internal olefin adducts (**7-E** and **7-Z**) formed in a 2:1 ratio (Scheme 6). In a much slower secondary reaction, the mixture of **7-E** and **7-Z** converts at room temperature over several weeks essentially completely to the *Z*-2-pentene adduct **7-Z**.

The reactions of **2**-*d*_{0.43} with *n*-butane, *n*-hexane, and *n*-heptane proceed similarly, but with several additional features. With *n*-butane, three different Pt-H signals are initially observed, at ($\delta = -22.2, -22.1,$ and -23.1); the first of these is much weaker than the other two, and disappears completely by the time reaction is complete. We ascribe these signals to platinum complexes of 1-butene, *E*-2-butene, and *Z*-2-butene, respectively; at the end of the reaction only the *E*- and *Z*-2-butene complexes are present in a 2.5:1 ratio. With both *n*-hexane and *n*-heptane, four different platinum hydride signals are observed by ¹H NMR. Displacement with PMe₃ and gc/ms analysis of the liberated olefins reveals the presence of the four possible internal olefins (*E*- and *Z*-2- and

3-enes in each case), indicating that the multiple signals correspond to the four isomeric platinum complexes as shown in Scheme 6. No hydride signal attributable to a 1-alkene adduct was observed with *n*-pentane, *n*-hexane, or *n*-heptane.

Scheme 6



Kinetics of C–H activation for linear alkanes. Reactions of **2-d_{0.43}** at 40 °C were examined as before, by following the disappearance of **2-d_{0.43}** by ¹H NMR at varying excess concentrations of *n*-alkanes. In all cases pseudo-first-order behavior is observed, rates are first order in alkane concentration, and the ratio of isomers remains relatively constant throughout the course of the reaction. Rate constants for both linear and cyclic alkanes at 40 °C are summarized in Table 1.

Table 1. Rate constants for reactions of alkanes with **2-d**_{0.43}

Substrate	k_2^a ($M^{-1} s^{-1}$)	k_{norm}^b
cyclopentane	$1.34(20) \times 10^{-3}$	1.34×10^{-4}
cyclohexane	$1.59(4) \times 10^{-3}$	1.33×10^{-4}
cycloheptane	$1.86(12) \times 10^{-3}$	1.33×10^{-4}
cyclooctane	$2.1(5) \times 10^{-3}$	1.31×10^{-4}
<i>n</i> -butane	$1.33(4) \times 10^{-3}$	1.33×10^{-4}
<i>n</i> -pentane	$1.02(3) \times 10^{-3}$	0.85×10^{-4}
<i>n</i> -hexane	$1.06(4) \times 10^{-3}$	0.76×10^{-4}
<i>n</i> -heptane	$9.5(18) \times 10^{-4}$	0.59×10^{-4}
methane ^c	$2.7(2) \times 10^{-4}$	0.68×10^{-4}

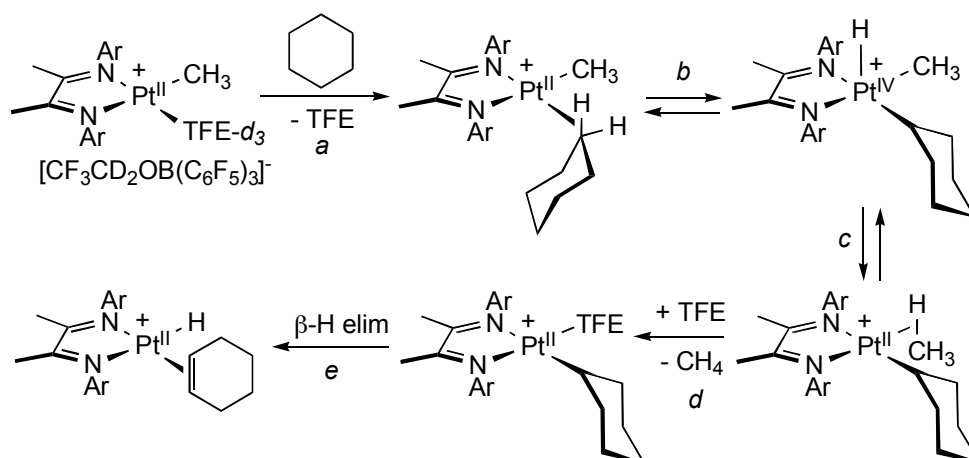
^aSecond-order rate constant at 40 °C

^bNormalized rate per C–H bond

^cData from reference 2f

Mechanism of alkane C–H activation. The reactions of linear and cyclic alkane substrates with **2** afford alkene-hydride cations $[(N-N)Pt^{II}(H)(alkene)]^+$. The most likely mechanism, based on previous work as well as present findings (see below), is shown (for cyclohexane) in Scheme 7.⁴ It involves (a) displacement of trifluoroethanol (TFE) by alkane to give a C–H σ complex, (b) oxidative cleavage to a 5-coordinate $[Pt^{IV}(methyl)(alkyl)(hydride)]$ intermediate, (c) reductive coupling to afford a methane C–H σ complex, (d), displacement of methane by TFE, and (e) β -H elimination. Questions of interest include: which step is rate-determining; what is the role and behavior of the proposed C–H σ complex intermediate; and how does reactivity vary with structure?

Scheme 7



There is precedent for either C–H coordination or oxidative C–H cleavage being rate-determining in alkane activation; a recent theoretical study supports the former (a) as rate-determining in the “real” Shilov system.⁵ For the reactions of linear and cyclic

alkanes with **2**, the same conclusion appears to hold. The extensive isotopic scrambling observed for the reaction of **2**-*d*_{0.43} with C₆D₁₂, giving CH₂D₂ and CHD₃ (CD₄ is presumably also formed, but not detected by ¹H NMR) in addition to the CH₃D, and CH₄ obtained from reactions of all-protio substrates, indicates that reversible steps *c* and *d* along with C–H bond interchange in cyclohexane and methane C–H σ complexes (see below) are all fast relative to loss of methane, consistent with rate-determining C–H coordination. This conclusion is further supported by the small KIE ($k_{\text{H}}/k_{\text{D}} = 1.28(5)$), which is similar to values measured for iridium- and rhodium-based C–H activation systems where C–H coordination is rate-determining ($k_{\text{H}}/k_{\text{D}} \approx 1.1 - 1.4$),⁶ but considerably smaller than values for rate-determining oxidative cleavage of an alkane C–H bond by d⁸ metal centers ($k_{\text{H}}/k_{\text{D}} \approx 2.5 - 5$).⁷

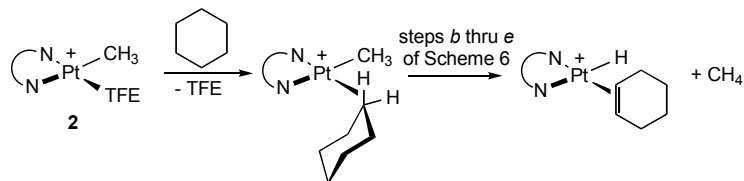
It is also notable, and consistent with rate-determining C–H coordination, that the second-order rate constants for reactions of **2** with cyclic hydrocarbons are roughly proportional to the number of C–H bonds present in the substrate (Table 1). Bergman and coworkers found that rate constants for the activation of *n*-alkanes by [Cp*(PMe₃)Rh] (Cp* = (h⁵-C₅Me₅)) are proportional to the number of secondary (-CH₂-) hydrogens in the *n*-alkane.^{6b} In that system, linear alkanes are more reactive than cycloalkanes (on a per C–H bond basis). In contrast, for the present system linear alkanes are less reactive, and the reactivity per C–H bond decreases for longer alkanes. We do not at present have a satisfying explanation for this trend. One possibility is that steric crowding inhibits C–H coordination in many of the possible conformations accessible to a linear alkane, a problem that should become more severe with increasing chain length but that would not

apply to cycloalkanes. However, such reasoning would not explain the low reactivity of methane (Table 1).

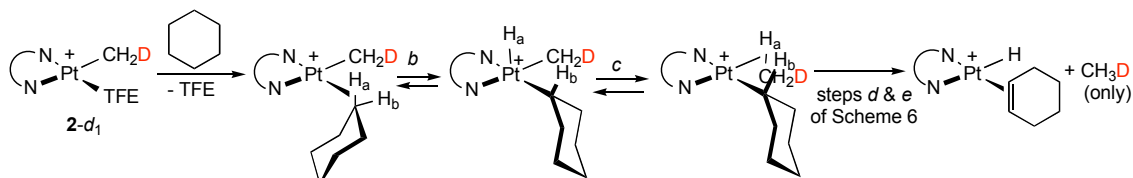
Additional information about the proposed mechanism can be deduced from quantitative details of isotopic scrambling in the methane liberated during reaction with hydrocarbon. Recall that some deuterium is introduced into **2** during the deuterolysis of **1** by $(\text{C}_6\text{F}_5)_3\text{BODCD}_2\text{CF}_3$ (Scheme 3). When the resulting 4:3 mixture of **2** and **2-d₁** reacts with a perprotio substrate, **2** liberates only CH_4 , while **2-d₁** releases a mixture of CH_3D and CH_4 . For the latter there are three possible scenarios, illustrated (for the example of cyclohexane) in Scheme 8. In case 1, step *b* is effectively irreversible; only a single C–H bond participates in the reaction, so only CH_3D will be generated from **2-d₁**, and the final ratio of CH_4 to CH_3D will be $4:3 = 1.33$.

In contrast, if steps *b* and *c* as well the interchange of coordinated C–H bonds are reversible and fast, there are two possible cases, depending upon how many C–H bonds of cyclohexane are sampled prior to dissociation of methane from the methane σ adduct (step *d*, Scheme 7). In case 2 there is fast exchange between geminal positions (H_a and H_b of cyclohexane, as well as all positions of coordinated methane); CH_3D and CH_4 will be generated in a 4:1 statistical ratio with deuterium being retained in the coordinated cyclohexene one-fifth of the time. Summing the methane generated from **2** and **2-d₁**, the expected ratio of $[\text{CH}_4]:[\text{CH}_3\text{D}]$ for case 2 is $23:12 = 1.92$. For case 3 both geminal and vicinal exchange are fast, so all 12 of the C–H bonds of cyclohexane participate in H/D exchange, giving an expected ratio of $[\text{CH}_4]:[\text{CH}_3\text{D}]$ of $31:4 = 7.75$.

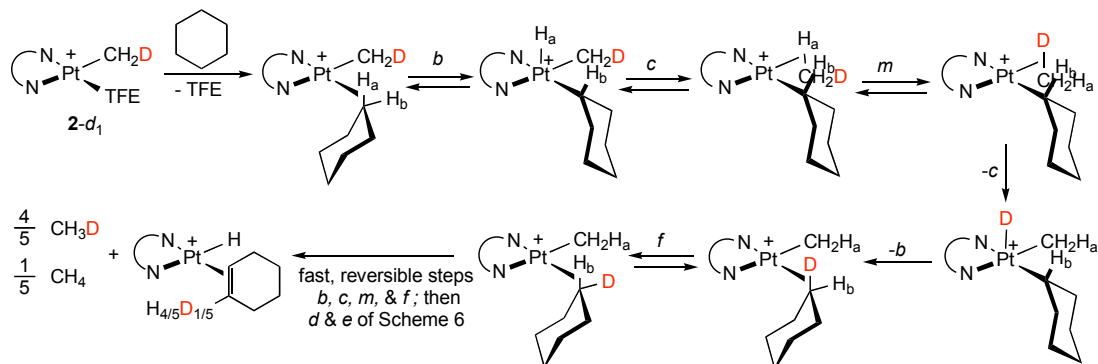
Scheme 8



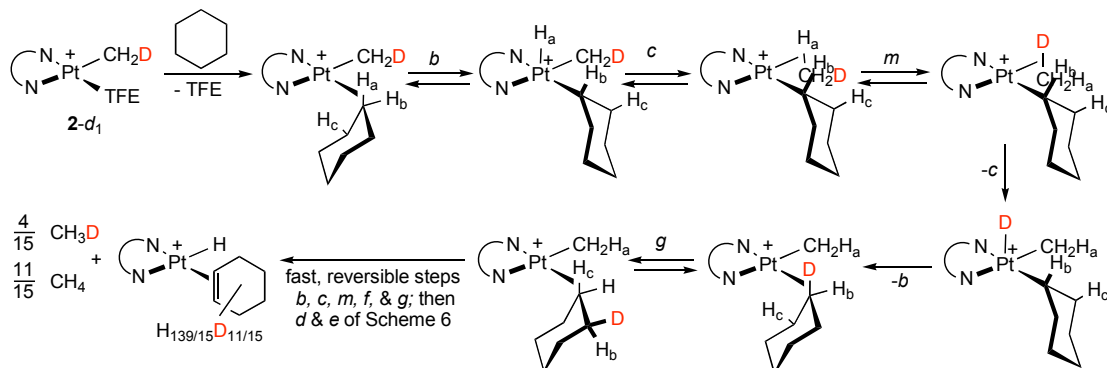
case 1: no scrambling of geminal or vicinal cyclohexane C-H bond(s) for cyclohexyl intermediate.



case 2: scrambling of geminal cyclohexane C-H bond for cyclohexyl intermediate (f); no vicinal scrambling.



case 3: scrambling of geminal (f) and vicinal (g) cyclohexane C-H bonds for cyclohexyl intermediate.



Predictions of net isotopologs of methane:

case 1: CH₄:CH₃D = 1.33

case 2: CH₄:CH₃D = 1.92

case 3: CH₄:CH₃D = 7.75

Observed: CH₄:CH₃D = 1.97(16)

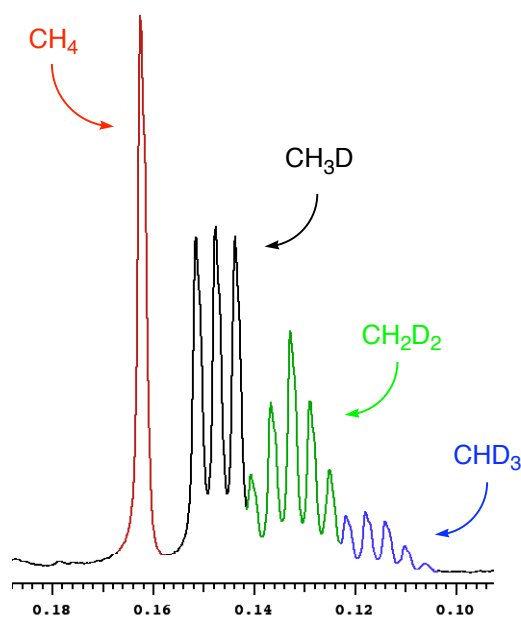
The experimentally observed ratio $[\text{CH}_4]:[\text{CH}_3\text{D}]$ from the reaction of C_6H_{12} with **2-*d*_{0.43}** is 1.97(16), for cyclohexane, and approximately the same for all the other alkanes and cycloalkanes examined. This finding is only consistent with case 2: fast geminal but slow vicinal C–H interchange. By way of comparison, in a metastable rhenium-pentane complex (observed at low temperature by NMR) geminal exchange is fast on the NMR timescale, whereas vicinal exchange takes place much more slowly (rates on the order of $1\text{--}10\text{ s}^{-1}$ at 173 K).⁸

For linear alkanes we have the additional option of coordinating/reacting at either terminal (methyl) or internal (methylene) positions. Jones and coworkers have shown that in a rhodium system (Tp^*LRh with $\text{L} = \text{CNCH}_2\text{CMe}_3$), coordination of secondary C–H bonds is preferred over primary C–H bonds by a factor of 1.5;^{7b} for the rhenium system cited above, coordination of pentane at the 2- and 3-positions is (very slightly) favored over statistical values.⁸ We observed a $[\text{CH}_4]:[\text{CH}_3\text{D}]$ ratio of $\sim 2:1$ for all four linear alkanes, which at first glance seems consistent with statistical scrambling involving only one methylene ($-\text{CH}_2-$) group, as with cycloalkanes. However, the predicted $[\text{CH}_4]:[\text{CH}_3\text{D}]$ ratio for participation of a single terminal methyl ($-\text{CH}_3$) group is $15:6 = 2.50$; if both primary and secondary C–H activations occur, the $[\text{CH}_4]:[\text{CH}_3\text{D}]$ ratio would be between 1.92 and 2.50, well within the uncertainty of this experimental determination.

In an attempt to gain further information on this question, we examined the methane produced by reaction of partially deuterated propanes ($\text{CD}_3\text{CH}_2\text{CD}_3$ and $\text{CH}_3\text{CD}_2\text{CH}_3$) with **2-*d*_{0.43}**. The former gives CH_4 (10%), CH_3D (26%), CH_2D_2 (29%), and CHD_3 (35%); exclusive reaction of secondary [C–H] bonds would give only CH_4 and

CH_3D , whereas exclusive reaction of primary $[\text{C-H}]$ bonds would give no CH_4 . Similarly, the latter isotopologue gives CH_4 (63%), CH_3D (32%), and CH_2D_2 (5%). These results are approximately consistent with statistical expectations; i.e., no preference between terminal and internal positions. It should be noted, however, that the reactions of propane (and ethane) with **2** do not give olefin-hydride products analogous to those found for higher linear alkanes; these reactions do appear to involve initial C-H activation, but the final products exhibit more complex NMR spectra and were not fully identified. Nonetheless, we believe that the inferences from these selective labeling experiments are probably valid. We also examined the reaction of **2**- $d_{0.43}$ with $\text{CD}_3\text{CH}_2\text{CH}_2\text{CD}_3$. All four isotopologues of methane (CH_4 , CH_3D , CH_2D_2 , and CHD_3) were observed, which, like the results obtained above, are consistent with a system that shows no preference between terminal and internal positions (Figure 2).

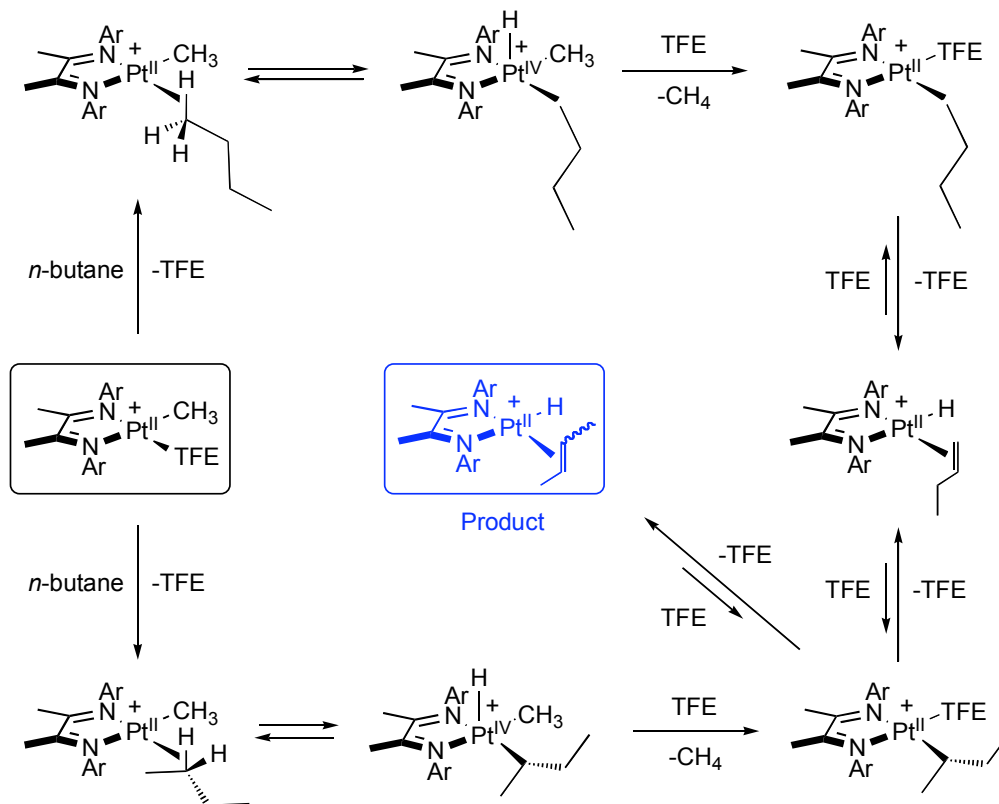
Figure 2. Methane isotopologues from the reaction of **2**- $d_{0.43}$ with $\text{CD}_3\text{CH}_2\text{CH}_2\text{CD}_3$



The failure to observe any evidence for terminal olefin adducts in the reactions of *n*-pentane, *n*-hexane, and *n*-heptane with **2-d**_{0.43} might also be taken to suggest a preference for internal reaction. However, it seems more likely that the terminal olefin complex is rapidly isomerized to the internal isomers via the olefin insertion/ β -H elimination sequence. Such a process has been shown to operate at -78 °C on the order of hours in a related [Tp⁺Pt] system; where the initially formed 1-pentene adduct isomerizes to 2-pentene adducts.^{4b} Our observation of a low transient amount of a terminal alkene adduct only in the case of *n*-butane (which has a small statistical advantage, relative to higher alkanes, for initial coordination and cleavage of primary C–H bonds) is consistent with this interpretation. There may well be a connection between this behavior and the failure to observe stable olefin-hydride products from propane and ethane, which can give only terminal olefin complexes.

A mechanism for the activation of linear alkanes consistent with all experimental observations is shown in Scheme 9 for *n*-butane. The initial rate-determining C–H coordination step is not selective, and both terminal and internal positions are activated. However, rapid isomerization via olefin insertion/ β -H elimination leads to only internal olefins in the final observed products.

Scheme 9



Conclusions

We have demonstrated C–H bond activation of various alkanes by $[(\text{N–N})\text{Pt}^{\text{II}}(\text{CH}_3)(\text{TFE-}d_3)]^+$ to generate $[(\text{N–N})\text{Pt}^{\text{II}}(\text{H})(\text{alkene})]^+$ cations. The small KIE ($k_{\text{H}}/k_{\text{D}} = 1.3$) for cyclohexane together with statistical isotopic scrambling in the methane released suggests that C–H bond coordination is rate determining. Comparing the relative rates of cyclic and linear alkanes indicates that the platinum center is relatively unselective with respect to different C–H bonds: the rate constants (per C–H bond) for the substrates examined all fall into a narrow range, and there does not appear to be any significant preference for either primary or secondary C–H bonds.

Experimental

General methods. All air- and/or moisture-sensitive compounds were manipulated by using standard high-vacuum line, Schlenk, or cannula techniques, or in a glove box under a nitrogen atmosphere. $\text{B}(\text{C}_6\text{F}_5)_3$ was purchased from Aldrich and sublimed at 90 °C at full vacuum and stored in a P_2O_5 dessicator in the glove box. Trifluoroethanol- d_3 was purchased from Cambridge Isotope Laboratories and dried over 3-Å molecular sieves for at least 5 days, then vacuum distilled onto $\text{B}(\text{C}_6\text{F}_5)_3$, and shortly thereafter distilled into a Strauss flask and stored in the glove box. All gasses were purchased from Matheson and dried using standard high vacuum line techniques over 4-Å molecular sieves. $\text{CD}_3\text{CH}_2\text{CD}_3$, $\text{CH}_3\text{CD}_2\text{CH}_3$, and $\text{CD}_3\text{CH}_2\text{CH}_2\text{CD}_3$ were purchased from CDN Isotopes and dried using standard high vacuum line techniques. All other alkanes were purchased from Aldrich and dried over calcium hydride and stored in the glove box. Compound **1** was synthesized according to literature procedures.^{2c} NMR spectra were recorded on a Varian Mercury 300 or Varian Inova 500 spectrometer.

C–H activation studies. Solutions of **2** were prepared by weighing **1** and $\text{B}(\text{C}_6\text{F}_5)_3$ (2 equivalents) into a volumetric flask and adding trifluoroethanol- d_3 . The suspension was shaken until all solids had dissolved to give a light yellow solution. This solution was then transferred into a J-Young NMR tube and degassed on a high-vacuum line to remove methane generated from the protonolysis. An initial ^1H NMR spectrum was acquired to confirm complete and clean formation of **2**. The desired alkane was then

added and the tube heated to 40 °C in an oil bath. After several hours, a second ^1H NMR spectrum was acquired to confirm formation of product.

Kinetics experiments. Stock solutions of **2** were prepared by weighing out 40 mg of **1** and 60 mg of $\text{B}(\text{C}_6\text{F}_5)_3$. Five milliliters of trifluoroethanol- d_3 were then added, and the solution turned light yellow after a few minutes. A total of 0.7 mL of this solution was added to a J-Young NMR tube. The NMR tube was degassed on a high-vacuum line, and an initial ^1H NMR spectrum was acquired to confirm complete and clean formation of **2**. Alkanes that are liquids at room temperature were then added by syringe, shaken briefly, and the tube was then inserted into an NMR spectrometer that had been preheated to 40 °C. Alkanes that are gases at room temperature were vacuum transferred into the NMR tube using a calibrated gas bulb on the high-vacuum line. After allowing a few minutes for the NMR tube to reach equilibrium, an array of 40 to 50 spectra was acquired. Kinetics was monitored by following the disappearance of either one of the backbone methyl peaks or one of the aryl peaks over time. Pseudo-first-order rate constants (k_{obs}) were then obtained by fitting the data to a first-order exponential function. Second-order rate constants were then obtained from a plot of k_{obs} versus [alkane].

References

- (1) (a) Luinstra, G. A.; Labinger, J. A.; Bercaw, J. E. *J. Am. Chem. Soc.* **1993**, *115*, 3004–3005. (b) Labinger, J. A.; Herring, A. M.; Lyon, D. K.; Luinstra, G. A.; Bercaw, J. E.; Horvath, I. T.; Eller, K. *Organometallics* **1993**, *12*, 895–905. (c) Luinstra, G. A.; Wang, L.; Stahl, S. S.; Labinger, J. A.; Bercaw, J. E. *Organometallics* **1994**, *13*, 755–756. (d) Hutson, A. C.; Lin, M.; Basickes, N.; Sen, A. *J. Organomet. Chem.* **1995**, *504*, 69–74.
- (2) (a) Stahl, S. S.; Labinger, J. A.; Bercaw, J. E. *J. Am. Chem. Soc.* **1996**, *118*, 5961–5976. (b) Johansson, L.; Tilset, M.; Labinger, J. A.; Bercaw, J. E. *J. Am. Chem. Soc.* **2000**, *122*, 10846–10855. (c) Zhong, H. A.; Labinger, J. A.; Bercaw, J. E. *J. Am. Chem. Soc.* **2002**, *124*, 1378–1399. (d) Heyduk, A. F.; Driver, T. G.; Labinger, J. A.; Bercaw, J. E. *J. Am. Chem. Soc.* **2004**, *126*, 15034–15035. (e) Driver, T. G.; Day, M. W.; Labinger, J. A.; Bercaw, J. E. *Organometallics* **2005**, *24*, 3644–3654. (f) Owen, J. S.; Labinger, J. A.; Bercaw, J. E. *J. Am. Chem. Soc.* **2006**, *128*, 2005–2016.
- (3) Deno, N. C.; LaVietes, D.; Mockus, J.; Scholl, P. C. *J. Am. Chem. Soc.* **1968**, *90*, 6457–6460.
- (4) (a) Zhong, H. A.; Labinger, J. A.; Bercaw, J. E. Unpublished results. (b) Kostelansky, C. N.; MacDonald, M. G.; White, P. S.; Templeton, J. L. *Organometallics* **2006**, *25*, 2993–2998.
- (5) Zhu, H.; Ziegler, T. *J. Organometal. Chem.* **2006**, *691*, 4486–4497.

- (6) (a) Janowicz, A. H.; Bergman, R. G. *J. Am. Chem. Soc.* **1983**, *105*, 3929–3939. (b) Periana, R. A.; Bergman, R. G. *J. Am. Chem. Soc.* **1986**, *108*, 7332–7346. (c) Alaimo, P. J.; Arndtsen, B. A.; Bergman, R. G. *Organometallics* **2000**, *19*, 2130–2143.
- (7) (a) Northcutt, T. O.; Wick, D. D.; Vetter, A. J.; Jones, W. D. *J. Am. Chem. Soc.* **2001**, *123*, 7257–7270. (b) Vetter, A. J.; Flaschenriem, C.; Jones, W. D. *J. Am. Chem. Soc.* **2005**, *127*, 12315–12322.
- (8) Lawes, D. J.; Geftakis, S.; Ball, G. E. *J. Am. Chem. Soc.* **2005**, *127*, 4134–4135.

Chapter 3

Investigating the Temperature Dependence of the Primary Kinetic Hydrogen Isotope Effect in the Protonolysis of Platinum(II) Methyl Complexes

Abstract

Protonolysis of $(\text{COD})\text{Pt}^{\text{II}}(\text{CH}_3)_2$ by trifluoroacetic acid gave abnormally large kinetic isotope effects (KIEs) as well as Arrhenius parameters that fall outside semi-classical limits. On the other hand, protonolysis of $(\text{tmeda})\text{Pt}^{\text{II}}(\text{CH}_3)\text{Cl}$ by trifluoroacetic acid gave only normal KIEs and classical Arrhenius parameters. We propose that the protonolysis of $(\text{COD})\text{Pt}^{\text{II}}(\text{CH}_3)_2$ proceeds by direct protonation at the M–C bond, while a stepwise oxidative addition/reductive elimination pathway occurs for the protonolysis of $(\text{tmeda})\text{Pt}^{\text{II}}(\text{CH}_3)\text{Cl}$. We further propose that the presence of abnormally large KIEs and Arrhenius parameters that fall outside semi-classical limits are indications that a concerted mechanism is operating.

Introduction

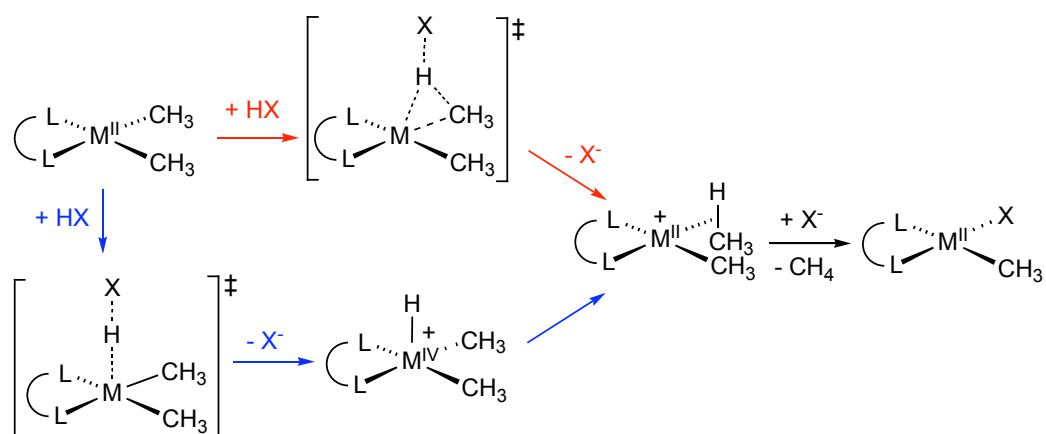
The selective activation and functionalization of alkane C–H bonds represent important areas of research. Over the past several decades, a number of examples of C–H bond activation by transition metals have appeared in the literature.¹ Of particular interest is the Shilov system, which catalytically converts methane to methanol and methyl chloride by aqueous platinum(II) salts in water.² Both the original Shilov system as well as related systems have since been developed and studied.³

Numerous experimental and theoretical studies have shown that the C–H activation step of the Shilov system governs the overall rate as well as the selectivity of the catalytic cycle.⁴ Unfortunately, direct detailed study of this step is difficult in the “real” Shilov system because of its complexity and interfering side reactions. Accordingly, many groups have investigated the microscopic reverse of the C–H activation step, namely protonolysis of alkylplatinum(II) model systems.⁵

Two alternative mechanisms for protonolysis have been proposed in the literature.⁶ As shown in Scheme 1, protonation can take place either by a concerted attack at the metal-carbon bond (the microscopic reverse of electrophilic C–H activation), or a stepwise prior oxidative addition on the central metal to generate a metal hydride followed by reductive elimination (the microscopic reverse of oxidatively adding a C–H bond across the metal). Both pathways involve the formation of a Pt(II)-methane σ adduct before the liberation of methane, which is supported by statistical deuterium scrambling in deuterolysis where methane dissociation is rate determining. The possibility for the latter pathway has been clearly shown plausible by the observation of

Pt(IV)–H intermediates in the protonolysis of several alkylplatinum(II) model systems. However, the ability to detect these intermediates can be difficult and is dependent on a number of factors such as solvent, temperature, and supporting ligands. The failure to observe a Pt(IV)–H intermediate does not necessarily rule out the oxidative addition pathway. As a result, indirect methods are often needed to probe the mechanism in cases where no intermediate can be observed.

Scheme 1



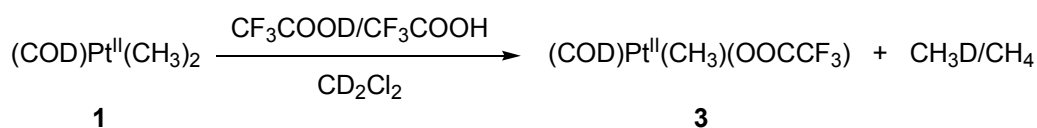
A powerful indirect method used to investigate the mechanism of protonolysis is to measure its kinetic isotope effect (KIE).⁷ A possible correlation between the above two pathways and the magnitude of the KIE at 298 K (normal KIEs, 1.3–5.0 for the concerted pathway; inverse KIEs, 0.3–0.7 for the stepwise pathway) has been recently proposed based on the studies of a number of phosphine-ligated platinum(II) methyl complexes.^{6b} In order to further explore the mechanisms of C–H activation by platinum(II), we studied the protonolysis chemistry of a series of platinum(II) methyl complexes. To our great surprise, abnormally large KIEs (greater than 10) at room temperature and higher were

observed for the protonolysis of $(\text{COD})\text{Pt}^{\text{II}}(\text{CH}_3)_2$ (COD = 1,5-cyclooctadiene). This discovery prompted us to examine the temperature dependence of the KIE for several platinum(II) methyl complexes. These results are described in the following sections. A correlation between the mechanisms and the abnormally large KIEs is also proposed.

Results and Discussion

Protonolysis of (COD)Pt^{II}(CH₃)₂. Protonolysis of (COD)Pt^{II}(CH₃)₂ **1** with two equivalents of B(C₆F₅)₃ in anhydrous TFE-*d*₃ at room temperature (COD = 1,5-cyclooctadiene) cleanly generates [(COD)Pt^{II}CH₃(OCD₂CF₃)]⁺ **2** and methane. Surprisingly, a non-negligible amount of CH₄ is present in addition to CH₃D. Because no deuterium incorporation is observed in either the methyl or COD ¹H NMR signals of the product, residual H⁺ in the solvent must be responsible for the CH₄ formed. Addition of a 9.5:1 mixture of CF₃COOD:CF₃COOH to a solution of **1** in CD₂Cl₂ at room temperature gives (COD)Pt^{II}(CH₃)(OOCF₃) **3** and a CH₃D:CH₄ ratio of 0.54:1 by ¹H NMR (no other isotopologues of methane are observed), leading to an abnormally large kinetic isotope effect (*k*_H/*k*_D) of 17.6 (Scheme 2). Again, deuterium incorporation into **3** is not observed. Furthermore, no platinum(IV) hydride intermediates are detected by ¹H NMR in the protonolysis of **1** in CD₂Cl₂ at -80 °C.

Scheme 2



KIE temperature dependence for the protonolysis of (COD)Pt^{II}(CH₃)₂. The literature on the protonolysis of platinum(II) methyl bonds is quite extensive, and to the best of our knowledge, no other research group has reported a *k*_H/*k*_D at room temperature greater than 10.⁸ KIE values greater than 10 at room temperature are generally

acknowledged as an indicator for significant contribution of quantum mechanical tunneling in proton transfer reactions.⁹ Tunneling is a fundamental phenomenon originating from wave-particle duality. According to the de Broglie relation ($\lambda = h/p = h/[2mk_B T]^{1/2}$), protons moving with thermal velocities at ordinary temperatures have wavelengths between 1 to 2 Å.¹⁰ Since the barriers of proton transfer reactions have a total width of a few Ångströms, we may expect the tunnel effect to be of importance in some cases.

$$k = (k_B T/h) \times Q_t \times Z_t \times Z_r \times Z_v \times \exp(-E_a/RT) \quad \text{Equation (1)}$$

$$Z_t = \exp [(TS_{t,a} - E_{t,a})/RT] \quad \text{translational partition function}$$

$$Z_r = \exp [(TS_{r,a} - E_{r,a})/RT] \quad \text{rotational partition function}$$

$$Z_v = \exp [(TS_{v,a} - E_{v,a})/RT] \quad \text{vibrational partition function}$$

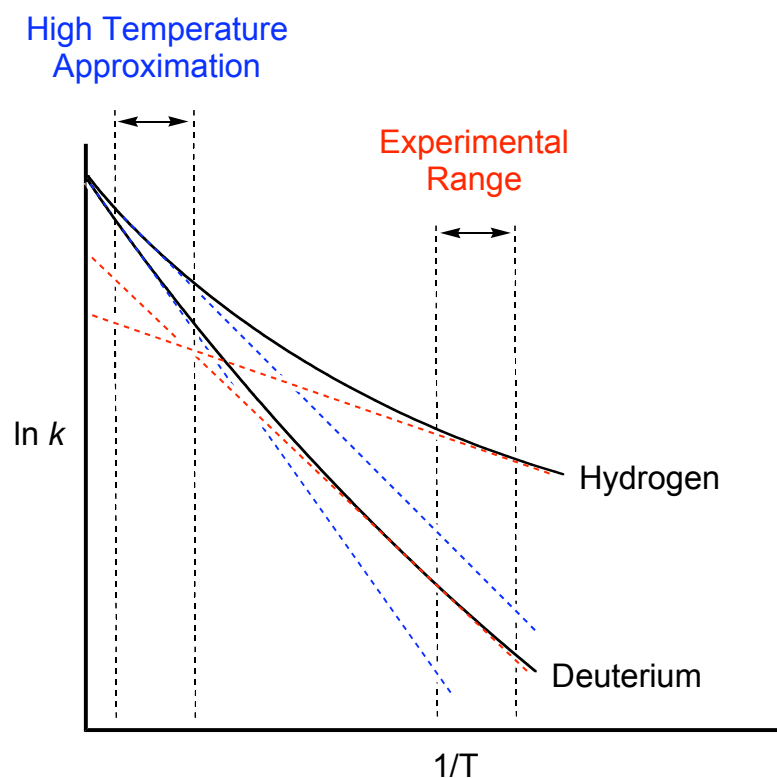
In the presence of tunneling, the rate constant is modified by a tunneling correction factor, Q_t (Equation 1).¹¹ Since E_a , the activation electronic energy, is assumed to be isotope insensitive, only Q_t and the partition functions will contribute to the KIE. The presence of significant tunneling can be experimentally determined by examining the temperature dependence of the KIE.¹² This behavior is due to the fact that both $Q_{t,H}/Q_{t,D}$ (subject to $\lambda = h/[2mk_B T]^{1/2}$) and $Z_{v,H}/Z_{v,D}$ (subject to thermal excitation of vibronic states) are temperature dependent within normal experimental temperature ranges. A plot of $\ln(k_H/k_D)$ against $1/T$ gives a curve, although this curvature is not discernible over temperature ranges typical of most experiments, allowing the use of the Arrhenius relation to approximate these situations (Equation 2, Figure 1). Correlating the Arrhenius relation with the Eyring equation (Equation 3: $Z_v^{\text{exc}} =$ partition function of excited

vibronic states; ZPE = zero-point vibrational energy), one can obtain limits for the Arrhenius parameters associated with proton transfer reactions in the absence of tunneling: $0.5 < A_H/A_D < 2^{1/2}$ (calculations on model systems suggest 0.7–1.2 is a more realistic range)¹³ and $(E_a^D - E_a^H) < 1.2$ kcal/mol (zero-point energy difference of O-H stretching of the proton source). Proton transfer reactions with $(E_a^D - E_a^H)$ greater, and A_H/A_D smaller, than these predictions indicate the substantial involvement of tunneling.

$$\frac{k_H}{k_D} = A_H/A_D \exp[-(E_a^H - E_a^D)/RT] \quad \text{Equation (2)}$$

$$\frac{k_H}{k_D} = \frac{Q_{t,H} \times Z_{t,H} \times Z_{r,H} \times Z_{v,H}^{\text{exc}}}{Q_{t,D} \times Z_{t,D} \times Z_{r,D} \times Z_{v,D}^{\text{exc}}} \times e^{-\Delta\Delta\text{ZPE}/RT} \quad \text{Equation (3)}$$

Figure 1. Arrhenius plots with incidence of tunneling of H and D



Since highly accurate measurements of the $\text{CH}_3\text{D}:\text{CH}_4$ ratio across a wide temperature range are needed to calculate reliable KIEs and the corresponding Arrhenius parameters, we screened a variety of solvents in order to find the one that gives the best ^1H NMR signals. We selected 1,2-dichloroethane- d_4 as the solvent because of its convenient temperature range, and the fact that it gives well-separated and sharp ^1H NMR signals for both CH_3D and CH_4 .

The $\text{CH}_3\text{D}:\text{CH}_4$ ratio for the protonolysis of **1** with a mixture of CF_3COOD and CF_3COOH was measured from 0 to 80 °C in twenty degree intervals. For each given temperature, multiple runs were made. The total amounts of acid, solvent, and platinum complex were kept constant. The ratio of $\text{CF}_3\text{COOD}:\text{CF}_3\text{COOH}$ was varied from 5:1 to 20:1, but the ratio of $\text{CF}_3\text{COOH}:\mathbf{1}$ was kept at a minimum of 15:1 to ensure that during the course of the reaction, the concentrations of the acids remain relatively constant. Highly reproducible and consistent results were obtained for all temperatures. The results are summarized in Table 1, and show an interesting temperature dependence. In all cases, only **3** is observed by ^1H NMR. Protonolysis of **3** to give $(\text{COD})\text{Pt}^{\text{II}}(\text{OOC}\text{CF}_3)_2$ is not observed even after heating at 80 °C for 12 hours, and no other isotopologues of methane are detected.

Using the values from Table 1, a plot of $\ln k_{\text{H}}/k_{\text{D}}$ versus $1/T$ gives a straight line ($R^2 = 0.9991$) with $A_{\text{H}}/A_{\text{D}} = 0.075 \pm 0.007$ and $E_{\text{a}}^{\text{D}} - E_{\text{a}}^{\text{H}} = 3.2 \pm 0.1$ kcal/mol (Figure 2). These values are indicative of a tunneling pathway for the protonolysis of the platinum methyl bond since $A_{\text{H}}/A_{\text{D}}$ is considerably less than 0.7, and $E_{\text{a}}^{\text{D}} - E_{\text{a}}^{\text{H}}$ is much larger than 1.2 kcal/mol.

Table 1. Temperature dependence of k_H/k_D in the protonolysis of **1** by TFA (determined by the average of 3 runs at each temperature)

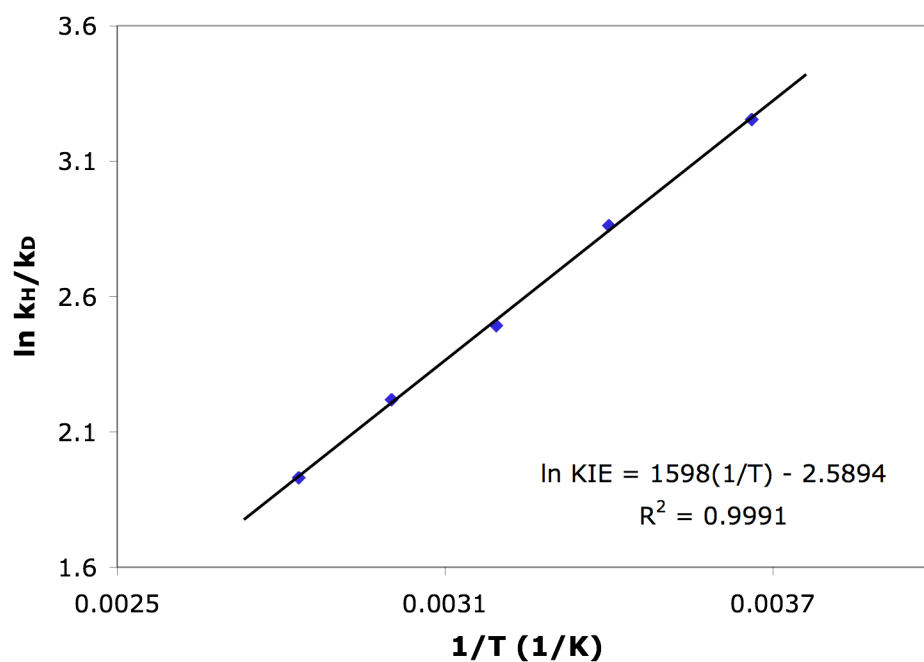
Temperature K	k_H/k_D
273	25.9 ± 0.3
294	17.5 ± 0.3
313	12.1 ± 0.3
333	9.2 ± 0.3
353	6.9 ± 0.3

Calculated Parameters:

$$A_H/A_D = 0.075 \pm 0.007$$

$$E_a^D - E_a^H = 3.2 \pm 0.1 \text{ kcal/mol}$$

Figure 2. Plot of $\ln(k_H/k_D)$ over $1/T$ for **1**



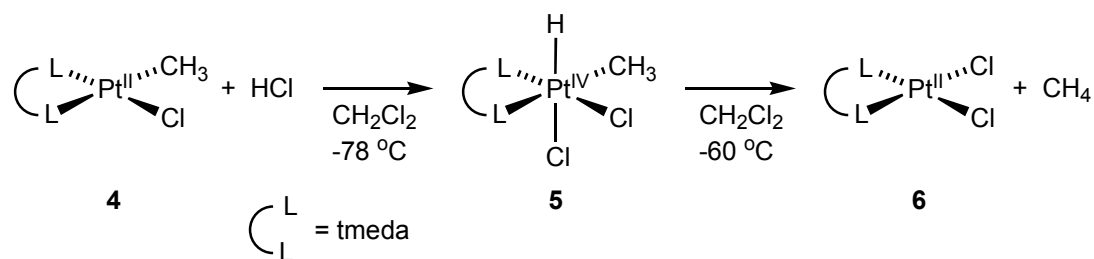
The lack of isotope scrambling and incorporation of deuterium into Pt-CH₃, and the absence of isotopologues of methane besides CH₃D and CH₄ suggest a mechanism involving rate determining proton attack followed by fast methane loss. The presence of a

large positive kinetic isotope effect further suggests that the rate determining proton transfer involves direct protonation at the metal-carbon bond. An oxidative addition reductive elimination pathway would generally result in a small positive or inverse KIE, something not observed in our case. A concerted mechanism is further suggested by the failure to observe any Pt(IV)-H intermediates in the protonolysis of **1** at -80 °C in CD₂Cl₂; one might expect the electron withdrawing COD ligand to disfavor the formation of a Pt(IV) intermediate.

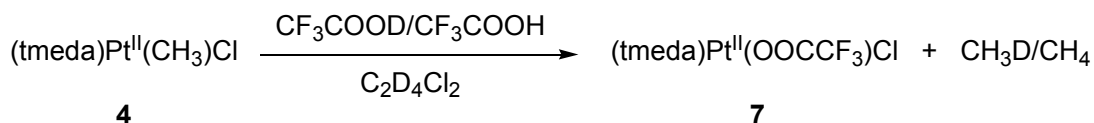
Protonolysis of (tmeda)Pt^{II}(CH₃)Cl. The results of the protonolysis of **1** prompted us to examine a different system under similar conditions in which the presence of an oxidative addition/reductive elimination mechanism has been supported by the observation of Pt(IV)-H. If a correlation does exist between proton tunneling/abnormally large KIEs and the concerted protonation mechanism, we would expect to see normal or inverse KIEs as well as a classical KIE-temperature relationship for a system that operates by an oxidative addition/reductive elimination mechanism. Towards that regard, we decided to study the protonolysis of (tmeda)Pt^{II}(CH₃)Cl **4** (tmeda = N,N,N',N'-tetramethyl-ethylenediamine).^{6a} Previous work has shown that addition of excess HCl (dissolved in diethyl ether) at -78 °C to a methylene chloride solution of **4** leads to oxidative addition of HCl to generate (tmeda)Pt(CH₃)(H)Cl₂ **5**. Upon warming to -60 °C, the reductive elimination of methane is observed along with formation of (tmeda)PtCl₂ **6** (Scheme 3). The presence of only a single methyl group also eliminates deuterium scrambling that is often observed in the protonolysis of dimethylplatinum(II) species that undergo oxidative addition, therefore allowing us to measure the KIE of protonolysis under competitive conditions across a wide temperature range. Addition of a 2:1 mixture

of $\text{CF}_3\text{COOD}:\text{CF}_3\text{COOH}$ to a solution of **4** in $\text{DCE-}d_4$ at room temperature gives $(\text{tmeda})\text{Pt}(\text{OOCF}_3)\text{Cl}$ **7** and a $\text{CH}_3\text{D}:\text{CH}_4$ ratio of 0.45:1 by ^1H NMR, leading to a kinetic isotope effect ($k_{\text{H}}/k_{\text{D}}$) of 4.4. No other isotopologues of methane are observed (Scheme 4).

Scheme 3



Scheme 4



The temperature dependence of $k_{\text{H}}/k_{\text{D}}$ for the protonolysis of **4** was then investigated (Table 2). In sharp contrast to **1**, the KIEs measured for the protonolysis of **4** are much less temperature dependent. A linear correlation between $\ln(k_{\text{H}}/k_{\text{D}})$ and $1/T$ was obtained, giving $A_{\text{H}}/A_{\text{D}} = 1.1 \pm 0.1$ and $(E_{\text{a}}^{\text{D}} - E_{\text{a}}^{\text{H}}) = 0.8 \pm 0.1$ kcal/mol for **4** (Figure 3). Unlike the system examined earlier, the results for **4** all fall within semi-classical limits. It should be noted that the involvement of proton tunneling cannot always be ruled out for systems with normal KIEs and Arrhenius parameters that fall within semi-classical limits. For example, temperature-independent KIEs have been observed for enzymatic

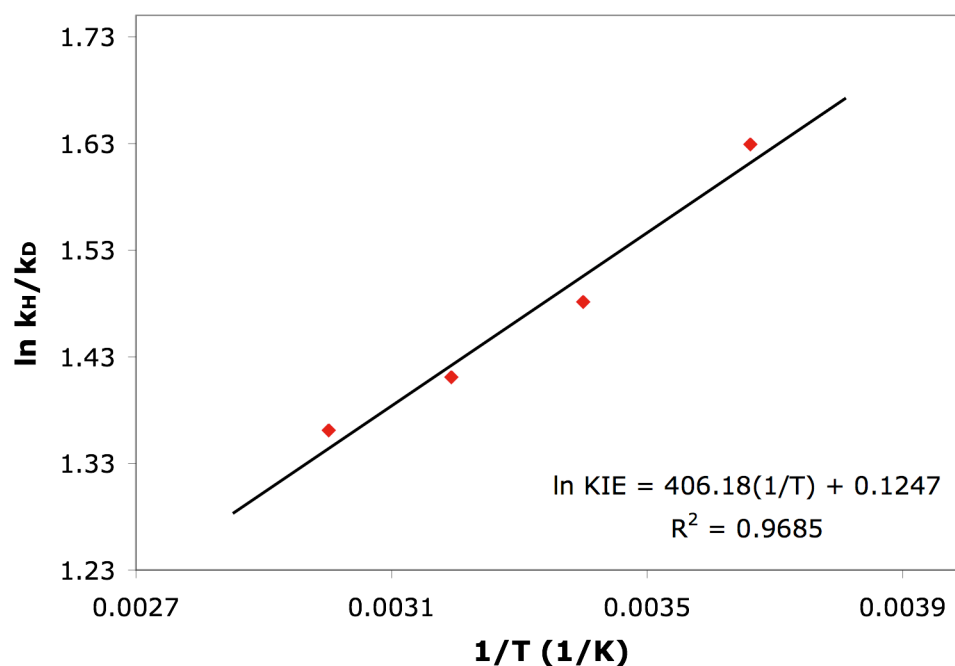
systems that have been shown to have significant proton tunneling.¹⁴ A recent DFT study also suggests that proton tunneling might play a major role in the reductive elimination of methane from $(\text{PPh}_3)_2\text{Pt}^{\text{II}}(\text{CH}_3)(\text{H})$ even though the observed KIE is 3.3 at 248 K in toluene.¹⁵

Table 2. Temperature dependence of $k_{\text{H}}/k_{\text{D}}$ in the protonolysis of **4** by TFA (determined by the average of 3 runs at each temperature)

Temperature K	$k_{\text{H}}/k_{\text{D}}$
273	5.1 ± 0.5
294	4.4 ± 0.5
313	4.1 ± 0.5
333	3.9 ± 0.5

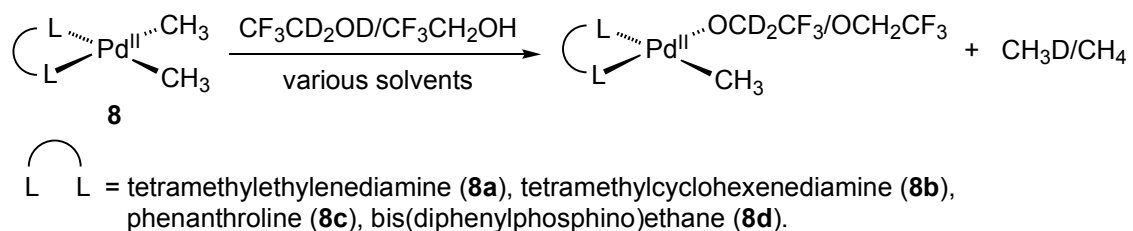
Calculated Parameters:
 $A_{\text{H}}/A_{\text{D}} = 1.1 \pm 0.1$
 $E_{\text{a}}^{\text{D}} - E_{\text{a}}^{\text{H}} = 0.8 \pm 0.1 \text{ kcal/mol}$

Figure 3. Plot of $\ln(k_{\text{H}}/k_{\text{D}})$ over $1/T$ for **4**



Abnormally large kinetic isotope effects and C–H bond activation. A number of general mechanisms for C–H activation by transition metal complexes have been identified, including (1) electrophilic activation, (2) oxidative addition, (3) σ -bond metathesis, (4) 1,2-addition to metal-ligand multiple bonds, (5) H-atom abstraction by metal-oxo complexes, and (6) metalloradical activation.^{1f} Abnormally large KIEs at room temperature or higher have been observed for C–H activations involving the latter four mechanisms.^{7a,16} Previous to our work, reactions involving electrophilic activation or oxidative addition as well as their corresponding microscopic reverse processes, protonolysis of a metal alkyl or reductive elimination, have been reported to exhibit only normal or inverse KIEs at similar temperatures.^{6,7} In addition to the discovery of abnormally large KIEs in the protonolysis of **1**, we recently observed KIEs greater than 20 in the protonolysis of several dimethylpalladium(II) complexes **8a–d** at room temperature (Scheme 5).¹⁷ The temperature dependence of $k_{\text{H}}/k_{\text{D}}$ for the protonolysis of **8d** was examined, and the corresponding Arrhenius parameters were also found to fall outside the semi-classical limits ($A_{\text{H}}/A_{\text{D}} = 0.34 \pm 0.06$ and $(E_{\text{a}}^{\text{D}} - E_{\text{a}}^{\text{H}}) = 2.4 \pm 0.1$ kcal/mol). A concerted mechanism was proposed for these systems.

Scheme 5



Aside from enzymatic C–H activations, few systematic studies of the temperature dependence of $k_{\text{H}}/k_{\text{D}}$ for C–H activation or the microscopic reverse have been carried out.¹⁸ Temperature-dependent KIEs typical of tunneling have been found for the intramolecular aromatic C–H activation of $\text{Cp}^* \text{ZrPh}_2$ via σ -bond metathesis¹⁹ as well as in a recent study on C–H activation by an oxoiron(IV) porphyrin radical cation.²⁰ KIEs have been measured for methane C–H activation by rhodium(II) porphyrin via the metalloradical mechanism at two different temperatures,^{16c} and parameters calculated from those data fall outside the semi-classical limits ($k_{\text{H}}/k_{\text{D}} = 8.2$ at 296 K and 5.1 at 353 K, $A_{\text{H}}/A_{\text{D}} = 0.43$, $E_{\text{a}}^{\text{D}} - E_{\text{a}}^{\text{H}} = 1.7$ kcal/mol). It has been proposed, based on analysis of equilibrium isotope effects (EIEs), that factors such as partition quotients and zero-point energy differences can account for the large KIEs observed in 1,2-addition of C–H bond across Ti–N multiple bonds,^{16a} so that tunneling does not necessarily need to be invoked; a similar argument was offered for the above-cited metalloradical C–H activation. In light of the temperature parameters, we would suggest that tunneling may be a more reasonable explanation for all of these large KIE values.

The temperature dependence of $k_{\text{H}}/k_{\text{D}}$ and mechanism. The temperature dependence of $k_{\text{H}}/k_{\text{D}}$ in the protonolysis of **1** and **4** suggests that a correlation exists between the mechanisms and the measured KIEs. In particular, the electronic nature of the ligand appears to have a large effect. A stepwise mechanism involving a Pt(IV)–*H* intermediate is favored in the presence of the electron rich tmeda ligand. Normal KIEs as well as Arrhenius parameters that fall within the semi-classical limits are observed for the protonolysis of **4**.²¹ On the other hand, the more electron deficient COD ligand disfavors the formation of a Pt(IV)–*H* intermediate. In this case, direct protonation at the M–C

bond occurs. Our work on methylplatinum(II) as well as methylpalladium(II) complexes suggest that the presence of large KIEs and Arrhenius parameters that fall outside semi-classical limits are indications that a concerted mechanism is operating.

Conclusions

In summary, we found that the electronic nature of the ligand can have a large effect on the temperature dependence of k_H/k_D in the protonolysis of methylplatinum(II) complexes. Protonolysis of $(\text{COD})\text{Pt}^{\text{II}}(\text{CH}_3)_2$ by TFA gave abnormally large KIEs at room temperature and higher as well as Arrhenius parameters that fall outside semi-classical limits. When the electron-deficient COD was replaced with the more electron-rich tmeda ligand, normal KIEs and classical Arrhenius parameters were observed. Based on our experimental results, we believe that the protonolysis of $(\text{COD})\text{Pt}^{\text{II}}(\text{CH}_3)_2$ proceeds by direct protonation at the M–C bond, while a stepwise oxidative addition/reductive elimination pathway occurs for the protonolysis of $(\text{tmeda})\text{Pt}^{\text{II}}(\text{CH}_3)\text{Cl}$. We further propose that the presence of abnormally large KIEs and Arrhenius parameters that fall outside semi-classical limits are indications that a concerted mechanism is operating. Further theoretical studies on the protonolysis of methylplatinum(II) complexes will be discussed in the following chapter.

Experimental

General methods. All air- and/or moisture-sensitive compounds were manipulated by using standard high-vacuum line, Schlenk, or cannula techniques, or in a glove box under a nitrogen atmosphere. $B(C_6F_5)_3$ was purchased from Aldrich and sublimed at 90 °C at full vacuum and stored in a P_2O_5 dessicator in the glove box. Trifluoroethanol- d_3 was purchased from Cambridge Isotope Laboratories and dried over 3-Å molecular sieves for at least 5 days, then vacuum distilled onto $B(C_6F_5)_3$, and shortly thereafter distilled into a Strauss flask and stored in the glove box. TFA- d_1 and DCE- d_4 were purchased from Cambridge Isotope Laboratories and stored under nitrogen in the glove box. TFA- d_0 was purchased from Sigma-Aldrich and stored in the glove box. CD_2Cl_2 was purchased from Cambridge Isotope Laboratories and dried over Na_2SO_4 right before use. $(COD)Pt^{II}(CH_3)_2$ **1** was purchased from Strem Chemicals and stored under nitrogen in the glove box. $(tmeda)Pt^{II}(CH_3)Cl$ **4** was prepared according to literature procedures. All NMR tubes were dried overnight in a 180 °C oven. Protonolysis studies were performed in a screw cap NMR tube with a PTFE/silicone septum. The error introduced by residual protons from the glass surface of NMR tubes was found to be negligible by 1H NMR spectroscopy with internal standard (within 1H NMR error). All NMR spectra were recorded at room temperature on a Varian Mercury 300 spectrometer.

Protonolysis of 1. Stock solutions of 10:1 TFA- d_1 /TFA- d_0 and **1** in DCE- d_4 were prepared in the glove box in glass vials with PTFE/silicone septa. The vials with the stock solutions were then placed in an ice or oil bath with three screw-cap NMR tubes sealed

with PTFE/silicone septa at a constant temperature (273 K, 294 K, 313 K, 333 K, 353 K). After the solutions were given a few minutes to equilibrate, the TFA- d_1 /TFA- d_0 mixture (0.2 mL) and **1**/DCE- d_4 solution (0.7 mL) were slowly transferred into the NMR tubes by syringes. After quickly shaking the tubes outside the bath to homogenize the mixtures, the NMR tubes were inserted back into the bath. The solutions were kept in the bath for 10 minutes before they were taken out for NMR analysis. The average CH₃D/CH₄ ratios of three runs at each temperature were used. An analogous procedure was used for the protonolysis of **1** in CD₂Cl₂ at room temperature. Protonolysis of **1** in TFE- d_3 was accomplished by weighing **1** and B(C₆F₅)₃ (2 equivalents) into a J-Young NMR tube and then adding TFE- d_3 .

Protonolysis of 4. A procedure analogous to **1** was used for the protonolysis of **4**. A 2:1 TFA- d_1 /TFA- d_0 mixture was used as the acid source. Data were acquired at 4 different temperatures (273 K, 294 K, 313 K, 333 K). The average CH₃D/CH₄ ratios of three runs at each temperature were used.

References

- (1) (a) Crabtree, R. H. *Chem. Rev.* **1995**, *95*, 987–1007. (b) Arndtsen, B. A.; Bergman, R. G.; Mobley, T. A.; Peterson, T. H. *Acc. Chem. Res.* **1995**, *28*, 154–162. (c) Stahl, S. S.; Labinger, J. A.; Bercaw, J. E. *Angew. Chem. Int. Ed.* **1998**, *37*, 2180–2192. (d) Sen, A. *Acc. Chem. Res.* **1998**, *31*, 550–557. (e) Jia, C.; Kitamura, T.; Fujiwara, Y. *Acc. Chem. Res.* **2001**, *34*, 633–639. (f) Labinger, J. A.; Bercaw, J. E. *Nature* **2002**, *417*, 507–514. (g) Jones, W. D. *Acc. Chem. Res.* **2003**, *36*, 140–146. (h) Lersch, M.; Tilset, M. *Chem. Rev.* **2005**, *105*, 2471–2526. (i) Vedernikov, A. N. *Curr. Org. Chem.* **2007**, *11*, 1401–1416. (j) Bergman, R. G. *Nature* **2007**, *446*, 391–391.
- (2) (a) Goldshlegger, N. F.; Tyabin, M. B.; Shilov, A. E.; Shteinman, A. A. *Zh. Fiz. Khim.* **1969**, *43*, 2174–2175. (b) Goldshlegger, N. F.; Eskova, V. V.; Shilov, A. E.; Shteinman, A. A. *Zh. Fiz. Khim.* **1972**, *46*, 1353–1354. (c) Shilov, A. E.; Shul'pin, G. B. *Chem. Rev.* **1997**, *97*, 2879–2932.
- (3) (a) Labinger, J. A.; Herring, A. M.; Bercaw, J. E. *J. Am. Chem. Soc.* **1990**, *112*, 5628–5629. (b) Siegbahn, P. E. M.; Crabtree, R. H. *J. Am. Chem. Soc.* **1996**, *118*, 4442–4450. (c) Wick, D. D.; Goldberg, K. I. *J. Am. Chem. Soc.* **1997**, *119*, 10235–10236. (d) Periana, R. A.; Taube, D. J.; Gamble, S.; Taube, H.; Satoh, T.; Fujii, H. *Science*, **1998**, *280*, 560–564. (e) Heiberg, H.; Johansson, L.; Gropen, O.; Ryan, O. B.; Swang, O.; Tilset, M. *J. Am. Chem. Soc.* **2000**, *122*, 10831–10845. (f) Johansson, L.; Tilset, M.; Labinger, J. A.; Bercaw, J. E. *J. Am. Chem. Soc.* **2000**, *122*, 10846–10855. (g) Lin, J.; Shen, C.; Garcia-Zayas, E. A.; Sen, A. *J. Am. Chem. Soc.* **2001**, *123*, 1000–1001. (h) Zhong, H. A.; Labinger, J. A.; Bercaw, J. E. *J. Am. Chem. Soc.*

- 2002**, *124*, 1378–1399. (i) Jensen, M. P.; Wick, D. D.; Reinartz, S.; White, P. S.; Templeton, J. L.; Goldberg, K. I. *J. Am. Chem. Soc.* **2003**, *125*, 8614–8624. (j) Heyduk, A. F.; Driver, T. G.; Labinger, J. A.; Bercaw, J. E. *J. Am. Chem. Soc.* **2004**, *126*, 15034–15035. (k) Owen, J. S.; Labinger, J. A.; Bercaw, J. E. *J. Am. Chem. Soc.* **2006**, *128*, 2005–2016. (l) Khaskin, E.; Zavalij, P. Y.; Vedernikov, A. N. *J. Am. Chem. Soc.* **2006**, *128*, 13054–13055. (m) Chen, G. S.; Labinger, J. A.; Bercaw, J. E. *Proc. Natl. Acad. Sci. U.S.A.* **2007**, *104*, 6915–6920. (n) West, N. M.; White, P. S.; Templeton, J. L. *J. Am. Chem. Soc.* **2007**, *129*, 12372–12373.
- (4) (a) Luinstra, G. A.; Labinger, J. A.; Bercaw, J. E. *J. Am. Chem. Soc.* **1993**, *115*, 3004–3005. (b) Labinger, J. A.; Herring, A. M.; Lyon, D. K.; Luinstra, G. A.; Bercaw, J. E.; Horvath, I. T.; Eller, K. *Organometallics* **1993**, *12*, 895–905. (c) Luinstra, G. A.; Wang, L.; Stahl, S. S.; Labinger, J. A.; Bercaw, J. E. *Organometallics* **1994**, *13*, 755–756. (d) Hutson, A. C.; Lin, M.; Basicckes, N.; Sen, A. *J. Organomet. Chem.* **1995**, *504*, 69–74.
- (5) (a) Hill, G. S.; Rendina, L. M.; Puddephatt, R. J. *Organometallics* **1995**, *14*, 4966–4968. (b) Stahl, S. S.; Labinger, J. A.; Bercaw, J. E. *J. Am. Chem. Soc.* **1995**, *117*, 9371–9372. (c) Romeo, R.; Plutino, M. R.; Elding, L. I. *Inorg. Chem.* **1997**, *36*, 5909–5916. (d) Wik, B. J.; Lersch, M.; Tilset, M. *J. Am. Chem. Soc.* **2002**, *124*, 12116–12117. (e) Wik, B. J.; Ivanovic-Burmazovic, I.; Tilset, M.; Eldik, R. V. *Inorg. Chem.* **2006**, *45*, 3613–3621. (f) Parmene, J.; Ivanovic-Burmazovic, I.; Tilset, M.; Eldik, R. V. *Inorg. Chem.* **2009**, *48*, 9092–9103.
- (6) (a) Stahl, S. S.; Labinger, J. A.; Bercaw, J. E. *J. Am. Chem. Soc.* **1996**, *118*, 5961–5976. (b) Romeo, R.; D'Amico, G. *Organometallics* **2006**, *25*, 3435–3446.

- (7) (a) Ryabov, A. D. *Chem. Rev.* **1990**, *90*, 403–424. (b) Jones, W. D. *Acc. Chem. Res.* **2003**, *36*, 140–146, and references therein.
- (8) KIEs greater than 10 are reported for the protonolysis of (dfepe)Pt(CH₃)₂ at low temperatures, although the tunneling effect was not characterized: Bennett, B. L.; Hoerter, J. M.; Houlis, J. F.; Roddick, D. M. *Organometallics* **2000**, *19*, 615–621.
- (9) (a) Bell, R. P. *Chem. Soc. Rev.* **1974**, *4*, 513–544. (b) Bell, R. P. *The Proton in Chemistry*; Cornell University Press: Ithaca, New York, **1973**. (c) Bell, R. P. *The Tunnel Effect in Chemistry*; Chapman and Hall: London, **1980**.
- (10) Caldin, E. F. *Chem. Rev.* **1969**, *69*, 135–156.
- (11) (a) Moore, W. J. *Physical Chemistry*; Prentice-Hall Inc., New Jersey, 3rd Ed., **1962**. (b) Melander, L.; Saunders, W. H. *Reaction Rates of Isotopic Molecules*; Krieger: Malabar, Florida, **1987**.
- (12) (a) Kwart, H. *Acc. Chem. Res.* **1982**, *15*, 401–408. (b) Limbach, H.; Lopez, J. M.; Kohen, A. *Phil. Trans. R. Soc. B* **2006**, *361*, 1399–1415.
- (13) Schneider, M. E.; Stern, M. J. *J. Am. Chem. Soc.* **1972**, *95*, 1517–1522.
- (14) Klinman, J. P.; Sharma, S. C. *J. Am. Chem. Soc.* **2008**, *130*, 17632–17633.
- (15) Datta, A.; Hrovat, D. A.; Borden, W. T. *J. Am. Chem. Soc.* **2008**, *130*, 2726–2727.
- (16) (a) Slaughter, L. M.; Wolczanski, P. T.; Klinckman, T. R.; Cundari, T. R. *J. Am. Chem. Soc.* **2000**, *122*, 7953–7975. (b) Yoshizawa, K. *Coord. Chem. Rev.* **2002**, *226*, 251–259, and references therein. (c) Cui, W.; Wayland, B. B. *J. Am. Chem. Soc.* **2004**, *126*, 8266–8274.
- (17) Bercaw, J. E.; Chen, G. S.; Labinger, J. A.; Lin, B. L. *J. Am. Chem. Soc.* **2008**, *130*, 17654–17655.

- (18) Kohen, A. in *Hydrogen-Transfer Reactions*, Hynes, J. T.; Klinman, J. P.; Limbach, H. H.; Schowen, R. L., Eds.; Wiley-VCH: Weinheim, Germany, **2007**; Vol. 4, pp. 1311–1340.
- (19) Schock, L. E.; Brock, C. P.; Marks, T. J. *Organometallics* **1987**, *6*, 232–241.
- (20) Pan, Z.; Horner, J. H.; Newcomb, M. *J. Am. Chem. Soc.* **2008**, *130*, 7776–7777.
- (21) Our results suggest that the correlation between the observation of inverse KIEs and a stepwise mechanism may be limited to phosphine-ligated systems.

Chapter 4

Computational Studies on the Protonolysis of Platinum(II) Methyl Complexes

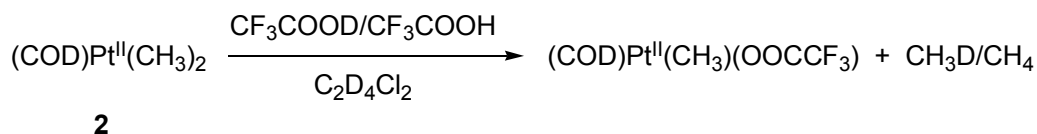
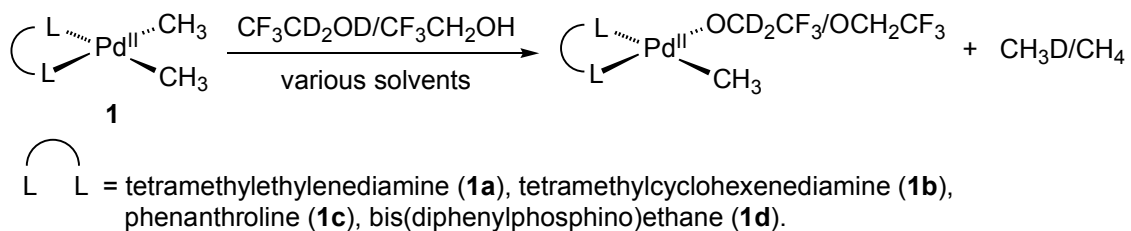
Abstract

The protonolysis of $(\text{tmeda})\text{Pt}^{\text{II}}(\text{CH}_3)\text{Cl}$ and $(\text{COD})\text{Pt}^{\text{II}}(\text{CH}_3)_2$ by trifluoroacetic acid were studied using density functional theory (TFA). Protonolysis of $(\text{tmeda})\text{Pt}^{\text{II}}(\text{CH}_3)\text{Cl}$ was found to occur through a stepwise mechanism, while a concerted pathway was found to be favored for $(\text{COD})\text{Pt}^{\text{II}}(\text{CH}_3)_2$. While computation was able to reproduce the KIEs for the protonolysis of $(\text{tmeda})\text{Pt}^{\text{II}}(\text{CH}_3)\text{Cl}$ by TFA, calculated KIEs (without tunneling corrections) for the protonolysis of $(\text{COD})\text{Pt}^{\text{II}}(\text{CH}_3)_2$ by TFA were much smaller than those observed experimentally, suggesting that tunneling is most likely the reason behind the abnormally large KIEs observed experimentally.

Introduction

Recently, we discovered the presence of abnormally large KIEs (greater than 10 at 298 K) in the protonolysis of several dimethylpalladium(II) complexes **1a–d** and (COD)Pt^{II}(CH₃)₂ **2** (COD = 1,5-cyclooctadiene) (Scheme 1).¹ The magnitude and temperature dependence of the KIEs suggest that proton tunneling is involved in the protonolysis. The existence of these systems with KIEs outside the range of conventionally observed values has motivated us to further investigate the relationship between observed KIEs and the mechanisms involved.

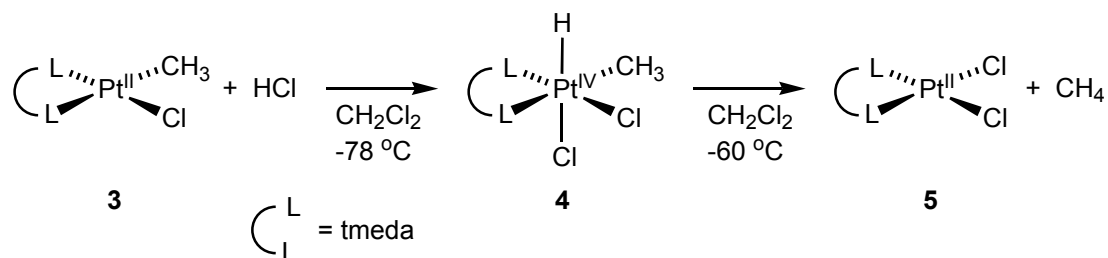
Scheme 1



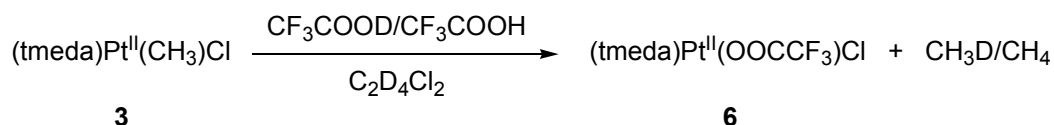
While the possibility of the oxidative addition route cannot be firmly excluded for **1a–d** and **2**, we believe that they proceed by direct protonation at the M–C bond and that there is a connection between that mechanism and the observed abnormally large KIEs. We favor the concerted mechanism for a number of reasons: Pd(IV)–H intermediates are not easily accessible; the electron-deficient COD ligand will disfavor formation of

Pt(IV)–H; no Pt(IV)–H is observed by ^1H NMR in the protonolysis of **2** at -80 °C in CD_2Cl_2 ; no scrambling of H/D between methyl/methane positions is observed in any of these systems.

Scheme 2



Scheme 3



The results of the protonolysis of **1a–d** and **2** prompted us to study a different system in which the presence of an oxidative addition/reductive elimination mechanism has been supported by the observation of Pt(IV)–H. Towards that regard, we studied the protonolysis of $(\text{tmeda})\text{Pt}^{\text{II}}(\text{CH}_3)\text{Cl}$ **3** ($\text{tmeda} = \text{N,N,N}',\text{N}'\text{-tetramethyl-ethylenediamine}$).² Previous work has shown that addition of excess HCl (dissolved in diethyl ether) at -78 °C to a methylene chloride solution of **3** leads to oxidative addition of HCl to generate $(\text{tmeda})\text{Pt}^{\text{IV}}(\text{CH}_3)(\text{H})\text{Cl}_2$ **4**. Upon warming to -60 °C, the reductive elimination of methane is observed along with formation of $(\text{tmeda})\text{Pt}^{\text{II}}\text{Cl}_2$ **5** (Scheme 2). We studied the protonolysis of **3** by trifluoroacetic acid to give $(\text{tmeda})\text{Pt}^{\text{II}}(\text{OOCF}_3)\text{Cl}$ **6** (Scheme 3). Unlike **1a–d** and **2**, normal KIEs and classical Arrhenius parameters were obtained. We

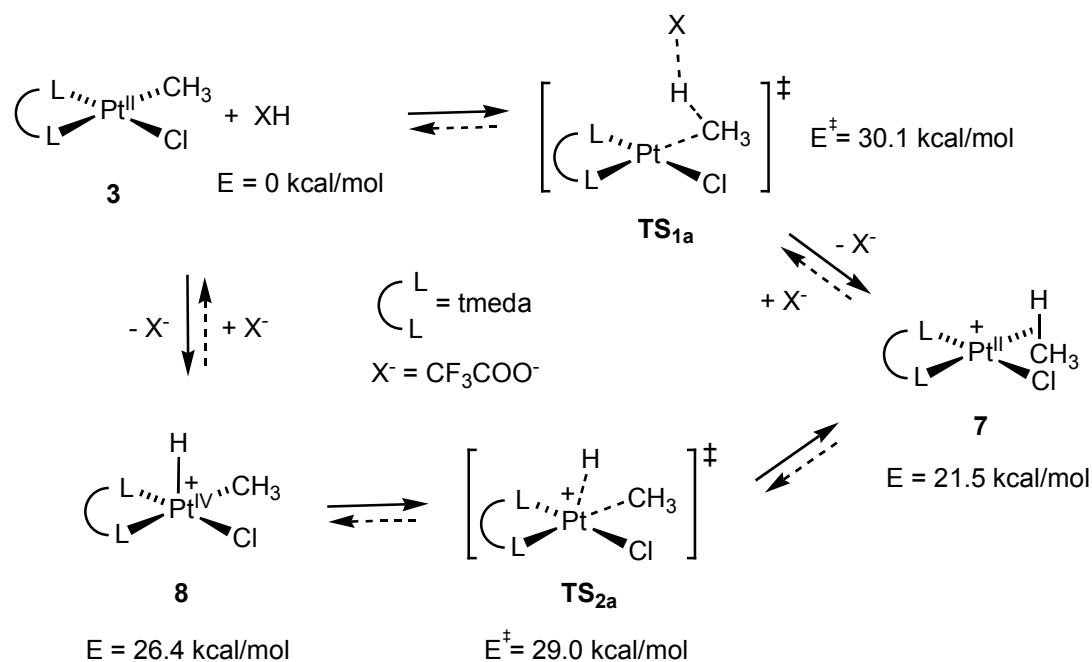
believe that the protonolysis of **3** proceeds through a stepwise oxidative addition/reductive elimination mechanism.

In the previous chapter, we suggested that the electronic nature of the ligand can have a large effect on the preferred mechanism for protonolysis. We also proposed that the presence of abnormally large KIEs and Arrhenius parameters that fall outside semi-classical limits are indications that a concerted mechanism is operating. In order to further support our proposals, we studied the protonolysis of **2** and **3** using density functional theory (DFT). Our results are described in the following sections.

Results and Discussion

Protonolysis of (tmeda)Pt^{II}(CH₃)Cl by trifluoroacetic acid-*d*₀ in 1,2-dichloroethane (Computational Results). Density functional theory (DFT) was used to examine the mechanism of the protonolysis of **3** by trifluoroacetic acid (TFA). A transition state, **TS_{1a}**, was located prior to the formation of the Pt(II)-methane σ adduct **7** for the concerted pathway. As expected, no intermediate could be located from **3** to **7**. The activation barrier for this pathway was calculated to be 30.1 kcal/mol (Scheme 4).

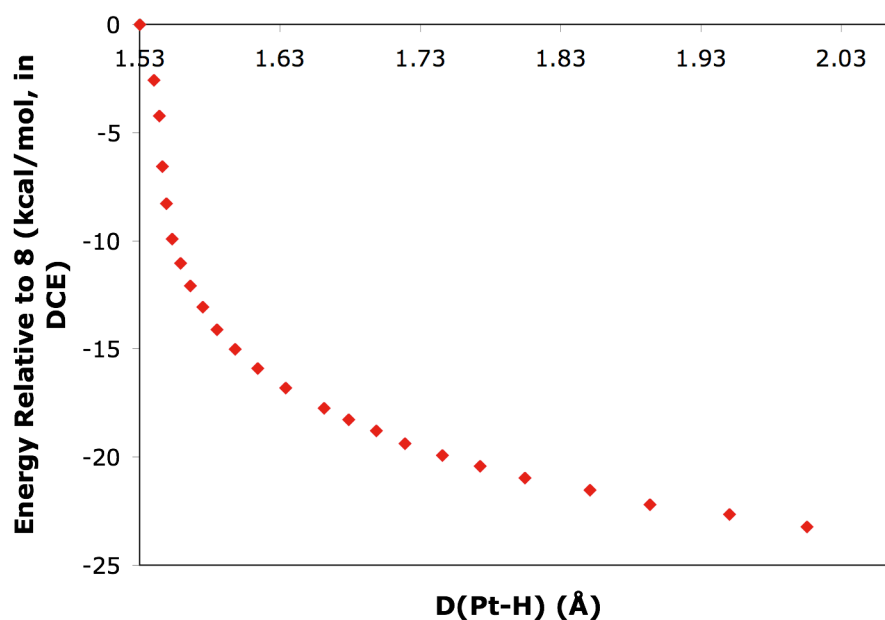
Scheme 4



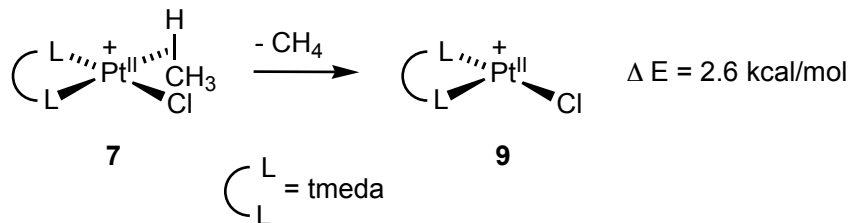
In contrast, a Pt(IV)-H intermediate **8** was found for the stepwise pathway.³ A transition state, **TS_{2a}**, was located for the reductive elimination from **8** to **7**. However, no transition state could be located for the proton transfer reaction from TFA to **3** to form **8**.

A potential energy surface scan for the reverse process shows that the energy (in 1,2-dichloroethane) decreases monotonically as the platinum hydrogen distance increases (Figure 1). No maximum can be found along the potential surface; it appears that the activation barrier from **3** to **8** is approximately equal to the corresponding reaction energy. This result suggests that reductive elimination is the rate-determining step for the stepwise pathway. As a consequence, the activation energy of the stepwise pathway was calculated to be 29.0 kcal/mol, which is slightly lower than the concerted pathway. (It should be emphasized that DFT is generally more reliable at predicting qualitative trends rather than quantitative values, especially for activation barriers).

Figure 1. Potential energy surface scan for the deprotonation of **8** by CF_3COO^- to give **3**



Scheme 5



The dissociation of methane from **7** can occur either through a dissociative or associative pathway. Although no transition state could be located for either mechanism, the activation barrier for dissociation should not be greater than the barrier of the dissociative pathway, which is assumed to be approximately equal to the energy of methane dissociation from **7** to form **9**. According to computational results, the dissociation of methane is a slightly uphill process; thus a comparably small activation barrier is expected for the dissociative pathway (Scheme 5). Therefore, computation predicts reductive elimination from **8** as the rate-determining step for the overall reaction. Furthermore, our computational results indicate that the reverse process, the stepwise proton loss from **7** to regenerate **3**, is much slower than loss of methane, which is consistent with the absence of deuterated methane isotopologues other than CH₃D in the protonolysis experiments reported earlier.

Our experimental (Chapter 3) and computational results both support the stepwise pathway in the protonolysis of **3** by TFA in DCE. The small difference between the activation barriers of the two pathways (1.1 kcal/mol) seems to suggest that the slightly disfavored concerted mechanism can compete with the preferred stepwise mechanism. The observation of normal KIEs for **3** is consistent with our earlier proposal that there

might be a connection between the concerted mechanism and the presence of abnormally large KIEs.

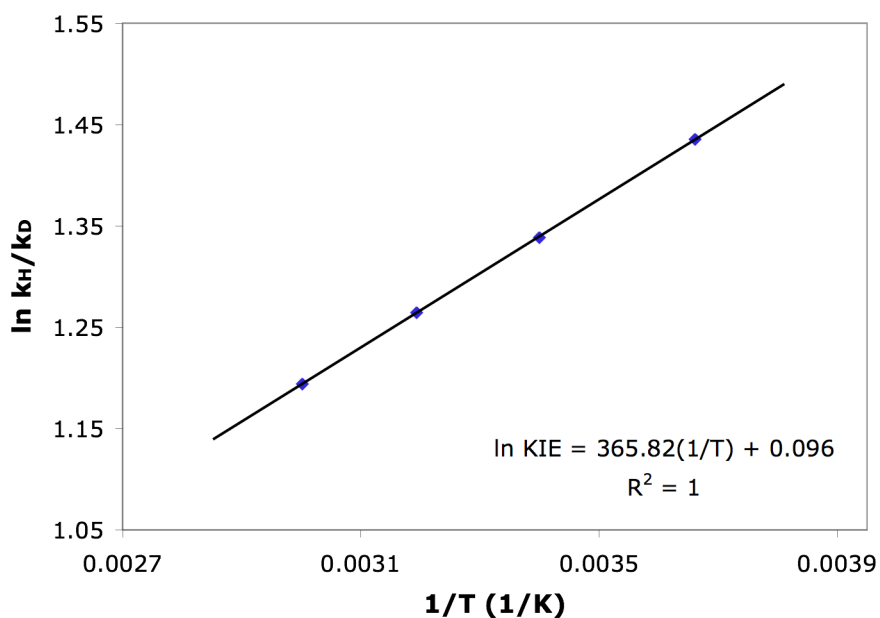
Calculated KIEs for the protonolysis of (tmeda)Pt^{II}(CH₃)Cl by trifluoroacetic acid in DCE. Through vibrational frequency analysis of the optimized complexes, we calculated KIEs for the protonolysis of **3** by TFA at various temperatures without tunneling corrections (Table 1). The calculated KIEs match closely the values obtained by experiments (For comparison see Chapter 3, Table 2). A plot of the calculated $\ln(k_H/k_D)$ over $1/T$ shows that the experimentally obtained Arrhenius parameters can be accurately reproduced (Figure 2), suggesting that proton tunneling does not play an important role in the protonolysis of **3** (For comparison see Chapter 3, Figure 3). The agreement between experiment and computation also indicates that current computational methodologies can be reliably used to predict qualitative trends for the systems in question.

Table 1. Calculated KIEs (without tunneling corrections) for the protonolysis of **3** by TFA at various temperatures

Temperature K	k_H/k_D
273	4.2
294	3.8
313	3.5
333	3.3

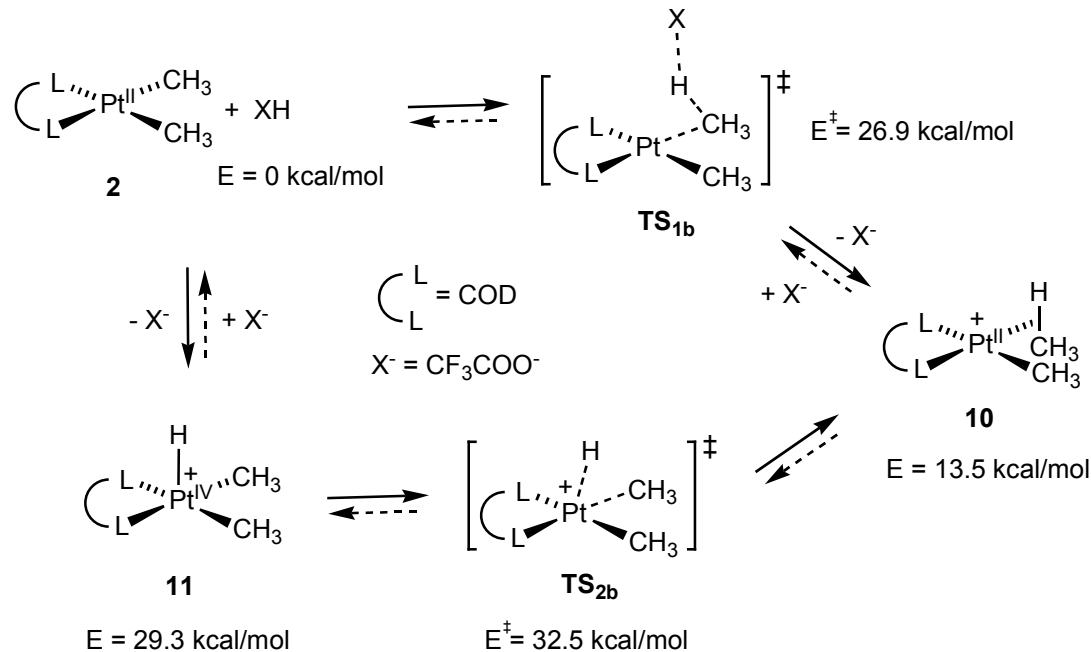
Calculated Parameters:
 $A_H/A_D = 1.1$
 $E_a^D - E_a^H = 0.7$ kcal/mol

Figure 2. Plot of calculated $\ln(k_H/k_D)$ over $1/T$ (without tunneling corrections) for **3**



Protonolysis of (COD)Pt^{II}(CH₃)₂ by trifluoroacetic acid-*d*₀ in DCE (Computation Results). DFT was also used to examine the mechanism of the protonolysis of **2** by TFA. Similar to the protonolysis of **3**, no intermediate could be located from **2** to the Pt(II)-methane σ adduct **10** for the concerted pathway, while a Pt(IV)-*H* intermediate **11** was found for the stepwise mechanism (Scheme 6).

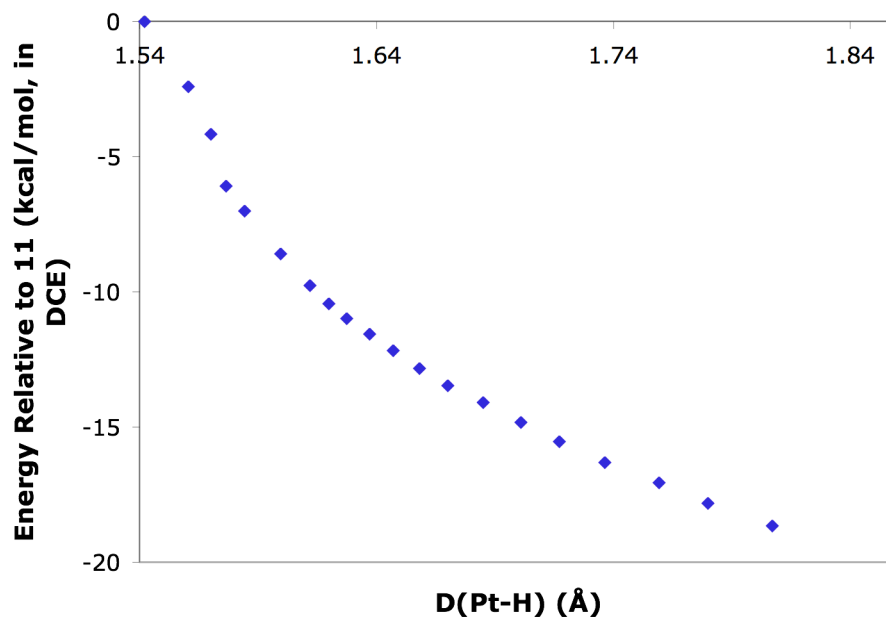
Scheme 6



The activation energy for the concerted pathway (TS_{1b}) of **2** was calculated to be 26.9 kcal/mol, ~ 3 kcal/mol lower than the activation energy for the concerted pathway corresponding to **3** (TS_{1a}) (30.1 kcal/mol). Similar to the protonolysis of **3**, a transition state, TS_{2b} , was located for reductive elimination. Once again, no transition state could be located for the reaction of TFA with **2** to give **11**. A potential energy surface scan for the reverse process, deprotonation of **11** by TFA to form **2**, shows that the energy decreases monotonically as the platinum hydrogen distance increases, similar to the deprotonation of **8** by TFA to form **3** (Figure 3). Assuming that the activation barrier for the formation of **11** is approximately equal to its reaction energy, reductive elimination from **11** to form **10** is the rate-determining step for the concerted mechanism. Interestingly, the activation energy for the stepwise mechanism in the protonolysis of **2** (32.5 kcal/mol) is about ~ 3 kcal/mol higher than the activation energy for the stepwise mechanism corresponding to

3 (29.0 kcal/mol). So by changing the ligand from tmeda to COD, the activation barrier for the concerted pathway is lowered in energy, while the barrier for the stepwise pathway increases.

Figure 3. Potential energy surface scan for the deprotonation of **11** by CF_3COO^- to give **2**



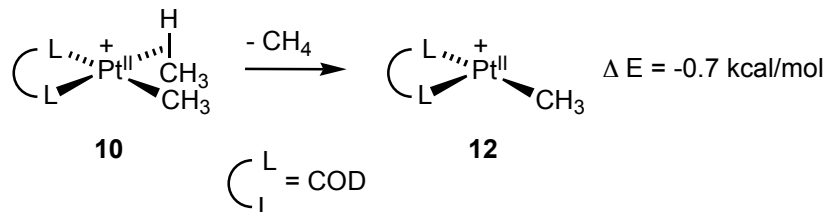
For the protonolysis of **2**, the barrier for the concerted pathway is calculated to be 5.6 kcal/mol lower than the stepwise pathway, opposite of the computational results obtained for **3** (concerted pathway is slightly higher in energy than the stepwise pathway). As proposed earlier, the stepwise mechanism is disfavored by the presence of the electron-deficient COD ligand because formal oxidation of the platinum center is involved. Accordingly, a lower activation barrier was calculated for **3** compared to **2** for the same pathway because tmeda is much more electron donating than COD. As a result,

the formation of the Pt(IV)-*H* intermediate from **3** (26.4 kcal/mol) is energetically disfavored by ~ 3 kcal/mol more than that corresponding to **2** (29.3 kcal/mol).

In contrast, the presence of the electron-deficient COD ligand appears to favor the concerted pathway. A comparison of the two different pathways shows that, in the transition state, the distance between the platinum center and the transferred proton is longer for the concerted pathway compared to the stepwise pathway for both **2** and **3** (Pt-H distance in **TS_{1b}** is ~ 0.56 Å longer than the Pt-H distance in **TS_{2b}**; Pt-H distance in **TS_{1a}** is ~ 0.22 Å longer than the Pt-H distance in **TS_{2a}**). These results suggest that the formal oxidation state of the platinum center probably does not play an important role in the concerted mechanism; changes of electron density at platinum from ligand variations will not have a large effect on the activation barrier. The stronger trans influence of COD compared to tmeda might be an important factor leading to a lower activation barrier for the concerted pathway. Our computation shows that the Pt^{II}-CH₃ bond length of **2** is ~ 0.03 Å longer than **3**. As a result, the Pt^{II}-CH₃ bond of **2** is more polarized, making it easier to accept a proton to the anionic methyl ligand compared to **3**.

The dissociation of methane from **10** to form **12** is roughly a thermoneutral process (Scheme 7); thus a small activation barrier is expected, as in the case of **7** going to **9** in the protonolysis of **3**. Therefore, computation predicts the protonation of the Pt^{II}-C bond as the rate determining step for the protonolysis of **2** by TFA. This result is consistent with experiment: CH₃D was the only deuterated methane isotopologue observed, and no deuterium incorporation into the resultant Pt^{II}-CH₃ of the product was detected.

Scheme 7



Calculated KIEs for the Protonolysis of (COD)Pt^{II}(CH₃)₂ by Trifluoroacetic Acid in DCE. As shown in Table 2, the calculated KIEs for the protonolysis of **2** are much smaller than the experimental KIEs at low temperatures (See Chapter 3, Table 1). As the temperature increases, the hydrogen tunneling contribution to the KIE is expected to decrease; thus the calculated and experimental KIEs gradually approach each other. A plot of the calculated $\ln(k_{\text{H}}/k_{\text{D}})$ over $1/T$ affords Arrhenius parameters within the theoretical semi-classical limits (Figure 4). Based on these calculations, it appears that hydrogen tunneling is most likely the reason behind the abnormally large experimental KIEs as well as their temperature-dependence behavior for the protonolysis of **2**.

Table 2. Calculated KIEs (without tunneling corrections) for the protonolysis of **2** by TFA at various temperatures

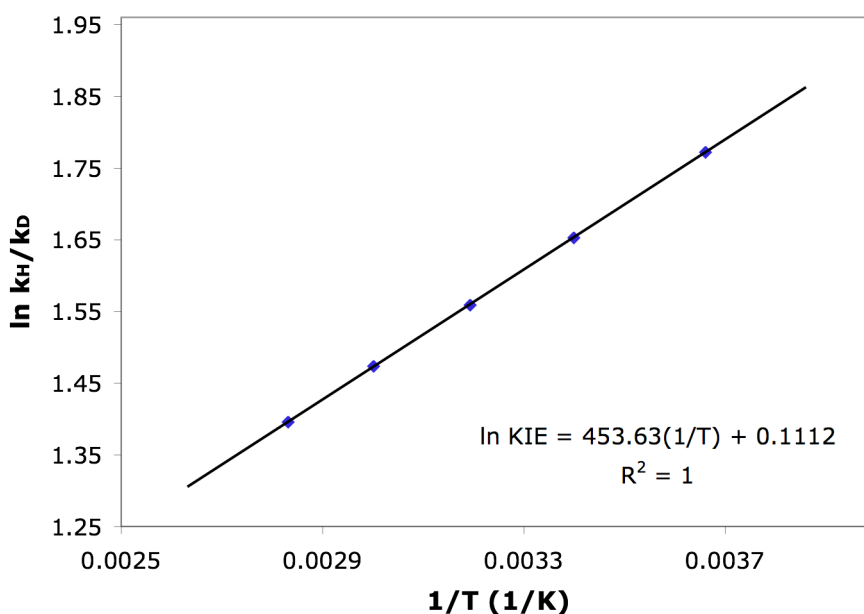
Temperature K	k_H/k_D
273	5.9
294	5.2
313	4.8
333	4.4
353	4.0

Calculated Parameters:

$$A_H/A_D = 1.1$$

$$E_a^D - E_a^H = 0.9 \text{ kcal/mol}$$

Figure 4. Plot of calculated $\ln(k_H/k_D)$ over $1/T$ (without tunneling corrections) for **2**



The microscopic reverse C–H bond activation process. Our computational results indicate that the activation barrier for the protonolysis of **3** (29.0 kcal/mol) is

greater than the barrier for the protonolysis of **2** (26.9 kcal/mol). For the same two systems, the opposite trend is observed for the microscopic reverse C-H bond activation process from the σ adducts (**7**, 7.5 kcal/mol; **10**, 13.4 kcal/mol). These results suggest that in these two cases, the system that undergoes slower protonolysis has a faster C-H bond cleavage step. However, the significant contribution of proton tunneling associated with **2** will lower the energy required in the C-H bond breaking process. How much this tunneling effect will have on the rate of C-H activation will require further investigation.

Conclusions

In summary, our computational studies have shown that protonolysis of methylplatinum(II) complexes can occur through either a concerted or stepwise pathway and can be highly ligand dependent. The two ligands (tmeda and COD) investigated have opposite effects on the barriers of the two pathways. Our work suggests that an electron-rich ligand (tmeda) will favor the stepwise mechanism, while an electron-deficient ligand (COD) with stronger trans influence will favor the concerted mechanism. While computation was able to reproduce the KIEs for the protonolysis of (tmeda)Pt^{II}(CH₃)Cl by TFA, calculated KIEs (without tunneling corrections) for the protonolysis of (COD)Pt^{II}(CH₃)₂ by TFA were much smaller than those observed experimentally, suggesting that tunneling is most likely the reason behind the abnormally large KIEs observed experimentally. Our computational studies are consistent with all previous experimental results and further support our proposal that abnormally large KIEs and Arrhenius parameters that fall outside semi-classical limits are indications that a concerted mechanism is operating.

Experimental

Computational Methods. All computations were performed using the Gaussian03 software package unless otherwise stated.⁴ All species were treated as singlets. Geometries were optimized by density functional theory method (BP86) with a hybrid basis set (Pd and Pt: LANL2TZ(*f*),^{5,6} consisting of Wadt and Hay relativistic effective core potentials (RECPs),^{5a} valence triple- ζ contraction functions, and an *f*-orbital polarization function; all other elements: 6-31+G(*d*), an all-electron basis set developed by Pople et al.⁷). A harmonic oscillator model was used for vibration frequency analysis of the optimized structures. All frequencies of the minima are positive, while transition states have one and only one negative frequency. The vibration mode of the negative frequency in the transition state was confirmed to be the one that corresponds to the reaction coordinate.

Gas phase enthalpies (with PV term) and entropies (pressure = 1 atm, 298.15 K) of all species were obtained via frequency calculations with appropriate isotopic contents at various temperatures. No scaling factor was used for the calculated frequencies. An implicit solvation model, the CPCM polarizable continuum model, was then employed for the calculation of solvation energies. The sum of the gas phase enthalpies and the solvation energies was used directly as the enthalpies in DCE. For reactions wherein different numbers of reactants and transition states are involved (the difference designated as n), an nPV error is introduced due to the absence of PV term in the liquid state, which underestimates the activation barrier of a biomolecular reaction by an ~ 0.6 kcal/mol error at room temperature. Such a small error is generally ignored in the

literature and is not essential as far as comparisons between reaction pathways with the same n are concerned. Finally, the gas phase entropies were converted to corresponding entropies (1 M in DCE) according to Wertz's method.⁸

Geometries for the potential energy surface scan were optimized by density function theory B3LYP method as implemented in the Jaguar 6.5 program package.⁹ The Pt hydride distance was fixed at a certain value, while all other structural parameters were fully optimized during the optimization of each point of the potential energy surface. The Pt was treated by LACVP**, a basis set consisting of the Wadt and Hay relativistic effective core potentials (RECPs) and valence double- ζ contraction functions. A modified variant of Pople's all-electron basis set, 6-31G**, where the six d functions have been reduced to five, was used for all other elements. Single point energy and CPCM solvation energy (in dichloroethane) calculations were then performed for the optimized geometries by the Gaussian03 software package using the BP86 method and the same hybrid basis described earlier. Electronic energies plus the corresponding solvation energies were used to calculate the energies of each point of the potential energy surface.

References

- (1) Bercaw, J. E.; Chen, G. S.; Labinger, J. A.; Lin, B. L. *J. Am. Chem. Soc.* **2008**, *130*, 17654–17655.
- (2) Stahl, S. S.; Labinger, J. A.; Bercaw, J. E. *J. Am. Chem. Soc.* **1996**, *118*, 5961–5976.
- (3) The reaction for the formation of the Pt(IV)–*H* intermediate is calculated to be uphill. However, such an intermediate can be observed experimentally, suggesting that it should be more energetically favorable than the starting material. This discrepancy can be attributed to the absence of strongly coordinating Cl⁻ in the computational system as compared to the experimental system.
- (4) Gaussian03, Revision D.01, Frisch, M. J.; Trucks, G. W.; Schlegel, H. B.; Scuseria, G. E.; Robb, M. A.; Cheeseman, J. R.; Montgomery, J. A.; Vreven, T.; Kudin, K. N.; Burant, J. C.; Millam, J. M.; Iyengar, S. S.; Tomasi, J.; Barone, V.; Mennucci, B.; Cossi, M.; Scalmani, G.; Rega, N.; Petersson, G. A.; Nakatsuji, H.; Hada, M.; Ehara, M.; Toyota, K.; Fukuda, R.; Hasegawa, J.; Ishida, M.; Nakajima, T.; Honda, Y.; Kitao, O.; Nakai, H.; Klene, M.; Li, X.; Knox, J. E.; Hratchian, H. P.; Cross, J. B.; Bakken, V.; Adamo, C.; Jaramillo, J.; Gomperts, R.; Stratmann, R. E.; Yazyev, O.; Austin, A. J.; Cammi, R.; Pomelli, C.; Ochterski, J. W.; Ayala, P. Y.; Morokuma, K.; Voth, G. A.; Salvador, P.; Dannenberg, J. J.; Zakrzewski, V. G.; Dapprich, S.; Daniels, A. D.; Strain, M. C.; Farkas, O.; Malick, D. K.; Rabuck, A. D.; Raghavachari, K.; Foresman, J. B.; Ortiz, J. V.; Cui, Q.; Baboul, A. G.; Clifford, S.; Cioslowski, J.; Stefanov, B. B.; Liu, G.; Liashenko, A.; Piskorz, P.; Komaromi, I.; Martin, R. L.; Fox, D. J.; Keith, T.; Al-Laham, M. A.; Peng, C. Y.; Nanayakkara,

- A.; Challacombe, M.; Gill, P. M. W.; Johnson, B.; Chen, W.; Wong, M. W.; Gonzalez, C.; Pople, J. A. Gaussian, Inc., Wallingford, CT, **2004**.
- (5) (a) Hay, P. J.; Wadt, W. R. *J. Chem. Phys.* **1985**, *82*, 299–310. (b) Ehlers, A.W.; Bohme, M.; Dapprich, S.; Gobbi, A.; Hollwarth, A.; Jonas, V.; Kohler, K. F.; Stegmann, R.; Veldkamp, A.; Frenking, G. *Chem. Phys. Lett.* **1993**, *208*, 111–114. (c) Roy, L.E.; Hay, P. J.; Martin, R. L. *J. Chem. Theory Comput.* **2008**, *4*, 1029–1031.
- (6) (a) Feller, D. *J. Comp. Chem.* **1996**, *17*, 1571–1586. (b) Schuchardt, K. L.; Didier, B. T.; Elsethagen, T.; Sun, L.; Gurumoorthi, V.; Chase, J.; Li, J.; Windus, T. L. *J. Chem. Inf. Model.* **2007**, *47*, 1045–1052.
- (7) (a) Hariharan, P. C.; Pople, J. A. *Chem. Phys. Lett.* **1972**, *16*, 217–219. (b) Franel, M. M.; Pietro, W. J.; Hehre, W. J.; Binkley, J. S.; Gordon, M. S.; DeFrees, D. J.; Pople, J. A. *J. Chem. Phys.* **1982**, *77*, 3654–3665.
- (8) Wertz, D. H. *J. Am. Chem. Soc.* **1980**, *102*, 5316–5322.
- (9) Jaguar, version 6.5, Schrodinger, LLC, New York, **2005**.

Chapter 5

Selective Oxidation of sp^3 C–H Bonds in Water Catalyzed by a Glycinate-Platinum(II) Complex

Abstract

In aqueous solution, $[\text{Pt}^{\text{II}}(\text{glycinato})\text{Cl}_2]^-$ catalyzes oxidation by $[\text{Pt}^{\text{IV}}\text{Cl}_6]^{2-}$ of the methyl group of *p*-toluenesulfonate to the corresponding alcohol and aldehyde, with no further oxidation to the carboxylic acid. Both rate and selectivity are improved in comparison to the original Shilov system that employs $[\text{Pt}^{\text{II}}\text{Cl}_n(\text{H}_2\text{O})_{4-n}]^{2-n}$ as the catalyst.

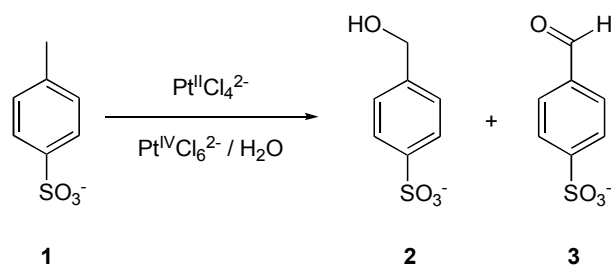
Introduction

The selective catalytic transformation of C–H bonds remains an important academic and practical challenge. Over the past several decades, a number of examples of C–H bond activation by transition metal complexes have appeared in the literature.¹ The Shilov system, an aqueous solution of $[\text{Pt}^{\text{II}}\text{Cl}_4]^{2-}$ and $[\text{Pt}^{\text{IV}}\text{Cl}_6]^{2-}$ salts that oxidizes alkanes to alcohols (and alkyl chlorides),² has attracted a great deal of attention since its original discovery.³ Despite several attractive features, the Shilov system is impractical because of low reaction rates, expensive oxidant, and catalyst instability. Overoxidation is an additional problem that lowers alcohol selectivities.^{4,5}

Analogous systems based on Pt^{II} , Pd^{II} , or Hg^{II} have been found to give better selectivities in strongly acidic solvents such as trifluoroacetic acid or fuming sulfuric acid, because the products are esters which tend to be considerably less subject to further oxidation than the corresponding alcohols.⁶ However, to date the added cost and complexity of converting such esters to desirable products have precluded any practical application of these reactions. Improving the performance of aqueous catalysts for direct conversion to alcohols would hence be desirable. While earlier efforts to modify the original Shilov system by the addition of ligands resulted in much lower (most often zero) yields of the desired products,^{5b,7} we report here that the anionic ligated platinum complex $\text{K}[\text{Pt}^{\text{II}}(\text{glycinato})\text{Cl}_2]$ can catalyze sp^3 C–H bond oxidation in water, with improvements in both activity and selectivity, and without the requirement for strong acids to protect the alcohol from overoxidation.

We have previously used sodium *p*-toluenesulfonate **1** as a model water-soluble substrate. The original Shilov system oxidizes **1** at the methyl position to a mixture of the corresponding alcohol **2** and aldehyde **3** (Scheme 1); further oxidation to the carboxylic acid **4** was not observed.^{5a} Selectivity for **2** versus **3** drops off from ~ 10:1 during the early course of the reaction (~ 10% conversion) to ~ 2:1 at ~ 45% conversion. Oxidation at the aromatic ring positions does not occur, and the reaction remains visibly homogeneous for the majority of the reaction time, although deposition of platinum metal is eventually observed after long periods of heating. Products **2** and **3** are formed sequentially; overoxidation of **2** to **3** becomes more prevalent as the concentration of **2** increases, which explains the decrease in selectivity at higher conversions.^{5b,7}

Scheme 1



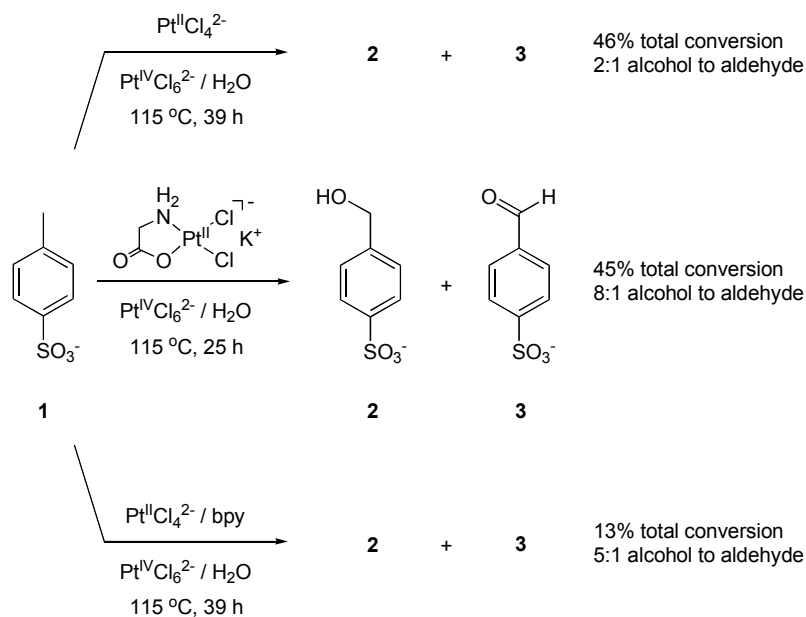
We and others have previously observed that good electron donor ligands can promote faster C–H activation in some cases.⁸ This phenomenon has been interpreted in terms of higher electron density at the metal center facilitating the displacement of a solvent ligand by coordination of a C–H bond, which has been shown to be the rate-determining step in several model systems.⁹ Glycine appeared to be an attractive choice to test this approach, as it is anionic and hence will tend to generate a more electron-rich

platinum center. It is also inexpensive, and contains relatively few C–H bonds that could make the catalyst prone to destructive self-oxidation. $\text{K}[\text{Pt}^{\text{II}}(\text{glycinato})\text{Cl}_2]\cdot 2\text{KCl}$ was previously prepared in high yield by addition of one equivalent of glycine and KOH to $\text{K}_2\text{Pt}^{\text{II}}\text{Cl}_4$ in water. Notably, recrystallization from a 9:1 ethanol:water mixture gave $\text{K}[\text{Pt}^{\text{II}}(\text{glycine})\text{Cl}_2]$ **5**, but only in 30% yield, accompanied by precipitation of a substantial amount of platinum metal.¹⁰ This observation suggests that **5** can oxidize ethanol (as can the original Shilov system, but only at elevated temperature⁵) under very mild conditions and hence might be a promising candidate for an oxidation catalyst. Our studies on **5** and its ability to catalyze selective C–H bond oxidation are described in the following sections.

Results and Discussion

Oxidation of *p*-toluenesulfonate using $\text{K}[\text{Pt}^{\text{II}}(\text{glycine})\text{Cl}_2]$. Under conditions similar to those for the Shilov system ($115\text{ }^\circ\text{C}$, $[\text{Pt}^{\text{II}}]_0 = 0.013\text{ M}$, $[\text{Pt}^{\text{IV}}]_0 = 0.11\text{ M}$, $[\mathbf{1}]_0 = 0.155\text{ M}$) but using **5** as the catalyst and $\text{Pt}^{\text{IV}}\text{Cl}_6^{2-}$ as the oxidant, **1** is oxidized to a mixture of **2** and **3** in water. After 25 hours, 45% of **1** is converted to products, and the selectivity for **2** versus **3** is 8:1 (Scheme 2). On replacing **5** with $\text{Pt}^{\text{II}}\text{Cl}_4^{2-}$ and keeping all other conditions the same, 39 hours are required to convert a similar percentage of **1** to products, and the selectivity for **2** versus **3** is only 2:1. For comparison, both conversion and selectivity are reduced by addition of bipyridine to the Shilov system (39 hours, 13% converted, 5:1 selectivity for **2** over **3**).^{5b} In all three cases, neither overoxidation to the carboxylic acid **4** nor precipitation of platinum metal is observed, and no more than trace amounts of any other product are detected by ^1H NMR.

Scheme 2



The improvements in selectivity and rate with **5** as the catalyst is notable, especially given the fact that $\text{Pt}^{\text{II}}\text{Cl}_4^{2-}$ is generated from $\text{Pt}^{\text{IV}}\text{Cl}_6^{2-}$, so that the solution increasingly contains the components of the original Shilov system. To examine the consequences of that process, the course of the reaction was monitored over time by ^1H NMR (Table 1, Figure 1). Initially, the rate of conversion using **5**/ $\text{Pt}^{\text{IV}}\text{Cl}_6^{2-}$ is about twice as fast as the original Shilov ($\text{Pt}^{\text{II}}\text{Cl}_4^{2-}/\text{Pt}^{\text{IV}}\text{Cl}_6^{2-}$) system. As the reaction proceeds and more $\text{Pt}^{\text{II}}\text{Cl}_4^{2-}$ is generated from $\text{Pt}^{\text{IV}}\text{Cl}_6^{2-}$, the difference between the two systems decreases, although overall conversion and selectivity are always better for the system starting with **5** at any point in time. In both cases, platinum metal formation is visible only at the end of the long heating period.

Table 1. Oxidation of **1** using **5** or $\text{Pt}^{\text{II}}\text{Cl}_4^{2-}$ as the catalyst and $\text{Pt}^{\text{IV}}\text{Cl}_6^{2-}$ as the oxidant at 105 °C

	System 1 ^a	System 2 ^b
Time (hours)	% converted (2:3)	% converted (2:3)
12	5 (2 only)	3 (2 only)
24	12 (2 only)	6 (2 only)
42	21 (>20:1)	12 (12:1)
66	33 (13:1)	23 (8:1)
90	42 (9:1)	32 (7:1)
109	46 (8:1)	36 (6:1)
132	53 (4:1)	44 (4:1)
179	58 (3:1)	48 (2:1)

^a $[\mathbf{5}]_0 = 0.013 \text{ M}$, $[\text{Pt}^{\text{IV}}\text{Cl}_6^{2-}]_0 = 0.11 \text{ M}$, $[\mathbf{1}]_0 = 0.155 \text{ M}$.

^b $[\text{Pt}^{\text{II}}\text{Cl}_4^{2-}]_0 = 0.013 \text{ M}$, $[\text{Pt}^{\text{IV}}\text{Cl}_6^{2-}]_0 = 0.11 \text{ M}$, $[\mathbf{1}]_0 = 0.155 \text{ M}$.

Figure 1. Formation of **2** (◆) and **3** (▲) using **5** as the catalyst and $\text{Pt}^{\text{IV}}\text{Cl}_6^{2-}$ as the oxidant; formation of **2** (■) and **3** (×) using $\text{Pt}^{\text{II}}\text{Cl}_4^{2-}$ as the catalyst and $\text{Pt}^{\text{IV}}\text{Cl}_6^{2-}$ as the oxidant (105 °C, $[\text{Pt}^{\text{II}}]_0 = 0.013 \text{ M}$, $[\text{Pt}^{\text{IV}}]_0 = 0.11 \text{ M}$, $[\mathbf{1}]_0 = 0.155 \text{ M}$)

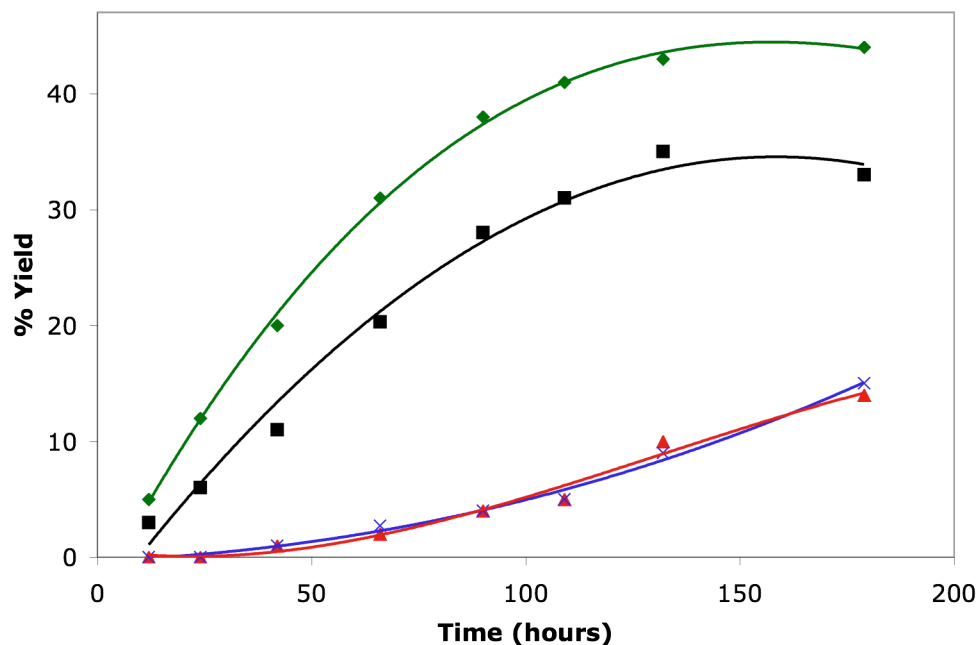


Figure 1 shows that while the rate of formation of **2** is faster with system 1, the rate of formation of **3** is about the same for both systems. However, since both $[\mathbf{2}]$ and total $[\text{Pt}^{\text{II}}]$ are higher at any given time in system 1, this finding implies that whereas **5** catalyzes the oxidation of **1** to **2** *faster* than $\text{Pt}^{\text{II}}\text{Cl}_4^{2-}$, it catalyzes oxidation of **2** to **3** *slower* than $\text{Pt}^{\text{II}}\text{Cl}_4^{2-}$. The combination of faster hydroxylation of **1** and slower overoxidation of **2** by **5** results in higher overall yield and selectivity.

Testing for heterogeneous reactions. The appearance of platinum metal after prolonged heating raises the possibility of heterogeneously catalyzed reactions; in particular, the higher selectivities with the glycinate ligand might be caused by inhibiting

formation of Pt^0 , which can catalyze dehydrogenation of **2** to **3**. No reaction is observed upon heating colloidal platinum with **1**, and activity is still observed in the presence of elemental mercury (a standard test for heterogeneous activity¹¹); there is some decrease in activity, but this could be due to the fact that Hg^0 is known to reduce both Pt^{II} and Pt^{IV} .^{5b} When **2** was prepared independently and subjected to the same conditions, the rate of formation of **3** was found to be somewhat slower using **5** as the catalyst than with the original Shilov system,¹² but the data do not rule out suppression of Pt^0 formation by the glycinate ligand as contributing to the increased selectivity.

Conclusions

Existing processes for selective oxidation of benzylic C–H bonds generally favor carboxylic acids, or in a few select cases aldehydes, as major products.¹³ We find here that the moderately selective oxidation to alcohols exhibited by the original Shilov system can be enhanced, in both activity and selectivity, by coordination of a simple anionic ligand. A practical process based on this chemistry will require not only further improvement but, most crucially, replacement of Pt^{IV} with a cheaper terminal oxidant (as has been accomplished, albeit only to a very limited extent, with the Shilov system¹⁴).

Experimental

General methods. Compound **2** was prepared by literature methods.¹⁵ All other chemicals are commercially available and used as received without further purification. NMR spectra were recorded at room temperature on a Varian Mercury 300 spectrometer.

Synthesis of compound 5. $\text{K}[\text{Pt}^{\text{II}}(\text{glycine})\text{Cl}_2]$ was synthesized by using a modified literature procedure.¹⁰ $\text{K}_2\text{Pt}^{\text{II}}\text{Cl}_4$ (1g, 2.4 mmol) and glycine (0.18g, 2.4 mmol) were added to a round bottom flask. Water (25 mL) was added, and the reaction mixture was heated to 100 °C using an oil bath. After heating for 10 minutes, 1 equivalent of KOH (0.135g in 20 mL water) was added dropwise to the reaction mixture over the course of 10 minutes. The color of the solution turned from red to yellow. The reaction mixture was allowed to cool down to room temperature, and the solvent was removed under vacuum to give a yellow residue. Pure $\text{K}[\text{Pt}^{\text{II}}(\text{glycine})\text{Cl}_2]$ was recrystallized from a 9:1 ethanol:water mixture. Yield: 0.27g, 30%.

Oxidation of *p*-toluenesulfonate and compound 2. Reactions were carried out on solutions of 0.013 M $\text{K}_2\text{Pt}^{\text{II}}\text{Cl}_4$ or $\text{K}[\text{Pt}^{\text{II}}(\text{glycine})\text{Cl}_2]$, 0.11 M $\text{Na}_2\text{Pt}^{\text{IV}}\text{Cl}_6$, and 0.155 M sodium *p*-toluenesulfonate in 3 mL of D_2O . In a typical experiment, the reaction mixture was prepared by weighing the desired compounds into a 20 mL glass vial and adding D_2O . A magnetic stir bar was then added, and the vial was sealed using a Teflon screw cap. The vial was then heated to the desired temperature using an oil bath. Formation of products was monitored by following the growth of the corresponding ^1H NMR signals.

Direct oxidation of **2** (prepared independently) to **3** was carried out using the same procedure. The starting materials and products are all known compounds.

References

- (1) (a) Crabtree, R. H. *Chem. Rev.* **1995**, *95*, 987–1007. (b) Arndtsen, B. A.; Bergman, R. G.; Mobley, T. A.; Peterson, T. H. *Acc. Chem. Res.* **1995**, *28*, 154–162. (c) Stahl, S. S.; Labinger, J. A.; Bercaw, J. E. *Angew. Chem. Int. Ed.* **1998**, *37*, 2180–2192. (d) Sen, A. *Acc. Chem. Res.* **1998**, *31*, 550–557. (e) Jia, C.; Kitamura, T.; Fujiwara, Y. *Acc. Chem. Res.* **2001**, *34*, 633–639. (f) Labinger, J. A.; Bercaw, J. E. *Nature* **2002**, *417*, 507–514. (g) Jones, W. D. *Acc. Chem. Res.* **2003**, *36*, 140–146. (h) Lersch, M.; Tilset, M. *Chem. Rev.* **2005**, *105*, 2471–2526. (i) Vedernikov, A. N. *Curr. Org. Chem.* **2007**, *11*, 1401–1416. (j) Bergman, R. G. *Nature* **2007**, *446*, 391–391. (k) Dyker, G., Ed. *Handbook of C–H Transformations*; Wiley-VCH: Weinheim, Germany, **2005**, and references therein.
- (2) (a) Goldshlegger, N. F.; Tyabin, M. B.; Shilov, A. E.; Shteinman, A. A. *Zh. Fiz. Khim.* **1969**, *43*, 2174–2175. (b) Goldshlegger, N. F.; Eskova, V. V.; Shilov, A. E.; Shteinman, A. A. *Zh. Fiz. Khim.* **1972**, *46*, 1353–1354. (c) Shilov, A. E.; Shul'pin, G. B. *Chem. Rev.* **1997**, *97*, 2879–2932.
- (3) (a) Hill, G. S.; Rendina, L. M.; Puddephatt, R. J. *Organometallics* **1995**, *14*, 4966–4968. (b) Stahl, S. S.; Labinger, J. A.; Bercaw, J. E. *J. Am. Chem. Soc.* **1995**, *117*, 9371–9372. (c) Siegbahn, P. E. M.; Crabtree, R. H. *J. Am. Chem. Soc.* **1996**, *118*, 4442–4450. (d) Stahl, S. S.; Labinger, J. A.; Bercaw, J. E. *J. Am. Chem. Soc.* **1996**, *118*, 5961–5976. (e) Wick, D. D.; Goldberg, K. I. *J. Am. Chem. Soc.* **1997**, *119*, 10235–10236. (f) Romeo, R.; Plutino, M. R.; Elding, L. I. *Inorg. Chem.* **1997**, *36*, 5909–5916. (g) Bartlett, K. L.; Goldberg, K. I.; Borden, W. T. *J. Am. Chem. Soc.*

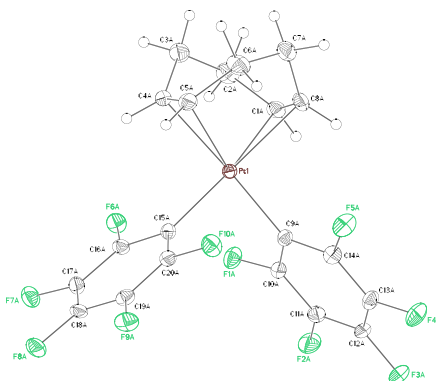
- 2000**, *122*, 1456–1465. (h) Heiberg, H.; Johansson, L.; Gropen, O.; Ryan, O. B.; Swang, O.; Tilset, M. *J. Am. Chem. Soc.* **2000**, *122*, 10831–10845. (i) Bartlett, K. L.; Goldberg, K. I.; Borden, W. T. *Organometallics* **2001**, *20*, 2669–2678. (j) Wik, B. J.; Lersch, M.; Tilset, M. *J. Am. Chem. Soc.* **2002**, *124*, 12116–12117. (k) Jensen, M. P.; Wick, D. D.; Reinartz, S.; White, P. S.; Templeton, J. L.; Goldberg, K. I. *J. Am. Chem. Soc.* **2003**, *125*, 8614–8624. (l) Driver, T. G.; Day, M. W.; Labinger, J. A.; Bercaw, J. E. *Organometallics*, **2005**, *24*, 3644–3654. (m) Khaskin, E.; Zavalij, P. Y.; Vedernikov, A. N. *J. Am. Chem. Soc.* **2006**, *128*, 13054–13055. (n) Romeo, R.; D'Amico, G. *Organometallics* **2006**, *25*, 3435–3446. (o) Weinberg, D. R.; Labinger, J. A.; Bercaw, J. E. *Organometallics*, **2007**, *26*, 167–172. (p) Williams, T. J.; Labinger, J. A.; Bercaw, J. E. *Organometallics*, **2007**, *26*, 281–287. (q) Driver, T. G.; Williams, T. J.; Labinger, J. A.; Bercaw, J. E. *Organometallics*, **2007**, *26*, 294–301. (r) West, N. M.; White, P. S.; Templeton, J. L. *J. Am. Chem. Soc.* **2007**, *129*, 12372–12373.
- (4) Horváth, I. T.; Cook, R. A.; Millar, J. M.; Gábor, K. *Organometallics* **1993**, *12*, 8–10.
- (5) (a) Labinger, J. A.; Herring, A. M.; Bercaw, J. E. *J. Am. Chem. Soc.* **1990**, *112*, 5628–5629. (b) Labinger, J. A.; Herring, A. M.; Lyon, D. K.; Luinstra, G. A.; Bercaw, J. E.; Horváth, I. T.; Eller, K. *Organometallics* **1993**, *12*, 895–905.
- (6) (a) Kao, L. C.; Hutson, A. C.; Sen, A. *J. Am. Chem. Soc.* **1991**, *113*, 700–701. (b) Periana, R. A.; Taube, D. J.; Evitt, E. R.; Loffler, D. G.; Wentreck, P. R.; Voss, G.; Masuda, T. *Science* **1993**, *259*, 340–343. (c) Periana, R. A.; Taube, D. J.; Gamble, S.; Taube, H.; Satoh, T.; Fujii, H. *Science* **1998**, *280*, 560–564. (d) An, Z.; Pan, X.; Liu, X.; Han, X.; Bao, X. *J. Am. Chem. Soc.* **2006**, *128*, 16028–16029.

- (7) Herring, A. M.; Lyon, D. K.; Labinger, J. A.; Bercaw, J. E. Unpublished results.
- (8) (a) Zhong, H. A.; Labinger, J. A.; Bercaw, J. E. *J. Am. Chem. Soc.* **2002**, *124*, 1378–1399. (b) Ziatdinov, V. R.; Oxgaard, J.; Mironov, O. A.; Young, K. J. H.; Goddard, W. A.; Periana, R. A. *J. Am. Chem. Soc.* **2006**, *128*, 7404–7405.
- (9) (a) Johansson, L.; Tilset, M.; Labinger, J. A.; Bercaw, J. E. *J. Am. Chem. Soc.* **2000**, *122*, 10846–10855. (b) Heyduk, A. F.; Driver, T. G.; Labinger, J. A.; Bercaw, J. E. *J. Am. Chem. Soc.* **2004**, *126*, 15034–15035. (c) Owen, J. S.; Labinger, J. A.; Bercaw, J. E. *J. Am. Chem. Soc.* **2006**, *128*, 2005–2016. (d) Chen, G. S.; Labinger, J. A.; Bercaw, J. E. *Proc. Natl. Acad. Sci. U.S.A.* **2007**, *104*, 6915–6920.
- (10) (a) Erickson, L. E.; McDonald, J. W.; Howie, J. K.; Clow, R. P. *J. Am. Chem. Soc.* **1968**, *90*, 6371–6382. (b) Erickson, L. E.; Dappen, A. J.; Uhlenhopp, J. C. *J. Am. Chem. Soc.* **1969**, *91*, 2510–2513. (c) Erickson, L. E.; Erickson, M. D.; Smith, B. L. *Inorg. Chem.* **1973**, *12*, 412–422.
- (11) Anton, D. R.; Crabtree, R. H. *Organometallics* **1983**, *2*, 855–859.
- (12) 115 °C, 20 hours. $[5]_0 = 0.013 \text{ M}$, $[\text{Pt}^{\text{IV}}\text{Cl}_6^{2-}]_0 = 0.11 \text{ M}$, $[2]_0 = 0.155 \text{ M}$, 27% converted. $[\text{Pt}^{\text{II}}\text{Cl}_4^{2-}]_0 = 0.013 \text{ M}$, $[\text{Pt}^{\text{IV}}\text{Cl}_6^{2-}]_0 = 0.11 \text{ M}$, $[2]_0 = 0.155 \text{ M}$, 33% converted.
- (13) (a) Ishii, Y.; Sakaguchi, S.; Iwahama, T. *Adv. Synth. Catal.* **2001**, *343*, 393–427. (b) Nomiya, K.; Hashino, K.; Nemoto, Y.; Watanabe, M. *J. Mol. Catal. A* **2001**, *176*, 79–86. (c) Wang, F.; Xu, J.; Li, X.; Gao, J.; Zhou, L.; Ohnishi, R. *Adv. Synth. Catal.* **2005**, *347*, 1987–1992.

- (14) (a) Freund, M. S.; Labinger, J. A.; Lewis, N. S.; Bercaw, J. E. *J. Mol. Cat.* **1994**, *87*, L11–L16. (b) Lin, M.; Shen, C.; Garcia-Zayas, E. A.; Sen, A. *J. Am. Chem. Soc.* **2001**, *123*, 1000–1001.
- (15) Hubbuck, A.; Bindewald, R.; Fohles, J.; Naithani, V. K.; Zahn, H. *Angew. Chem. Int. Ed. Engl.* **1980**, *19*, 394–396.

Appendix A. X-Ray Crystallographic Data for $(\text{COD})\text{Pt}^{\text{II}}(\text{C}_6\text{F}_5)_2$

While studying the protonolysis of $(\text{COD})\text{Pt}^{\text{II}}(\text{CH}_3)_2$ with $\text{B}(\text{C}_6\text{F}_5)_3$ in anhydrous $\text{TFE-}d_3$, it was discovered that if a large excess of $\text{B}(\text{C}_6\text{F}_5)_3$ was used, crystals would form in the reaction flask overnight. X-ray analysis of these crystals found that two perfluorophenyl groups were transferred from $\text{B}(\text{C}_6\text{F}_5)_3$ to platinum to give $(\text{COD})\text{Pt}^{\text{II}}(\text{C}_6\text{F}_5)_2$.



$(\text{COD})\text{Pt}^{\text{II}}(\text{C}_6\text{F}_5)_2$

Note: The crystallographic data have been deposited in the Cambridge Database (CCDC) and have been placed on hold pending further instructions from me. The deposition number is 694649. Ideally the CCDC would like the publication to contain a footnote of the type: "Crystallographic data have been deposited at the CCDC, 12 Union Road, Cambridge CB2 1EZ, UK and copies can be obtained on request, free of charge, by quoting the publication citation and the deposition number 694649."

Table 1. Crystal data and structure refinement for (COD)Pt^{II}(C₆F₅)₂ (CCDC 694649)

Empirical formula	C ₂₀ H ₁₂ F ₁₀ Pt
Formula weight	637.39
Crystallization Solvent	Not given
Crystal Habit	Fragment
Crystal size	0.30 x 0.15 x 0.06 mm ³
Crystal color	Colorless



Data Collection

Type of diffractometer	Bruker KAPPA APEX II
Wavelength	0.71073 Å MoK α
Data Collection Temperature	100(2) K
θ range for 76096 reflections used in lattice determination	2.20 to 38.51°
Unit cell dimensions	a = 10.7452(4) Å b = 12.5728(5) Å c = 27.2752(10) Å
Volume	3684.8(2) Å ³
Z	8
Crystal system	Orthorhombic
Space group	P2 ₁ 2 ₁ 2 ₁
Density (calculated)	2.298 Mg/m ³
F(000)	2400
Data collection program	Bruker APEX2 v2.1-0
θ range for data collection	1.78 to 38.53°
Completeness to $\theta = 38.53^\circ$	99.8 %
Index ranges	-18 ≤ h ≤ 18, -22 ≤ k ≤ 21, -47 ≤ l ≤ 42
Data collection scan type	ω scans; 23 settings
Data reduction program	Bruker SAINT-Plus v7.34A
Reflections collected	122519
Independent reflections	20705 [R _{int} = 0.0418]
Absorption coefficient	7.719 mm ⁻¹
Absorption correction	Semi-empirical from equivalents
Max. and min. transmission	0.7476 and 0.4548

Table 1 (cont.)**Structure Solution and Refinement**

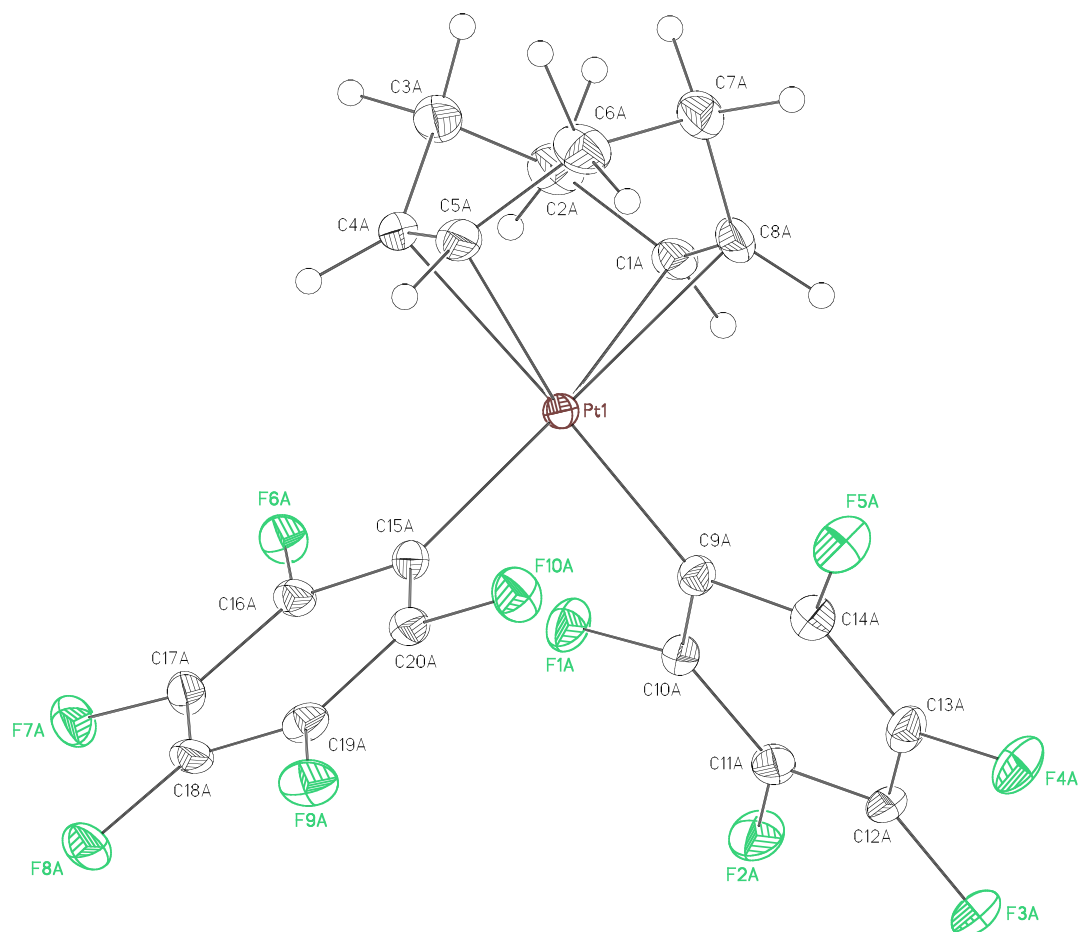
Structure solution program	SHELXS-97 (Sheldrick, 2008)
Primary solution method	Direct methods
Secondary solution method	Difference Fourier map
Hydrogen placement	Difference Fourier map
Structure refinement program	SHELXL-97 (Sheldrick, 2008)
Refinement method	Full matrix least-squares on F^2
Data / restraints / parameters	20705 / 0 / 655
Treatment of hydrogen atoms	Unrestrained
Goodness-of-fit on F^2	1.060
Final R indices [$I > 2\sigma(I)$, 18653 reflections]	$R1 = 0.0240$, $wR2 = 0.0405$
R indices (all data)	$R1 = 0.0308$, $wR2 = 0.0418$
Type of weighting scheme used	Sigma
Weighting scheme used	$w = 1/\sigma^2(Fo^2)$
Max shift/error	0.002
Average shift/error	0.000
Absolute structure determination	Anomalous differences
Absolute structure parameter	0.002(2)
Largest diff. peak and hole	2.955 and -1.501 e.Å ⁻³

Special Refinement Details

Crystals were mounted on a glass fiber using Paratone oil then placed on the diffractometer under a nitrogen stream at 100K.

Refinement of F^2 against ALL reflections. The weighted R-factor (wR) and goodness of fit (S) are based on F^2 , conventional R-factors (R) are based on F , with F set to zero for negative F^2 . The threshold expression of $F^2 > 2\sigma(F^2)$ is used only for calculating R-factors(gt) etc. and is not relevant to the choice of reflections for refinement. R-factors based on F^2 are statistically about twice as large as those based on F , and R-factors based on ALL data will be even larger.

All esds (except the esd in the dihedral angle between two l.s. planes) are estimated using the full covariance matrix. The cell esds are taken into account individually in the estimation of esds in distances, angles, and torsion angles; correlations between esds in cell parameters are only used when they are defined by crystal symmetry. An approximate (isotropic) treatment of cell esds is used for estimating esds involving l.s. planes.



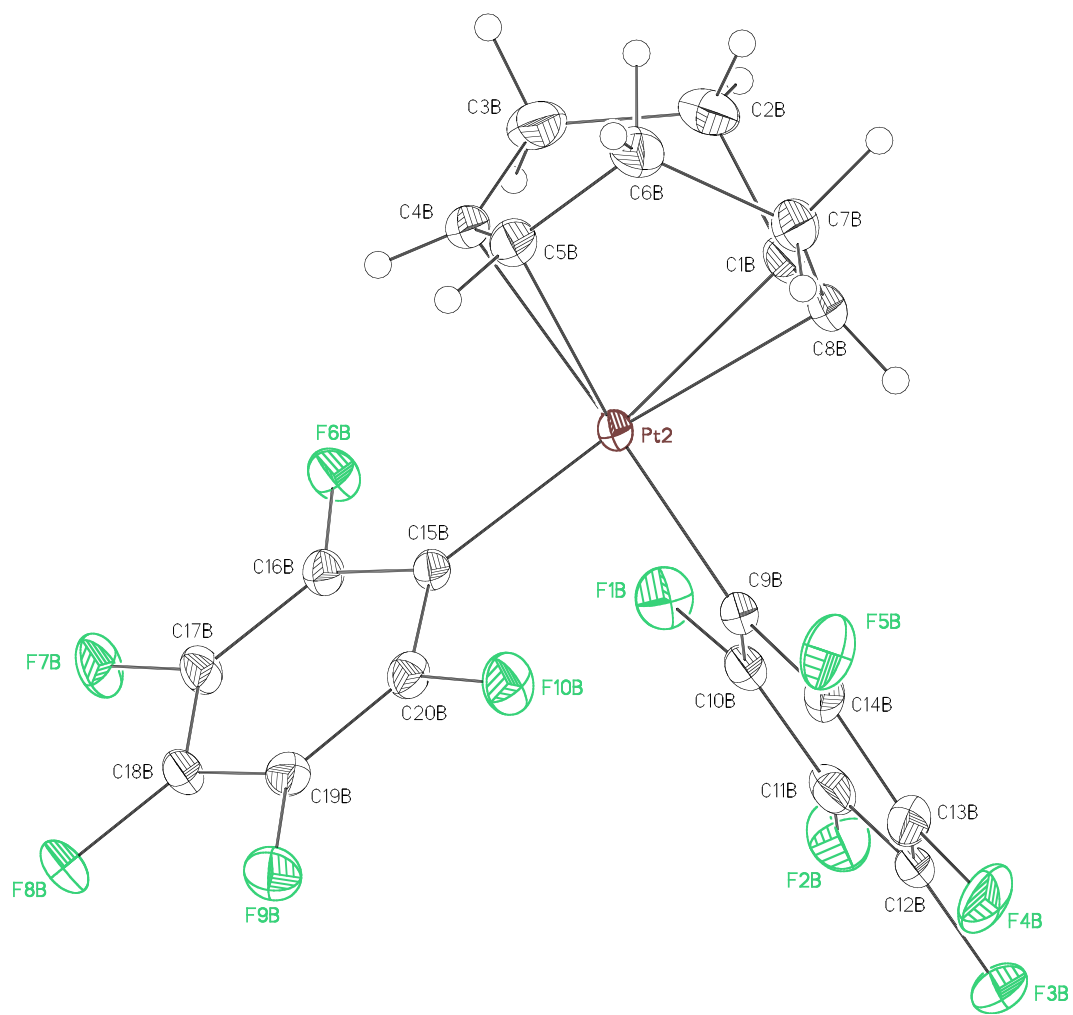


Table 2. Atomic coordinates ($\times 10^4$) and equivalent isotropic displacement parameters ($\text{\AA}^2 \times 10^3$) for (COD)Pt^{II}(C₆F₅)₂ (CCDC 694649). U(eq) is defined as the trace of the orthogonalized U^{ij} tensor.

	x	y	z	U _{eq}
Pt(1)	4779(1)	4987(1)	157(1)	12(1)
F(1A)	5492(2)	3005(1)	-521(1)	22(1)
F(2A)	6391(2)	2888(1)	-1443(1)	26(1)
F(3A)	7055(2)	4685(1)	-1928(1)	25(1)
F(4A)	6658(2)	6620(1)	-1508(1)	27(1)
F(5A)	5634(2)	6758(1)	-614(1)	24(1)
F(6A)	5875(1)	2788(1)	536(1)	19(1)
F(7A)	8029(2)	2272(1)	970(1)	22(1)
F(8A)	9824(2)	3784(1)	1102(1)	23(1)
F(9A)	9417(2)	5811(1)	813(1)	22(1)
F(10A)	7237(2)	6362(1)	399(1)	23(1)
C(1A)	2869(2)	4716(2)	-135(1)	18(1)
C(2A)	2243(3)	4002(2)	235(1)	25(1)
C(3A)	2485(3)	4298(2)	771(1)	23(1)
C(4A)	3798(2)	4675(2)	866(1)	18(1)
C(5A)	4168(3)	5724(2)	861(1)	19(1)
C(6A)	3381(3)	6675(2)	724(1)	25(1)
C(7A)	2488(3)	6486(2)	304(1)	22(1)
C(8A)	3028(2)	5806(2)	-100(1)	18(1)
C(9A)	5524(2)	4884(1)	-526(1)	14(1)
C(10A)	5749(2)	3920(2)	-759(1)	15(1)
C(11A)	6225(2)	3839(2)	-1225(1)	18(1)
C(12A)	6564(3)	4753(1)	-1478(1)	18(1)
C(13A)	6366(2)	5730(2)	-1259(1)	18(1)
C(14A)	5850(2)	5771(1)	-798(1)	16(1)
C(15A)	6468(2)	4602(1)	444(1)	14(1)
C(16A)	6733(2)	3569(1)	595(1)	15(1)
C(17A)	7843(2)	3278(1)	813(1)	16(1)
C(18A)	8752(2)	4033(2)	883(1)	16(1)
C(19A)	8532(2)	5073(2)	735(1)	16(1)
C(20A)	7413(2)	5325(1)	526(1)	15(1)
Pt(2)	1534(1)	6086(1)	7956(1)	14(1)
F(1B)	-638(2)	7767(1)	8164(1)	26(1)
F(2B)	-2850(2)	8091(1)	7725(1)	36(1)
F(3B)	-3624(2)	6779(2)	6998(1)	42(1)
F(4B)	-2145(2)	5127(1)	6709(1)	40(1)
F(5B)	112(2)	4871(1)	7099(1)	30(1)
F(6B)	874(2)	6733(1)	9063(1)	22(1)
F(7B)	-361(2)	5715(1)	9770(1)	26(1)
F(8B)	-1276(2)	3720(1)	9615(1)	27(1)
F(9B)	-934(2)	2768(1)	8728(1)	27(1)
F(10B)	300(2)	3769(1)	8016(1)	25(1)
C(1B)	2466(3)	7392(2)	7529(1)	22(1)
C(2B)	3587(3)	7801(2)	7807(1)	27(1)
C(3B)	3625(3)	7433(2)	8340(1)	28(1)
C(4B)	3223(2)	6291(2)	8415(1)	21(1)

C(5B)	3444(3)	5440(2)	8110(1)	22(1)
C(6B)	4223(3)	5465(2)	7649(1)	24(1)
C(7B)	3486(3)	5698(2)	7177(1)	24(1)
C(8B)	2437(3)	6484(2)	7244(1)	22(1)
C(9B)	-160(2)	6313(1)	7648(1)	16(1)
C(10B)	-968(2)	7112(2)	7795(1)	18(1)
C(11B)	-2105(3)	7286(2)	7580(1)	23(1)
C(12B)	-2501(3)	6626(2)	7209(1)	28(1)
C(13B)	-1750(3)	5794(2)	7058(1)	26(1)
C(14B)	-600(3)	5673(2)	7274(1)	20(1)
C(15B)	650(2)	5295(1)	8506(1)	14(1)
C(16B)	438(2)	5742(1)	8961(1)	16(1)
C(17B)	-200(3)	5240(1)	9335(1)	18(1)
C(18B)	-662(3)	4224(2)	9257(1)	19(1)
C(19B)	-480(2)	3749(1)	8810(1)	18(1)
C(20B)	159(2)	4279(1)	8447(1)	16(1)

Table 3. Selected bond lengths [Å] and angles [°] for (COD)Pt^{II}(C₆F₅)₂ (CCDC 694649)

Pt(1)-C(9A)	2.032(2)	Pt(2)-C(9B)	2.024(2)
Pt(1)-C(15A)	2.035(2)	Pt(2)-C(15B)	2.034(2)
Pt(1)-C(1A)	2.228(2)	Pt(2)-C(1B)	2.249(2)
Pt(1)-C(4A)	2.236(2)	Pt(2)-C(4B)	2.220(3)
Pt(1)-C(5A)	2.231(2)	Pt(2)-C(5B)	2.247(3)
Pt(1)-C(8A)	2.257(2)	Pt(2)-C(8B)	2.229(2)
C(9A)-Pt(1)-C(15A)	89.18(9)	C(9B)-Pt(2)-C(15B)	87.42(9)
C(9A)-Pt(1)-C(1A)	91.43(9)	C(9B)-Pt(2)-C(4B)	162.27(8)
C(15A)-Pt(1)-C(1A)	157.42(7)	C(15B)-Pt(2)-C(4B)	91.30(9)
C(9A)-Pt(1)-C(5A)	158.67(8)	C(9B)-Pt(2)-C(8B)	89.90(10)
C(15A)-Pt(1)-C(5A)	91.73(9)	C(15B)-Pt(2)-C(8B)	162.83(8)
C(1A)-Pt(1)-C(5A)	95.77(9)	C(4B)-Pt(2)-C(8B)	96.30(10)
C(9A)-Pt(1)-C(4A)	165.27(7)	C(9B)-Pt(2)-C(5B)	161.74(8)
C(15A)-Pt(1)-C(4A)	92.67(9)	C(15B)-Pt(2)-C(5B)	96.41(9)
C(1A)-Pt(1)-C(4A)	81.30(9)	C(4B)-Pt(2)-C(5B)	35.88(9)
C(5A)-Pt(1)-C(4A)	35.92(9)	C(8B)-Pt(2)-C(5B)	81.18(10)
C(9A)-Pt(1)-C(8A)	94.15(9)	C(9B)-Pt(2)-C(1B)	94.72(9)
C(15A)-Pt(1)-C(8A)	166.30(7)	C(15B)-Pt(2)-C(1B)	161.21(9)
C(1A)-Pt(1)-C(8A)	35.94(8)	C(4B)-Pt(2)-C(1B)	81.00(10)
C(5A)-Pt(1)-C(8A)	80.38(9)	C(8B)-Pt(2)-C(1B)	35.96(9)
C(4A)-Pt(1)-C(8A)	87.49(9)	C(5B)-Pt(2)-C(1B)	87.39(9)

Table 4. Bond lengths [Å] and angles [°] for (COD)Pt^{II}(C₆F₅)₂ (CCDC 694649)

Pt(1)-C(9A)	2.032(2)	Pt(2)-C(8B)	2.229(2)
Pt(1)-C(15A)	2.035(2)	Pt(2)-C(5B)	2.247(3)
Pt(1)-C(1A)	2.228(2)	Pt(2)-C(1B)	2.249(2)
Pt(1)-C(5A)	2.231(2)	F(1B)-C(10B)	1.349(3)
Pt(1)-C(4A)	2.236(2)	F(2B)-C(11B)	1.350(3)
Pt(1)-C(8A)	2.257(2)	F(3B)-C(12B)	1.352(3)
F(1A)-C(10A)	1.351(2)	F(4B)-C(13B)	1.339(3)
F(2A)-C(11A)	1.347(2)	F(5B)-C(14B)	1.353(3)
F(3A)-C(12A)	1.338(3)	F(6B)-C(16B)	1.360(2)
F(4A)-C(13A)	1.346(2)	F(7B)-C(17B)	1.341(2)
F(5A)-C(14A)	1.359(2)	F(8B)-C(18B)	1.339(3)
F(6A)-C(16A)	1.356(2)	F(9B)-C(19B)	1.345(2)
F(7A)-C(17A)	1.350(2)	F(10B)-C(20B)	1.349(2)
F(8A)-C(18A)	1.336(3)	C(1B)-C(8B)	1.382(4)
F(9A)-C(19A)	1.345(3)	C(1B)-C(2B)	1.514(4)
F(10A)-C(20A)	1.362(2)	C(1B)-H(1B)	0.93(3)
C(1A)-C(8A)	1.384(3)	C(2B)-C(3B)	1.525(4)
C(1A)-C(2A)	1.509(3)	C(2B)-H(2B1)	0.91(3)
C(1A)-H(1A)	0.96(3)	C(2B)-H(2B2)	0.92(4)
C(2A)-C(3A)	1.531(4)	C(3B)-C(4B)	1.514(3)
C(2A)-H(2A1)	1.03(4)	C(3B)-H(3B1)	0.97(4)
C(2A)-H(2A2)	0.93(3)	C(3B)-H(3B2)	0.96(4)
C(3A)-C(4A)	1.510(4)	C(4B)-C(5B)	1.376(3)
C(3A)-H(3A1)	1.01(3)	C(4B)-H(4B)	0.89(3)
C(3A)-H(3A2)	0.98(3)	C(5B)-C(6B)	1.510(4)
C(4A)-C(5A)	1.377(3)	C(5B)-H(5B)	1.01(2)
C(4A)-H(4A)	0.95(3)	C(6B)-C(7B)	1.541(4)
C(5A)-C(6A)	1.511(3)	C(6B)-H(6B1)	0.97(3)
C(5A)-H(5A)	1.01(3)	C(6B)-H(6B2)	0.94(3)
C(6A)-C(7A)	1.513(4)	C(7B)-C(8B)	1.510(4)
C(6A)-H(6A1)	1.03(4)	C(7B)-H(7B1)	1.06(3)
C(6A)-H(6A2)	1.06(3)	C(7B)-H(7B2)	0.88(3)
C(7A)-C(8A)	1.511(3)	C(8B)-H(8B)	0.88(3)
C(7A)-H(7A1)	0.97(3)	C(9B)-C(14B)	1.383(3)
C(7A)-H(7A2)	0.98(3)	C(9B)-C(10B)	1.387(3)
C(8A)-H(8A)	0.97(2)	C(10B)-C(11B)	1.373(4)
C(9A)-C(14A)	1.385(3)	C(11B)-C(12B)	1.375(4)
C(9A)-C(10A)	1.390(3)	C(12B)-C(13B)	1.384(4)
C(10A)-C(11A)	1.374(3)	C(13B)-C(14B)	1.377(4)
C(11A)-C(12A)	1.388(3)	C(15B)-C(16B)	1.382(3)
C(12A)-C(13A)	1.382(3)	C(15B)-C(20B)	1.392(3)
C(13A)-C(14A)	1.376(3)	C(16B)-C(17B)	1.380(3)
C(15A)-C(20A)	1.380(3)	C(17B)-C(18B)	1.386(3)
C(15A)-C(16A)	1.393(3)	C(18B)-C(19B)	1.371(3)
C(16A)-C(17A)	1.382(3)	C(19B)-C(20B)	1.376(3)
C(17A)-C(18A)	1.376(3)		
C(18A)-C(19A)	1.388(3)	C(9A)-Pt(1)-C(15A)	89.18(9)
C(19A)-C(20A)	1.369(3)	C(9A)-Pt(1)-C(1A)	91.43(9)
Pt(2)-C(9B)	2.024(2)	C(15A)-Pt(1)-C(1A)	157.42(7)
Pt(2)-C(15B)	2.034(2)	C(9A)-Pt(1)-C(5A)	158.67(8)
Pt(2)-C(4B)	2.220(3)	C(15A)-Pt(1)-C(5A)	91.73(9)

C(1A)-Pt(1)-C(5A)	95.77(9)	C(7A)-C(8A)-Pt(1)	110.57(16)
C(9A)-Pt(1)-C(4A)	165.27(7)	C(1A)-C(8A)-H(8A)	117.9(13)
C(15A)-Pt(1)-C(4A)	92.67(9)	C(7A)-C(8A)-H(8A)	116.1(13)
C(1A)-Pt(1)-C(4A)	81.30(9)	Pt(1)-C(8A)-H(8A)	101.5(16)
C(5A)-Pt(1)-C(4A)	35.92(9)	C(14A)-C(9A)-C(10A)	114.40(19)
C(9A)-Pt(1)-C(8A)	94.15(9)	C(14A)-C(9A)-Pt(1)	122.66(15)
C(15A)-Pt(1)-C(8A)	166.30(7)	C(10A)-C(9A)-Pt(1)	122.94(14)
C(1A)-Pt(1)-C(8A)	35.94(8)	F(1A)-C(10A)-C(11A)	117.32(18)
C(5A)-Pt(1)-C(8A)	80.38(9)	F(1A)-C(10A)-C(9A)	119.10(18)
C(4A)-Pt(1)-C(8A)	87.49(9)	C(11A)-C(10A)-C(9A)	123.58(19)
C(8A)-C(1A)-C(2A)	126.7(2)	F(2A)-C(11A)-C(10A)	121.55(19)
C(8A)-C(1A)-Pt(1)	73.16(14)	F(2A)-C(11A)-C(12A)	118.78(19)
C(2A)-C(1A)-Pt(1)	105.15(16)	C(10A)-C(11A)-C(12A)	119.67(18)
C(8A)-C(1A)-H(1A)	117.0(13)	F(3A)-C(12A)-C(13A)	120.88(18)
C(2A)-C(1A)-H(1A)	115.4(13)	F(3A)-C(12A)-C(11A)	120.31(17)
Pt(1)-C(1A)-H(1A)	101.3(17)	C(13A)-C(12A)-C(11A)	118.8(2)
C(1A)-C(2A)-C(3A)	114.7(2)	F(4A)-C(13A)-C(12A)	119.1(2)
C(1A)-C(2A)-H(2A1)	111.8(17)	F(4A)-C(13A)-C(14A)	121.56(18)
C(3A)-C(2A)-H(2A1)	100.3(19)	C(12A)-C(13A)-C(14A)	119.34(18)
C(1A)-C(2A)-H(2A2)	107(2)	F(5A)-C(14A)-C(13A)	116.21(17)
C(3A)-C(2A)-H(2A2)	107(2)	F(5A)-C(14A)-C(9A)	119.6(2)
H(2A1)-C(2A)-H(2A2)	116(3)	C(13A)-C(14A)-C(9A)	124.15(18)
C(4A)-C(3A)-C(2A)	113.5(2)	C(20A)-C(15A)-C(16A)	114.6(2)
C(4A)-C(3A)-H(3A1)	107.1(17)	C(20A)-C(15A)-Pt(1)	124.22(14)
C(2A)-C(3A)-H(3A1)	114.1(18)	C(16A)-C(15A)-Pt(1)	121.15(16)
C(4A)-C(3A)-H(3A2)	109.1(19)	F(6A)-C(16A)-C(17A)	116.49(16)
C(2A)-C(3A)-H(3A2)	109.0(16)	F(6A)-C(16A)-C(15A)	120.1(2)
H(3A1)-C(3A)-H(3A2)	104(2)	C(17A)-C(16A)-C(15A)	123.4(2)
C(5A)-C(4A)-C(3A)	124.6(2)	F(7A)-C(17A)-C(18A)	119.8(2)
C(5A)-C(4A)-Pt(1)	71.85(14)	F(7A)-C(17A)-C(16A)	120.9(2)
C(3A)-C(4A)-Pt(1)	110.29(17)	C(18A)-C(17A)-C(16A)	119.28(17)
C(5A)-C(4A)-H(4A)	117.3(16)	F(8A)-C(18A)-C(17A)	120.81(18)
C(3A)-C(4A)-H(4A)	115.9(17)	F(8A)-C(18A)-C(19A)	119.8(2)
Pt(1)-C(4A)-H(4A)	102.6(18)	C(17A)-C(18A)-C(19A)	119.3(2)
C(4A)-C(5A)-C(6A)	126.7(2)	F(9A)-C(19A)-C(20A)	121.81(18)
C(4A)-C(5A)-Pt(1)	72.24(13)	F(9A)-C(19A)-C(18A)	119.0(2)
C(6A)-C(5A)-Pt(1)	106.28(16)	C(20A)-C(19A)-C(18A)	119.2(2)
C(4A)-C(5A)-H(5A)	117.9(14)	F(10A)-C(20A)-C(19A)	116.68(19)
C(6A)-C(5A)-H(5A)	114.1(14)	F(10A)-C(20A)-C(15A)	119.1(2)
Pt(1)-C(5A)-H(5A)	103.6(16)	C(19A)-C(20A)-C(15A)	124.19(18)
C(5A)-C(6A)-C(7A)	114.70(18)	C(9B)-Pt(2)-C(15B)	87.42(9)
C(5A)-C(6A)-H(6A1)	109(2)	C(9B)-Pt(2)-C(4B)	162.27(8)
C(7A)-C(6A)-H(6A1)	109(2)	C(15B)-Pt(2)-C(4B)	91.30(9)
C(5A)-C(6A)-H(6A2)	109(2)	C(9B)-Pt(2)-C(8B)	89.90(10)
C(7A)-C(6A)-H(6A2)	110.2(19)	C(15B)-Pt(2)-C(8B)	162.83(8)
H(6A1)-C(6A)-H(6A2)	104(3)	C(4B)-Pt(2)-C(8B)	96.30(10)
C(8A)-C(7A)-C(6A)	113.4(2)	C(9B)-Pt(2)-C(5B)	161.74(8)
C(8A)-C(7A)-H(7A1)	103(2)	C(15B)-Pt(2)-C(5B)	96.41(9)
C(6A)-C(7A)-H(7A1)	110(2)	C(4B)-Pt(2)-C(5B)	35.88(9)
C(8A)-C(7A)-H(7A2)	111.7(14)	C(8B)-Pt(2)-C(5B)	81.18(10)
C(6A)-C(7A)-H(7A2)	107.7(16)	C(9B)-Pt(2)-C(1B)	94.72(9)
H(7A1)-C(7A)-H(7A2)	112(3)	C(15B)-Pt(2)-C(1B)	161.21(9)
C(1A)-C(8A)-C(7A)	124.3(2)	C(4B)-Pt(2)-C(1B)	81.00(10)
C(1A)-C(8A)-Pt(1)	70.90(13)	C(8B)-Pt(2)-C(1B)	35.96(9)

C(5B)-Pt(2)-C(1B)	87.39(9)	C(1B)-C(8B)-C(7B)	126.3(3)
C(8B)-C(1B)-C(2B)	125.5(3)	C(1B)-C(8B)-Pt(2)	72.80(15)
C(8B)-C(1B)-Pt(2)	71.24(13)	C(7B)-C(8B)-Pt(2)	106.48(15)
C(2B)-C(1B)-Pt(2)	110.01(16)	C(1B)-C(8B)-H(8B)	115.8(17)
C(8B)-C(1B)-H(1B)	115.7(18)	C(7B)-C(8B)-H(8B)	116.3(18)
C(2B)-C(1B)-H(1B)	117.2(18)	Pt(2)-C(8B)-H(8B)	103(2)
Pt(2)-C(1B)-H(1B)	100.8(19)	C(14B)-C(9B)-C(10B)	114.8(2)
C(1B)-C(2B)-C(3B)	113.3(2)	C(14B)-C(9B)-Pt(2)	122.10(17)
C(1B)-C(2B)-H(2B1)	109(3)	C(10B)-C(9B)-Pt(2)	123.06(16)
C(3B)-C(2B)-H(2B1)	106(2)	F(1B)-C(10B)-C(11B)	117.1(2)
C(1B)-C(2B)-H(2B2)	106(2)	F(1B)-C(10B)-C(9B)	119.6(2)
C(3B)-C(2B)-H(2B2)	114(2)	C(11B)-C(10B)-C(9B)	123.3(2)
H(2B1)-C(2B)-H(2B2)	109(3)	F(2B)-C(11B)-C(10B)	121.4(2)
C(4B)-C(3B)-C(2B)	114.1(2)	F(2B)-C(11B)-C(12B)	119.0(3)
C(4B)-C(3B)-H(3B1)	110.6(18)	C(10B)-C(11B)-C(12B)	119.5(2)
C(2B)-C(3B)-H(3B1)	112(2)	F(3B)-C(12B)-C(11B)	120.2(3)
C(4B)-C(3B)-H(3B2)	101.8(19)	F(3B)-C(12B)-C(13B)	120.1(3)
C(2B)-C(3B)-H(3B2)	107(2)	C(11B)-C(12B)-C(13B)	119.7(3)
H(3B1)-C(3B)-H(3B2)	110(3)	F(4B)-C(13B)-C(12B)	120.0(3)
C(5B)-C(4B)-C(3B)	127.4(2)	F(4B)-C(13B)-C(14B)	121.3(2)
C(5B)-C(4B)-Pt(2)	73.14(16)	C(12B)-C(13B)-C(14B)	118.7(2)
C(3B)-C(4B)-Pt(2)	105.50(17)	F(5B)-C(14B)-C(13B)	116.0(2)
C(5B)-C(4B)-H(4B)	117.0(17)	F(5B)-C(14B)-C(9B)	120.1(2)
C(3B)-C(4B)-H(4B)	114.4(17)	C(13B)-C(14B)-C(9B)	123.9(2)
Pt(2)-C(4B)-H(4B)	103(2)	C(16B)-C(15B)-C(20B)	114.37(19)
C(4B)-C(5B)-C(6B)	125.6(2)	C(16B)-C(15B)-Pt(2)	122.78(14)
C(4B)-C(5B)-Pt(2)	70.98(16)	C(20B)-C(15B)-Pt(2)	122.79(16)
C(6B)-C(5B)-Pt(2)	110.06(17)	F(6B)-C(16B)-C(17B)	116.06(18)
C(4B)-C(5B)-H(5B)	120.1(16)	F(6B)-C(16B)-C(15B)	119.90(19)
C(6B)-C(5B)-H(5B)	112.8(16)	C(17B)-C(16B)-C(15B)	124.04(18)
Pt(2)-C(5B)-H(5B)	102.4(18)	F(7B)-C(17B)-C(16B)	120.94(18)
C(5B)-C(6B)-C(7B)	114.5(2)	F(7B)-C(17B)-C(18B)	120.0(2)
C(5B)-C(6B)-H(6B1)	111(2)	C(16B)-C(17B)-C(18B)	119.05(19)
C(7B)-C(6B)-H(6B1)	107(2)	F(8B)-C(18B)-C(19B)	120.86(19)
C(5B)-C(6B)-H(6B2)	108.5(16)	F(8B)-C(18B)-C(17B)	120.0(2)
C(7B)-C(6B)-H(6B2)	112.0(15)	C(19B)-C(18B)-C(17B)	119.1(2)
H(6B1)-C(6B)-H(6B2)	103(3)	F(9B)-C(19B)-C(18B)	119.7(2)
C(8B)-C(7B)-C(6B)	114.0(2)	F(9B)-C(19B)-C(20B)	120.37(19)
C(8B)-C(7B)-H(7B1)	108.7(17)	C(18B)-C(19B)-C(20B)	119.91(18)
C(6B)-C(7B)-H(7B1)	109.5(19)	F(10B)-C(20B)-C(19B)	116.90(17)
C(8B)-C(7B)-H(7B2)	109.8(19)	F(10B)-C(20B)-C(15B)	119.59(19)
C(6B)-C(7B)-H(7B2)	107.7(19)	C(19B)-C(20B)-C(15B)	123.51(19)
H(7B1)-C(7B)-H(7B2)	107(3)		

Table 5. Anisotropic displacement parameters ($\text{\AA}^2 \times 10^4$) for (COD)Pt^{II}(C₆F₅)₂ (CCDC 694649). The anisotropic displacement factor exponent takes the form: $-2\pi^2 [h^2 a^{*2} U^{11} + \dots + 2 h k a^* b^* U^{12}]$.

	U ¹¹	U ²²	U ³³	U ²³	U ¹³	U ¹²
Pt(1)	105(1)	137(1)	104(1)	-3(1)	-3(1)	2(1)
F(1A)	328(10)	160(5)	175(6)	27(4)	44(6)	32(5)
F(2A)	345(10)	223(5)	211(7)	-40(5)	77(7)	74(6)
F(3A)	267(9)	344(6)	141(6)	18(5)	77(6)	31(6)
F(4A)	333(10)	242(5)	222(7)	68(5)	73(7)	-70(6)
F(5A)	339(10)	159(5)	229(7)	-33(5)	52(7)	-44(5)
F(6A)	165(7)	175(5)	234(7)	11(5)	-22(6)	-42(5)
F(7A)	226(8)	190(5)	254(7)	44(5)	-18(6)	43(5)
F(8A)	141(7)	325(6)	220(6)	-5(5)	-55(6)	29(6)
F(9A)	138(7)	266(6)	263(7)	-47(5)	-7(6)	-74(5)
F(10A)	225(8)	163(5)	297(8)	50(5)	-17(7)	-27(5)
C(1A)	119(10)	239(7)	179(10)	-10(7)	-20(9)	-11(7)
C(2A)	188(12)	245(9)	318(13)	7(9)	-10(10)	-46(9)
C(3A)	164(12)	269(9)	266(12)	69(9)	7(10)	-16(8)
C(4A)	140(11)	243(8)	146(9)	34(7)	14(8)	28(7)
C(5A)	176(12)	270(9)	126(9)	-43(7)	-6(9)	31(8)
C(6A)	249(14)	232(8)	266(12)	-76(8)	-9(11)	59(9)
C(7A)	238(14)	208(8)	225(11)	7(8)	-1(10)	71(8)
C(8A)	160(11)	225(8)	166(10)	12(7)	-45(9)	37(7)
C(9A)	131(9)	174(7)	122(8)	9(6)	-12(7)	-17(7)
C(10A)	164(10)	160(6)	139(8)	23(7)	11(8)	17(8)
C(11A)	185(11)	192(7)	148(9)	-20(7)	14(8)	48(8)
C(12A)	157(11)	256(8)	114(8)	8(6)	33(9)	30(8)
C(13A)	177(12)	201(7)	153(9)	43(7)	2(9)	-50(8)
C(14A)	166(11)	167(7)	163(9)	-14(7)	-13(8)	-27(7)
C(15A)	134(10)	181(6)	106(8)	-4(6)	-13(8)	7(7)
C(16A)	110(11)	177(7)	151(9)	-13(6)	-5(8)	-4(6)
C(17A)	176(11)	167(7)	150(9)	17(7)	-11(8)	27(7)
C(18A)	98(10)	250(8)	136(8)	-29(7)	-9(7)	25(7)
C(19A)	135(9)	205(7)	140(8)	-26(7)	11(8)	-44(9)
C(20A)	147(11)	151(6)	163(9)	21(6)	25(8)	11(6)
Pt(2)	134(1)	192(1)	102(1)	22(1)	7(1)	-7(1)
F(1B)	322(10)	214(5)	243(7)	-47(5)	11(7)	12(6)
F(2B)	279(10)	414(8)	391(10)	117(7)	94(8)	177(7)
F(3B)	156(9)	741(10)	348(10)	192(9)	-81(8)	-29(8)
F(4B)	493(12)	460(8)	256(8)	11(7)	-212(8)	-162(8)
F(5B)	426(10)	273(6)	203(7)	-79(5)	-59(7)	81(6)
F(6B)	265(9)	185(5)	194(7)	-28(5)	33(6)	-47(5)
F(7B)	350(10)	316(6)	125(6)	-25(5)	78(7)	-15(6)
F(8B)	258(9)	347(6)	204(7)	87(5)	71(6)	-67(6)
F(9B)	318(10)	213(5)	281(8)	15(5)	-24(7)	-110(6)
F(10B)	350(9)	248(5)	158(6)	-59(5)	18(7)	-33(6)
C(1B)	196(13)	245(9)	220(12)	81(8)	38(10)	-22(8)
C(2B)	207(14)	271(9)	320(13)	24(9)	40(11)	-57(9)
C(3B)	210(15)	342(10)	272(13)	-34(9)	-31(11)	-57(10)
C(4B)	151(12)	334(10)	154(10)	18(8)	-4(8)	-29(8)

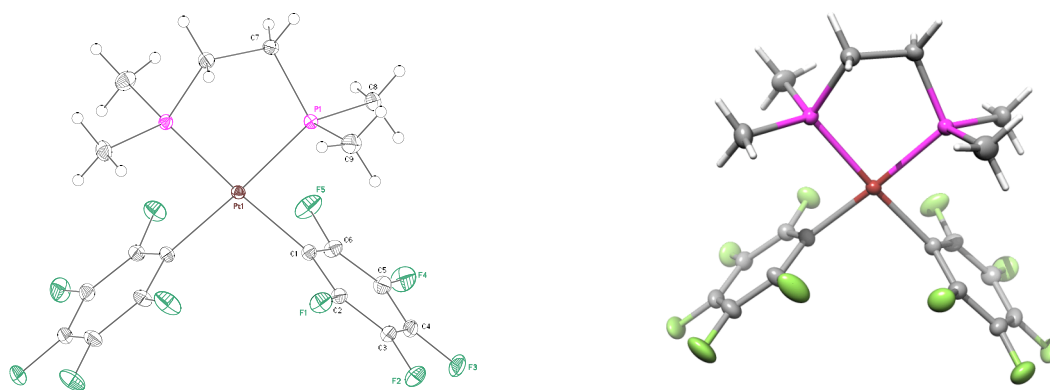
C(5B)	163(11)	280(9)	206(10)	48(8)	-3(10)	17(9)
C(6B)	179(13)	299(10)	249(12)	25(9)	39(10)	27(9)
C(7B)	218(13)	350(10)	154(9)	-3(8)	32(10)	-10(10)
C(8B)	185(13)	336(10)	142(10)	68(8)	23(9)	-27(9)
C(9B)	153(10)	191(7)	128(8)	32(6)	3(8)	-11(7)
C(10B)	176(12)	197(7)	157(9)	33(7)	27(8)	-13(7)
C(11B)	166(12)	286(9)	232(11)	112(9)	61(10)	45(9)
C(12B)	143(12)	476(13)	209(11)	179(10)	-16(10)	-61(10)
C(13B)	271(15)	324(9)	182(10)	59(9)	-67(11)	-96(9)
C(14B)	258(14)	214(8)	136(9)	17(7)	-20(9)	-12(8)
C(15B)	126(10)	182(7)	116(8)	18(6)	4(8)	8(6)
C(16B)	179(12)	156(6)	137(9)	-3(6)	1(8)	-1(7)
C(17B)	180(11)	221(7)	123(8)	-7(6)	46(9)	15(7)
C(18B)	167(12)	242(8)	166(10)	66(7)	25(9)	-11(8)
C(19B)	179(12)	181(7)	183(9)	23(7)	-24(9)	-29(7)
C(20B)	165(11)	199(7)	132(8)	-16(6)	3(8)	24(8)

Table 6. Hydrogen coordinates ($\times 10^4$) and isotropic displacement parameters ($\text{\AA}^2 \times 10^3$) for $(\text{COD})\text{Pt}^{\text{II}}(\text{C}_6\text{F}_5)_2$ (CCDC 694649)

	x	y	z	U_{iso}
H(1A)	3050(30)	4394(16)	-447(10)	4(5)
H(2A1)	1290(40)	4070(20)	223(12)	31(8)
H(2A2)	2570(40)	3320(20)	189(14)	37(9)
H(3A1)	1900(30)	4860(20)	904(11)	22(7)
H(3A2)	2310(30)	3679(19)	978(11)	16(7)
H(4A)	4340(30)	4176(18)	1023(10)	14(7)
H(5A)	4980(30)	5912(18)	1030(10)	17(7)
H(6A1)	2880(40)	6910(30)	1028(15)	51(11)
H(6A2)	3970(40)	7330(20)	644(13)	35(9)
H(7A1)	2320(40)	7150(20)	137(13)	34(9)
H(7A2)	1730(30)	6172(17)	441(10)	10(6)
H(8A)	3330(30)	6182(16)	-387(9)	7(5)
H(1B)	1800(30)	7860(20)	7485(11)	19(7)
H(2B1)	3550(40)	8520(30)	7819(14)	46(10)
H(2B2)	4270(40)	7600(20)	7627(12)	24(8)
H(3B1)	4430(40)	7560(20)	8488(13)	35(9)
H(3B2)	2990(40)	7820(20)	8513(12)	27(8)
H(4B)	2950(30)	6150(20)	8714(11)	14(6)
H(5B)	3260(30)	4694(17)	8225(10)	12(6)
H(6B1)	4650(40)	4790(20)	7601(14)	42(10)
H(6B2)	4880(30)	5949(17)	7696(9)	8(5)
H(7B1)	4100(30)	5990(20)	6904(12)	32(8)
H(7B2)	3190(30)	5090(20)	7068(11)	18(6)
H(8B)	1820(30)	6440(18)	7032(12)	17(7)

Appendix B. X-Ray Crystallographic Data for (dmpe)Pt^{II}(C₆F₅)₂

Analogous to (COD)Pt^{II}(CH₃)₂, protonolysis of (dmpe)Pt^{II}(CH₃)₂ with a large excess of B(C₆F₅)₃ in anhydrous TFE-*d*₃, led to the formation of crystals in the reaction flask. X-ray analysis of these crystals found that two perfluorophenyl groups were transferred from B(C₆F₅)₃ to platinum to give (dmpe)Pt^{II}(C₆F₅)₂.



(dmpe)Pt^{II}(C₆F₅)₂

Note: The crystallographic data have been deposited in the Cambridge Database (CCDC) and have been placed on hold pending further instructions from me. The deposition number is 752923. Ideally the CCDC would like the publication to contain a footnote of the type: "Crystallographic data have been deposited at the CCDC, 12 Union Road, Cambridge CB2 1EZ, UK and copies can be obtained on request, free of charge, by quoting the publication citation and the deposition number 752923."

Table 1. Crystal data and structure refinement for (dmpe)Pt^{II}(C₆F₅)₂ (CCDC 752923)


Empirical formula	C ₁₈ H ₁₆ F ₁₀ P ₂ Pt	
Formula weight	679.34	
Crystallization Solvent	Not given	
Crystal Habit	Block	
Crystal size	0.26 x 0.16 x 0.11 mm ³	
Crystal color	Colorless	
Data Collection		
Type of diffractometer	Bruker KAPPA APEX II	
Wavelength	0.71073 Å MoK α	
Data Collection Temperature	100(2) K	
θ range for 9794 reflections used in lattice determination	3.29 to 55.43°	
Unit cell dimensions	a = 19.7412(9) Å b = 8.5890(4) Å c = 13.0546(6) Å	β = 109.971(2)°
Volume	2080.39(17) Å ³	
Z	4	
Crystal system	Monoclinic	
Space group	C2/c	
Density (calculated)	2.169 Mg/m ³	
F(000)	1288	
Data collection program	Bruker APEX2 v2009.7-0	
θ range for data collection	2.20 to 58.06°	
Completeness to θ = 58.06°	98.0 %	
Index ranges	-42 \leq h \leq 46, -19 \leq k \leq 20, -24 \leq l \leq 31	
Data collection scan type	ω scans; 31 settings	
Data reduction program	Bruker SAINT-Plus v7.66A	
Reflections collected	106048	
Independent reflections	14561 [R _{int} = 0.0481]	
Absorption coefficient	6.989 mm ⁻¹	
Absorption correction	Semi-empirical from equivalents	
Max. and min. transmission	0.7514 and 0.5232	

Table 1 (cont.)**Structure Solution and Refinement**

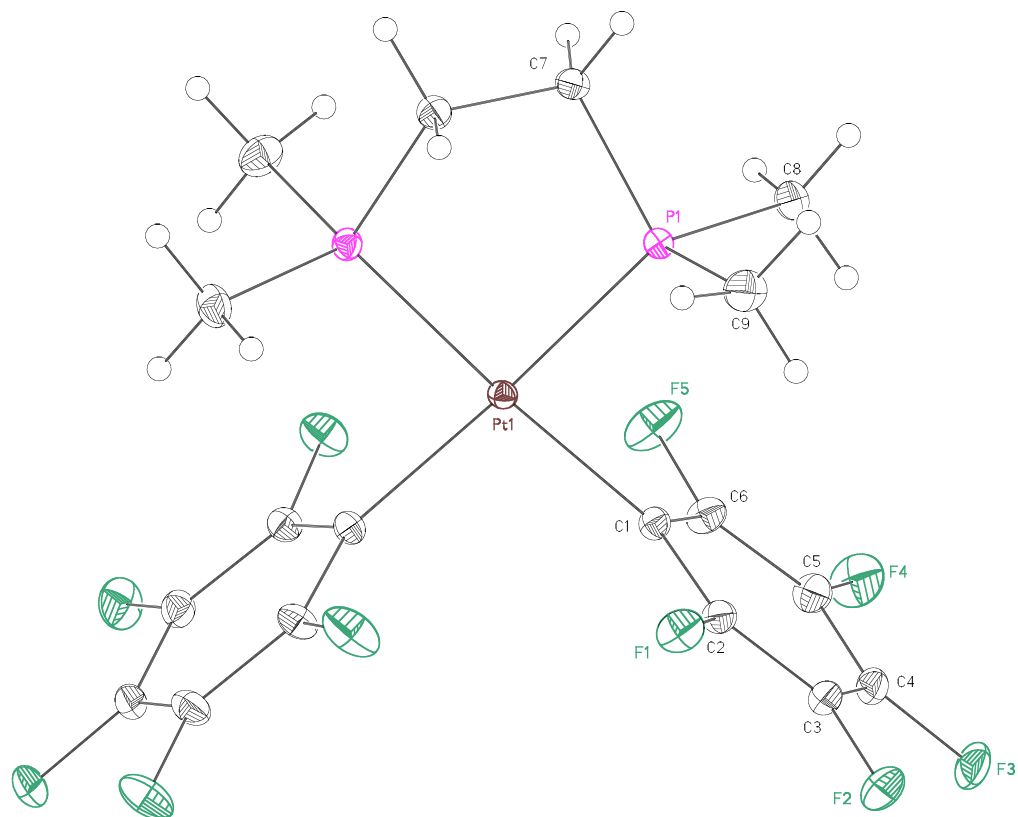
Structure solution program	SHELXS-97 (Sheldrick, 2008)
Primary solution method	Direct methods
Secondary solution method	Difference Fourier map
Hydrogen placement	Difference Fourier map
Structure refinement program	SHELXL-97 (Sheldrick, 2008)
Refinement method	Full matrix least-squares on F^2
Data / restraints / parameters	14561 / 0 / 173
Treatment of hydrogen atoms	Unrestrained
Goodness-of-fit on F^2	1.323
Final R indices [$I > 2\sigma(I)$, 13059 reflections]	$R1 = 0.0203$, $wR2 = 0.0382$
R indices (all data)	$R1 = 0.0265$, $wR2 = 0.0392$
Type of weighting scheme used	Sigma
Weighting scheme used	$w = 1/\sigma^2(Fo^2)$
Max shift/error	0.002
Average shift/error	0.000
Largest diff. peak and hole	3.677 and -1.553 e.Å ⁻³

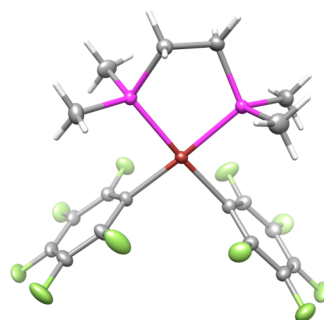
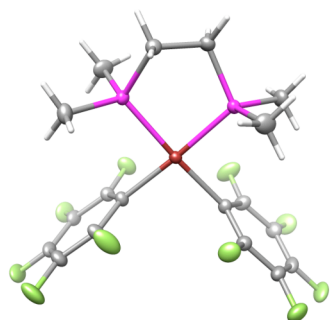
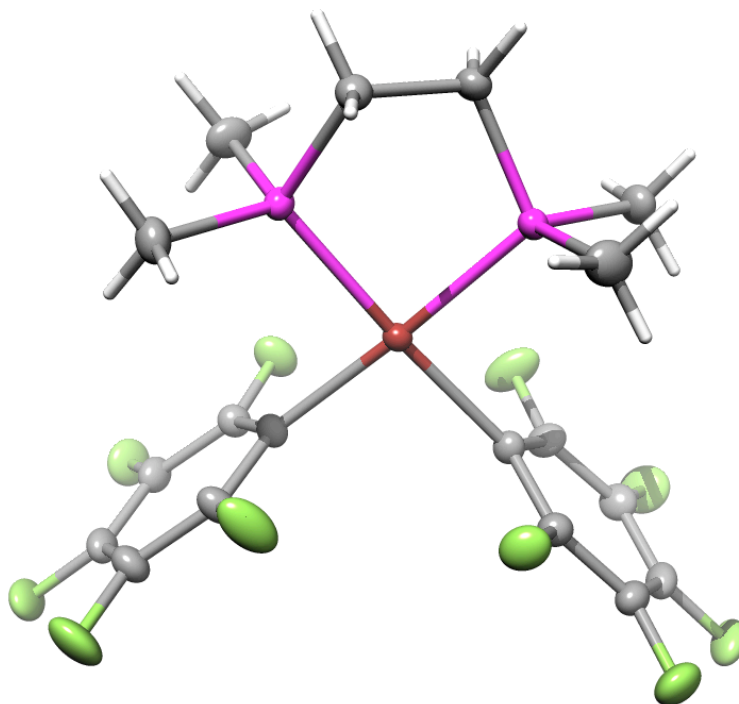
Special Refinement Details

Crystals were mounted on a glass fiber using Paratone oil then placed on the diffractometer under a nitrogen stream at 100K.

Refinement of F^2 against ALL reflections. The weighted R-factor (wR) and goodness of fit (S) are based on F^2 , conventional R-factors (R) are based on F , with F set to zero for negative F^2 . The threshold expression of $F^2 > 2\sigma(F^2)$ is used only for calculating R-factors(gt) etc. and is not relevant to the choice of reflections for refinement. R-factors based on F^2 are statistically about twice as large as those based on F , and R-factors based on ALL data will be even larger.

All esds (except the esd in the dihedral angle between two l.s. planes) are estimated using the full covariance matrix. The cell esds are taken into account individually in the estimation of esds in distances, angles, and torsion angles; correlations between esds in cell parameters are only used when they are defined by crystal symmetry. An approximate (isotropic) treatment of cell esds is used for estimating esds involving l.s. planes.





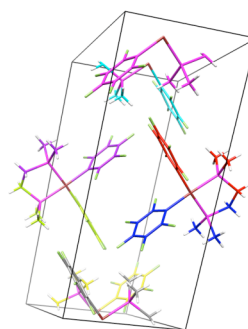
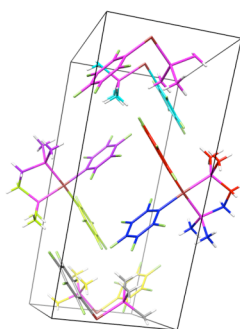
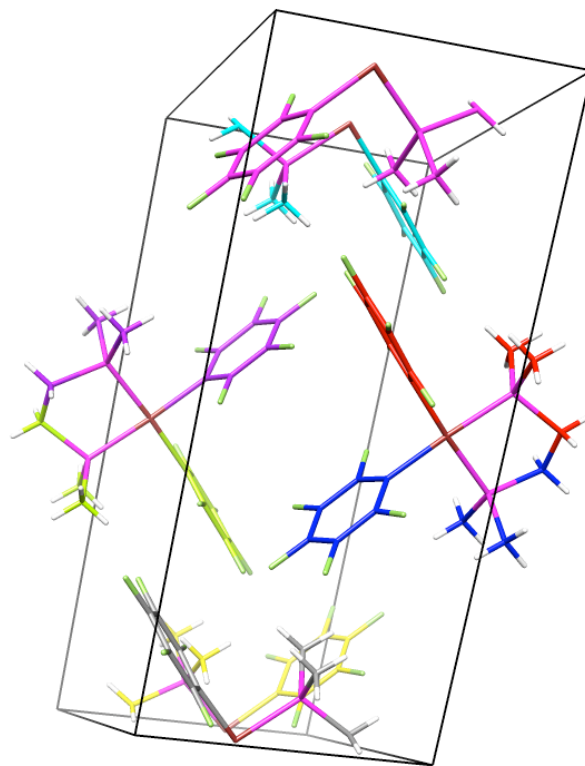


Table 2. Atomic coordinates ($\times 10^4$) and equivalent isotropic displacement parameters ($\text{\AA}^2 \times 10^3$) for $(\text{dmpe})\text{Pt}^{\text{II}}(\text{C}_6\text{F}_5)_2$ (CCDC 752923). $U(\text{eq})$ is defined as the trace of the orthogonalized U^{ij} tensor.

	x	y	z	U_{eq}
Pt(1)	10000	4247(1)	7500	8(1)
P(1)	9233(1)	6167(1)	7559(1)	10(1)
F(1)	8656(1)	2490(1)	5681(1)	18(1)
F(2)	7682(1)	412(1)	5855(1)	22(1)
F(3)	7723(1)	-605(1)	7850(1)	22(1)
F(4)	8758(1)	506(1)	9683(1)	26(1)
F(5)	9742(1)	2542(1)	9521(1)	24(1)
C(1)	9257(1)	2582(1)	7591(1)	11(1)
C(2)	8710(1)	2007(1)	6689(1)	12(1)
C(3)	8193(1)	956(1)	6754(1)	14(1)
C(4)	8207(1)	440(1)	7768(1)	15(1)
C(5)	8737(1)	992(1)	8696(1)	15(1)
C(6)	9243(1)	2034(1)	8582(1)	14(1)
C(7)	9726(1)	8019(1)	7796(1)	12(1)
C(8)	8824(1)	6048(1)	8603(1)	16(1)
C(9)	8485(1)	6428(1)	6290(1)	18(1)

Table 3. Selected bond lengths [Å] and angles [°] for (dmpe)Pt^{II}(C₆F₅)₂ (CCDC 752923)

Pt(1)-C(1)	2.0810(7)	C(1)-Pt(1)-C(1)#1	93.16(4)
Pt(1)-C(1)#1	2.0811(7)	C(1)-Pt(1)-P(1)	90.34(2)
Pt(1)-P(1)	2.2582(2)	C(1)#1-Pt(1)-P(1)	176.35(2)
Pt(1)-P(1)#1	2.2583(2)	C(1)-Pt(1)-P(1)#1	176.35(2)
		C(1)#1-Pt(1)-P(1)#1	90.34(2)
		P(1)-Pt(1)-P(1)#1	86.176(11)

Symmetry transformations used to generate equivalent atoms:

#1 -x+2,y,-z+3/2

Table 4. Bond lengths [Å] and angles [°] for (dmpe)Pt^{II}(C₆F₅)₂ (CCDC 752923)

Pt(1)-C(1)	2.0810(7)	C(9)-P(1)-Pt(1)	113.82(3)
Pt(1)-C(1)#1	2.0811(7)	C(7)-P(1)-Pt(1)	108.40(2)
Pt(1)-P(1)	2.2582(2)	C(6)-C(1)-C(2)	114.40(6)
Pt(1)-P(1)#1	2.2583(2)	C(6)-C(1)-Pt(1)	121.74(5)
P(1)-C(8)	1.8086(8)	C(2)-C(1)-Pt(1)	123.72(5)
P(1)-C(9)	1.8179(7)	F(1)-C(2)-C(3)	116.49(6)
P(1)-C(7)	1.8347(8)	F(1)-C(2)-C(1)	119.79(6)
F(1)-C(2)	1.3485(8)	C(3)-C(2)-C(1)	123.71(6)
F(2)-C(3)	1.3426(9)	F(2)-C(3)-C(2)	121.44(7)
F(3)-C(4)	1.3418(10)	F(2)-C(3)-C(4)	119.16(7)
F(4)-C(5)	1.3417(9)	C(2)-C(3)-C(4)	119.40(6)
F(5)-C(6)	1.3559(8)	F(3)-C(4)-C(5)	120.32(8)
C(1)-C(6)	1.3862(9)	F(3)-C(4)-C(3)	120.47(7)
C(1)-C(2)	1.3891(9)	C(5)-C(4)-C(3)	119.20(7)
C(2)-C(3)	1.3869(11)	F(4)-C(5)-C(6)	121.15(7)
C(3)-C(4)	1.3874(12)	F(4)-C(5)-C(4)	119.92(8)
C(4)-C(5)	1.3868(11)	C(6)-C(5)-C(4)	118.93(7)
C(5)-C(6)	1.3853(11)	F(5)-C(6)-C(5)	116.01(6)
C(7)-C(7)#1	1.5304(15)	F(5)-C(6)-C(1)	119.62(7)
C(7)-H(7A)	0.96(2)	C(5)-C(6)-C(1)	124.36(6)
C(7)-H(7B)	0.986(16)	C(7)#1-C(7)-P(1)	109.94(3)
C(8)-H(8A)	0.93(3)	C(7)#1-C(7)-H(7A)	109.3(14)
C(8)-H(8B)	0.94(2)	P(1)-C(7)-H(7A)	115.2(13)
C(8)-H(8C)	0.95(3)	C(7)#1-C(7)-H(7B)	113.4(11)
C(9)-H(9A)	0.96(2)	P(1)-C(7)-H(7B)	105.3(11)
C(9)-H(9B)	0.94(2)	H(7A)-C(7)-H(7B)	103.6(17)
C(9)-H(9C)	0.97(2)	P(1)-C(8)-H(8A)	110.8(16)
		P(1)-C(8)-H(8B)	110.2(15)
C(1)-Pt(1)-C(1)#1	93.16(4)	H(8A)-C(8)-H(8B)	110.4(19)
C(1)-Pt(1)-P(1)	90.34(2)	P(1)-C(8)-H(8C)	109.9(14)
C(1)#1-Pt(1)-P(1)	176.35(2)	H(8A)-C(8)-H(8C)	107(2)
C(1)-Pt(1)-P(1)#1	176.35(2)	H(8B)-C(8)-H(8C)	108.8(18)
C(1)#1-Pt(1)-P(1)#1	90.34(2)	P(1)-C(9)-H(9A)	108.6(14)
P(1)-Pt(1)-P(1)#1	86.176(11)	P(1)-C(9)-H(9B)	109.6(11)
C(8)-P(1)-C(9)	105.16(4)	H(9A)-C(9)-H(9B)	114(2)
C(8)-P(1)-C(7)	105.65(4)	P(1)-C(9)-H(9C)	112.7(12)
C(9)-P(1)-C(7)	105.37(4)	H(9A)-C(9)-H(9C)	107.2(19)
C(8)-P(1)-Pt(1)	117.51(3)	H(9B)-C(9)-H(9C)	104.5(18)

Symmetry transformations used to generate equivalent atoms:

#1 -x+2,y,-z+3/2

Table 5. Anisotropic displacement parameters ($\text{\AA}^2 \times 10^4$) for $(\text{dmpe})\text{Pt}^{\text{II}}(\text{C}_6\text{F}_5)_2$ (CCDC 752923). The anisotropic displacement factor exponent takes the form: $-2\pi^2 [h^2 a^{*2} U^{11} + \dots + 2 h k a^* b^* U^{12}]$.

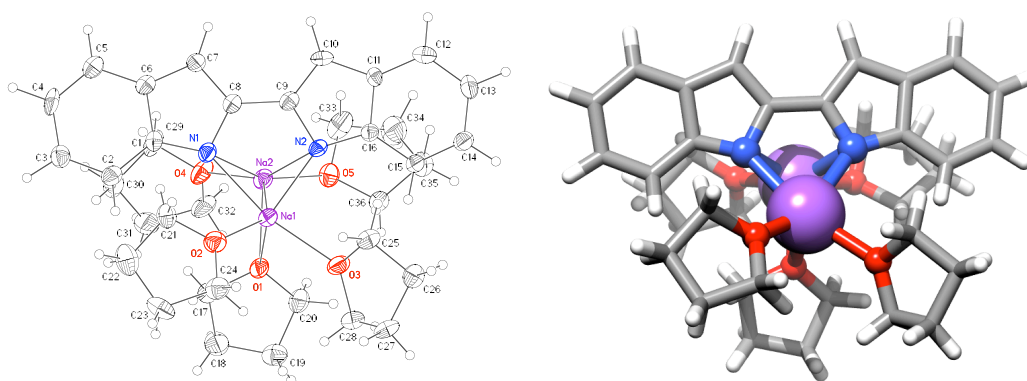
	U^{11}	U^{22}	U^{33}	U^{23}	U^{13}	U^{12}
Pt(1)	98(1)	80(1)	83(1)	0	39(1)	0
P(1)	96(1)	99(1)	108(1)	-9(1)	42(1)	0(1)
F(1)	226(2)	211(3)	107(1)	1(1)	46(1)	-40(2)
F(2)	150(2)	240(3)	228(2)	-54(2)	12(2)	-58(2)
F(3)	156(2)	171(3)	349(3)	34(2)	123(2)	-40(2)
F(4)	351(3)	261(3)	197(2)	63(2)	150(2)	-65(3)
F(5)	301(3)	292(3)	105(2)	6(2)	27(2)	-131(2)
C(1)	114(2)	118(2)	100(2)	0(1)	48(2)	-8(2)
C(2)	130(2)	118(2)	120(2)	-6(2)	46(2)	-8(2)
C(3)	114(2)	127(3)	177(2)	-18(2)	44(2)	-13(2)
C(4)	127(2)	117(2)	218(3)	9(2)	85(2)	-8(2)
C(5)	189(3)	138(3)	161(2)	20(2)	93(2)	-17(2)
C(6)	170(2)	137(3)	113(2)	7(2)	52(2)	-34(2)
C(7)	137(2)	104(2)	135(2)	-14(2)	60(2)	-3(2)
C(8)	162(2)	174(3)	181(2)	-25(2)	103(2)	-15(2)
C(9)	157(2)	182(3)	163(2)	0(2)	6(2)	18(2)

Table 6. Hydrogen coordinates ($\times 10^4$) and isotropic displacement parameters ($\text{\AA}^2 \times 10^3$) for $(\text{dmpe})\text{Pt}^{\text{II}}(\text{C}_6\text{F}_5)_2$ (CCDC 752923)

	x	y	z	U_{iso}
H(7A)	9430(12)	8930(30)	7595(18)	28(5)
H(7B)	9948(9)	8110(20)	8595(13)	18(4)
H(8A)	8533(13)	6910(30)	8575(19)	45(7)
H(8B)	9181(13)	5970(20)	9294(18)	28(5)
H(8C)	8520(12)	5160(30)	8484(17)	32(5)
H(9A)	8195(14)	5510(30)	6148(19)	34(6)
H(9B)	8664(11)	6700(30)	5730(15)	26(5)
H(9C)	8175(12)	7290(30)	6318(16)	33(5)

Appendix C. X-Ray Crystallographic Data for the Disodium Salt of 2,2'-Biindolyl

The disodium salt of 2,2'-biindolyl was generated by deprotonation of 2,2'-biindolyl with excess sodium hydride in tetrahydrofuran (THF). Excess sodium hydride was removed by filtration through celite, and the compound was recrystallized from a 1:1 mixture of THF and diethyl ether. X-ray analysis gave a very interesting structure.



Disodium Salt of 2,2'-Biindolyl

Note: The crystallographic data have been deposited in the Cambridge Database (CCDC) and have been placed on hold pending further instructions from me. The deposition number is 737620. Ideally the CCDC would like the publication to contain a footnote of the type: "Crystallographic data have been deposited at the CCDC, 12 Union Road, Cambridge CB2 1EZ, UK and copies can be obtained on request, free of charge, by quoting the publication citation and the deposition number 737620."

Table 1. Crystal data and structure refinement for the disodium salt of 2,2'-biindolyl (CCDC 737620)

Empirical formula	$C_{36}H_{50}N_2O_5Na_2$
Formula weight	636.76
Crystallization Solvent	Not given
Crystal Habit	Fragment
Crystal size	0.37 x 0.26 x 0.22 mm ³
Crystal color	Colorless

**Data Collection**

Type of diffractometer	Bruker KAPPA APEX II	
Wavelength	0.71073 Å MoK α	
Data Collection Temperature	100(2) K	
θ range for 8939 reflections used in lattice determination	2.50 to 23.28°	
Unit cell dimensions	a = 9.9039(9) Å b = 10.6892(10) Å c = 16.6715(15) Å	α = 100.643(4)° β = 93.452(4)° γ = 98.373(4)°
Volume	1709.2(3) Å ³	
Z	2	
Crystal system	Triclinic	
Space group	P-1	
Density (calculated)	1.237 Mg/m ³	
F(000)	684	
Data collection program	Bruker APEX2 v2.1-0	
θ range for data collection	1.96 to 25.27°	
Completeness to $\theta = 25.27^\circ$	89.4 %	
Index ranges	-11 ≤ h ≤ 11, -12 ≤ k ≤ 12, 0 ≤ l ≤ 19	
Data collection scan type	ω scans; 11 settings	
Data reduction program	Bruker SAINT-Plus v7.34A	
Reflections collected	5541	
Independent reflections	5541 [R _{int} = 0.0000]	
Absorption coefficient	0.103 mm ⁻¹	
Absorption correction	Semi-empirical from equivalents	
Max. and min. transmission	0.7452 and 0.6211	

Table 1 (cont.)**Structure Solution and Refinement**

Structure solution program	SHELXS-97 (Sheldrick, 2008)
Primary solution method	Direct methods
Secondary solution method	Difference Fourier map
Hydrogen placement	Difference Fourier map
Structure refinement program	SHELXL-97 (Sheldrick, 2008)
Refinement method	Full matrix least-squares on F^2
Data / restraints / parameters	5541 / 0 / 607
Treatment of hydrogen atoms	Unrestrained
Goodness-of-fit on F^2	1.836
Final R indices [$I > 2\sigma(I)$, 3576 reflections]	$R_1 = 0.0566$, $wR_2 = 0.0769$
R indices (all data)	$R_1 = 0.1247$, $wR_2 = 0.0835$
Type of weighting scheme used	Sigma
Weighting scheme used	$w = 1/\sigma^2(F_o^2)$
Max shift/error	0.002
Average shift/error	0.000
Largest diff. peak and hole	0.353 and -0.403 e.Å ⁻³

Special Refinement Details

Crystals were mounted in a loop using Paratone oil then placed on the diffractometer under a nitrogen stream at 100K.

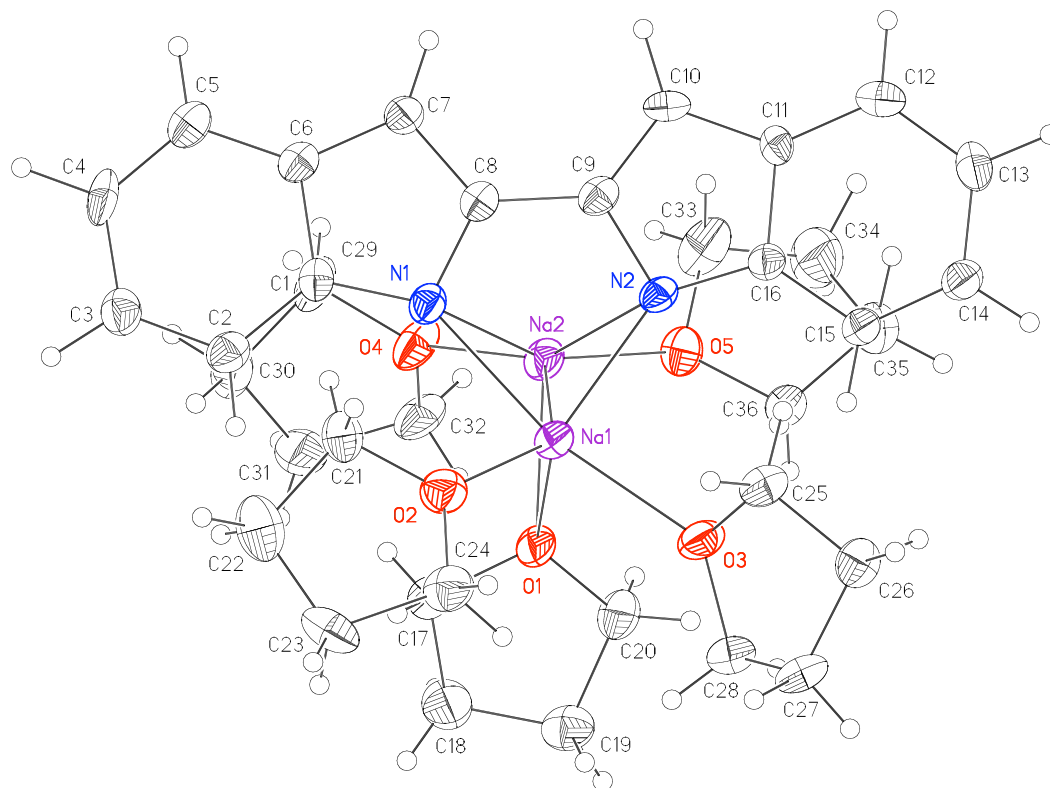
The crystals are twinned, containing two major components in an approximate 2:1 ratio. The transformation matrix for the components is shown below as is the summary from TWINABS.

Twin Law, Sample 1 of 1
 Transforms h1.1(1)->h1.2(2)
 0.07054 -0.92820 -0.07153
 -1.07235 -0.06955 0.07096
 0.00224 -0.00029 -0.99996

7364 data (2190 unique) involve domain 1 only, mean I/sigma 9.2
 7334 data (2159 unique) involve domain 2 only, mean I/sigma 6.0
 15098 data (4489 unique) involve 2 domains, mean I/sigma 8.7
 1 data (1 unique) involve 3 domains, mean I/sigma -0.3

TWINABS was used to prepare an HKLF5 type file for least-squares refinement against both components. No restraints were applied to hydrogen atoms; two hydrogen atoms refined to small displacement parameters..

Refinement of F^2 against ALL reflections. The weighted R-factor (wR) and goodness of fit (S) are based on F^2 , conventional R-factors (R) are based on F , with F set to zero for negative F^2 . The threshold expression of $F^2 > 2\sigma(F^2)$ is used only for calculating R-factors(gt) etc. and is not relevant to the choice of reflections for refinement. R-factors based on F^2 are statistically about twice as large as those based on F , and R-factors based on ALL data will be even larger.



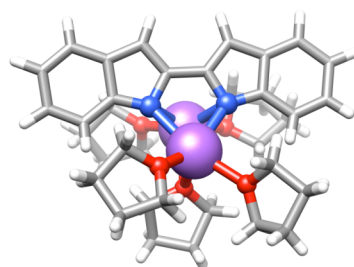
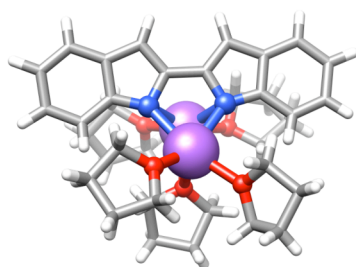
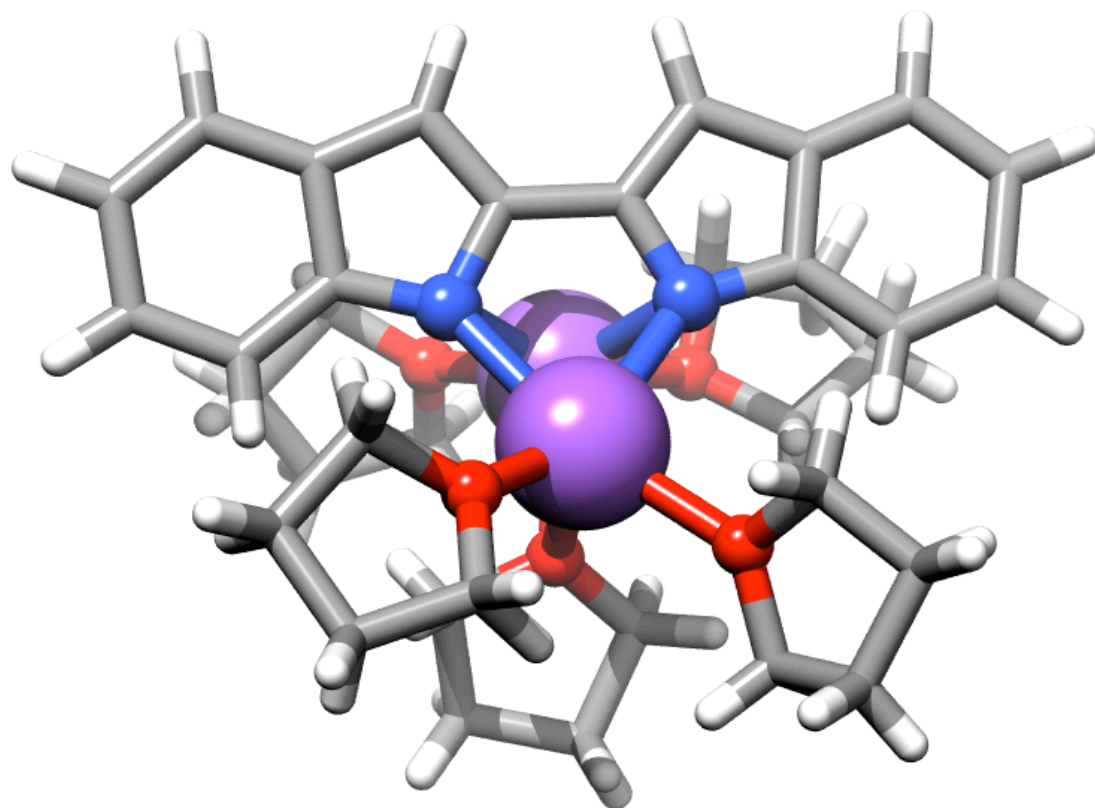


Table 2. Atomic coordinates ($\times 10^4$) and equivalent isotropic displacement parameters ($\text{\AA}^2 \times 10^3$) for the disodium salt of 2,2'-biindolyl (CCDC 737620). $U(\text{eq})$ is defined as the trace of the orthogonalized U^{ij} tensor.

	x	y	z	U_{eq}
Na(1)	5622(1)	3567(1)	3398(1)	26(1)
Na(2)	6507(1)	4332(1)	1831(1)	27(1)
O(1)	7214(2)	2647(2)	2429(2)	30(1)
O(2)	4075(2)	2144(2)	3868(2)	33(1)
O(3)	7046(2)	3857(2)	4625(1)	33(1)
O(4)	6137(2)	3520(2)	468(1)	34(1)
O(5)	8472(2)	5598(2)	1625(1)	32(1)
N(1)	4179(3)	3756(3)	2186(2)	24(1)
N(2)	6115(3)	5691(3)	3173(2)	21(1)
C(1)	3076(3)	3062(4)	1665(2)	21(1)
C(2)	2748(4)	1741(4)	1405(2)	28(1)
C(3)	1587(4)	1222(4)	872(2)	31(1)
C(4)	745(4)	2043(4)	603(2)	34(1)
C(5)	1070(4)	3358(4)	848(2)	30(1)
C(6)	2231(3)	3916(4)	1386(2)	23(1)
C(7)	2871(4)	5163(4)	1752(2)	24(1)
C(8)	4036(3)	5040(4)	2221(2)	20(1)
C(9)	5051(3)	6047(4)	2711(2)	23(1)
C(10)	5185(4)	7366(4)	2780(2)	24(1)
C(11)	6378(3)	7918(4)	3309(2)	20(1)
C(12)	7088(4)	9157(4)	3598(2)	29(1)
C(13)	8290(4)	9337(4)	4116(2)	30(1)
C(14)	8773(4)	8271(4)	4340(2)	28(1)
C(15)	8093(4)	7053(4)	4067(2)	28(1)
C(16)	6910(3)	6844(4)	3531(2)	22(1)
C(17)	6663(4)	1355(4)	1991(3)	34(1)
C(18)	7896(4)	647(5)	1821(3)	43(1)
C(19)	9001(4)	1413(4)	2461(3)	35(1)
C(20)	8706(4)	2776(4)	2551(3)	35(1)
C(21)	2637(4)	1765(4)	3571(3)	31(1)
C(22)	2389(5)	318(5)	3446(3)	48(1)
C(23)	3448(5)	8(4)	4067(3)	40(1)
C(24)	4307(5)	1316(4)	4425(3)	36(1)
C(25)	6720(4)	4756(5)	5327(2)	31(1)
C(26)	7864(4)	4847(4)	5983(3)	32(1)
C(27)	8136(5)	3466(4)	5831(3)	35(1)
C(28)	8035(5)	3128(5)	4903(3)	35(1)
C(29)	4953(4)	3221(4)	-120(2)	32(1)
C(30)	4972(4)	1841(4)	-540(3)	40(1)
C(31)	6512(5)	1764(5)	-544(3)	44(1)
C(32)	7210(4)	3004(5)	20(3)	37(1)
C(33)	8296(5)	6698(5)	1309(3)	46(1)
C(34)	9678(5)	7543(5)	1480(3)	54(1)
C(35)	10133(5)	7365(5)	2298(3)	49(1)
C(36)	9578(4)	5962(4)	2276(3)	34(1)

Table 3. Bond lengths [Å] and angles [°] for the disodium salt of 2,2'-biindolyl (CCDC 737620)

Na(1)-O(2)	2.276(3)	C(14)-C(15)	1.359(5)
Na(1)-O(3)	2.357(3)	C(14)-H(14)	0.97(3)
Na(1)-N(2)	2.356(3)	C(15)-C(16)	1.394(5)
Na(1)-N(1)	2.461(3)	C(15)-H(15)	0.95(3)
Na(1)-O(1)	2.497(2)	C(17)-C(18)	1.541(6)
Na(1)-Na(2)	3.0205(18)	C(17)-H(17A)	0.87(3)
Na(2)-O(4)	2.265(3)	C(17)-H(17B)	1.04(3)
Na(2)-O(5)	2.285(3)	C(18)-C(19)	1.510(6)
Na(2)-O(1)	2.383(3)	C(18)-H(18A)	0.95(4)
Na(2)-N(1)	2.436(3)	C(18)-H(18B)	1.04(3)
Na(2)-N(2)	2.518(3)	C(19)-C(20)	1.509(5)
Na(2)-C(8)	2.745(3)	C(19)-H(19A)	1.06(3)
Na(2)-C(9)	2.762(4)	C(19)-H(19B)	0.95(3)
O(1)-C(17)	1.449(5)	C(20)-H(20A)	1.07(4)
O(1)-C(20)	1.462(4)	C(20)-H(20B)	1.11(3)
O(2)-C(24)	1.427(5)	C(21)-C(22)	1.503(6)
O(2)-C(21)	1.453(4)	C(21)-H(21A)	1.06(3)
O(3)-C(28)	1.444(4)	C(21)-H(21B)	0.90(3)
O(3)-C(25)	1.456(4)	C(22)-C(23)	1.543(6)
O(4)-C(29)	1.439(4)	C(22)-H(22A)	1.00(4)
O(4)-C(32)	1.451(4)	C(22)-H(22B)	0.94(3)
O(5)-C(33)	1.403(5)	C(23)-C(24)	1.523(6)
O(5)-C(36)	1.451(4)	C(23)-H(23A)	1.05(3)
N(1)-C(1)	1.382(4)	C(23)-H(23B)	0.82(4)
N(1)-C(8)	1.392(4)	C(24)-H(24A)	1.09(4)
N(2)-C(16)	1.373(4)	C(24)-H(24B)	0.98(3)
N(2)-C(9)	1.406(4)	C(25)-C(26)	1.506(5)
C(1)-C(2)	1.383(5)	C(25)-H(25A)	1.03(3)
C(1)-C(6)	1.443(5)	C(25)-H(25B)	1.01(3)
C(2)-C(3)	1.388(5)	C(26)-C(27)	1.517(6)
C(2)-H(2)	0.91(3)	C(26)-H(26A)	0.97(3)
C(3)-C(4)	1.407(5)	C(26)-H(26B)	1.08(3)
C(3)-H(3)	1.01(3)	C(27)-C(28)	1.515(5)
C(4)-C(5)	1.373(5)	C(27)-H(27A)	0.89(4)
C(4)-H(4)	1.05(3)	C(27)-H(27B)	1.08(4)
C(5)-C(6)	1.400(5)	C(28)-H(28A)	1.11(3)
C(5)-H(5)	0.97(3)	C(28)-H(28B)	0.90(4)
C(6)-C(7)	1.400(5)	C(29)-C(30)	1.514(5)
C(7)-C(8)	1.391(5)	C(29)-H(29A)	1.08(3)
C(7)-H(7)	0.96(3)	C(29)-H(29B)	1.03(3)
C(8)-C(9)	1.448(4)	C(30)-C(31)	1.540(6)
C(9)-C(10)	1.379(5)	C(30)-H(30A)	0.99(3)
C(10)-C(11)	1.414(5)	C(30)-H(30B)	1.09(3)
C(10)-H(10)	0.99(3)	C(31)-C(32)	1.521(6)
C(11)-C(12)	1.390(5)	C(31)-H(31A)	0.91(4)
C(11)-C(16)	1.429(5)	C(31)-H(31B)	0.99(3)
C(12)-C(13)	1.396(5)	C(32)-H(32A)	0.90(3)
C(12)-H(12)	0.97(3)	C(32)-H(32B)	1.09(4)
C(13)-C(14)	1.401(5)	C(33)-C(34)	1.506(6)
C(13)-H(13)	1.00(3)	C(33)-H(33A)	1.07(3)

C(33)-H(33B)	0.90(3)	C(17)-O(1)-Na(2)	114.8(2)
C(34)-C(35)	1.465(6)	C(20)-O(1)-Na(2)	112.0(2)
C(34)-H(34A)	0.94(4)	C(17)-O(1)-Na(1)	112.6(2)
C(34)-H(34B)	1.03(4)	C(20)-O(1)-Na(1)	128.0(2)
C(35)-C(36)	1.512(6)	Na(2)-O(1)-Na(1)	76.45(7)
C(35)-H(35A)	1.14(5)	C(24)-O(2)-C(21)	104.7(3)
C(35)-H(35B)	0.96(3)	C(24)-O(2)-Na(1)	128.9(2)
C(36)-H(36A)	0.93(3)	C(21)-O(2)-Na(1)	126.0(2)
C(36)-H(36B)	1.06(4)	C(28)-O(3)-C(25)	108.5(3)
		C(28)-O(3)-Na(1)	132.8(2)
O(2)-Na(1)-O(3)	89.98(10)	C(25)-O(3)-Na(1)	117.1(2)
O(2)-Na(1)-N(2)	144.60(11)	C(29)-O(4)-C(32)	104.3(3)
O(3)-Na(1)-N(2)	97.53(11)	C(29)-O(4)-Na(2)	134.7(2)
O(2)-Na(1)-N(1)	97.04(10)	C(32)-O(4)-Na(2)	120.5(2)
O(3)-Na(1)-N(1)	168.07(11)	C(33)-O(5)-C(36)	108.1(3)
N(2)-Na(1)-N(1)	71.22(10)	C(33)-O(5)-Na(2)	115.9(2)
O(2)-Na(1)-O(1)	117.13(10)	C(36)-O(5)-Na(2)	119.1(2)
O(3)-Na(1)-O(1)	98.28(9)	C(1)-N(1)-C(8)	104.7(3)
N(2)-Na(1)-O(1)	96.03(9)	C(1)-N(1)-Na(2)	126.8(2)
N(1)-Na(1)-O(1)	87.13(9)	C(8)-N(1)-Na(2)	87.17(19)
O(2)-Na(1)-Na(2)	141.66(8)	C(1)-N(1)-Na(1)	139.7(2)
O(3)-Na(1)-Na(2)	125.23(8)	C(8)-N(1)-Na(1)	109.6(2)
N(2)-Na(1)-Na(2)	54.17(7)	Na(2)-N(1)-Na(1)	76.17(9)
N(1)-Na(1)-Na(2)	51.54(7)	C(16)-N(2)-C(9)	104.0(3)
O(1)-Na(1)-Na(2)	50.08(6)	C(16)-N(2)-Na(1)	139.2(2)
O(4)-Na(2)-O(5)	90.20(10)	C(9)-N(2)-Na(1)	113.3(2)
O(4)-Na(2)-O(1)	105.57(10)	C(16)-N(2)-Na(2)	124.5(2)
O(5)-Na(2)-O(1)	106.13(10)	C(9)-N(2)-Na(2)	84.40(19)
O(4)-Na(2)-N(1)	97.88(10)	Na(1)-N(2)-Na(2)	76.51(9)
O(5)-Na(2)-N(1)	159.08(11)	N(1)-C(1)-C(2)	128.4(3)
O(1)-Na(2)-N(1)	90.31(10)	N(1)-C(1)-C(6)	110.7(3)
O(4)-Na(2)-N(2)	156.03(10)	C(2)-C(1)-C(6)	120.8(4)
O(5)-Na(2)-N(2)	96.29(10)	C(3)-C(2)-C(1)	119.9(4)
O(1)-Na(2)-N(2)	94.77(10)	C(3)-C(2)-H(2)	116(2)
N(1)-Na(2)-N(2)	68.97(9)	C(1)-C(2)-H(2)	123(2)
O(4)-Na(2)-C(8)	103.07(10)	C(2)-C(3)-C(4)	119.8(4)
O(5)-Na(2)-C(8)	128.84(12)	C(2)-C(3)-H(3)	126.3(17)
O(1)-Na(2)-C(8)	116.80(10)	C(4)-C(3)-H(3)	113.6(17)
N(1)-Na(2)-C(8)	30.42(10)	C(5)-C(4)-C(3)	120.9(4)
N(2)-Na(2)-C(8)	55.38(10)	C(5)-C(4)-H(4)	119.8(14)
O(4)-Na(2)-C(9)	125.59(11)	C(3)-C(4)-H(4)	119.3(14)
O(5)-Na(2)-C(9)	103.89(11)	C(4)-C(5)-C(6)	120.9(4)
O(1)-Na(2)-C(9)	119.48(11)	C(4)-C(5)-H(5)	121(2)
N(1)-Na(2)-C(9)	55.88(11)	C(6)-C(5)-H(5)	117(2)
N(2)-Na(2)-C(9)	30.44(9)	C(5)-C(6)-C(7)	136.8(4)
C(8)-Na(2)-C(9)	30.48(9)	C(5)-C(6)-C(1)	117.7(4)
O(4)-Na(2)-Na(1)	137.57(8)	C(7)-C(6)-C(1)	105.5(3)
O(5)-Na(2)-Na(1)	128.90(8)	C(8)-C(7)-C(6)	107.1(4)
O(1)-Na(2)-Na(1)	53.47(6)	C(8)-C(7)-H(7)	120.6(19)
N(1)-Na(2)-Na(1)	52.29(7)	C(6)-C(7)-H(7)	132.2(19)
N(2)-Na(2)-Na(1)	49.32(7)	N(1)-C(8)-C(7)	112.0(3)
C(8)-Na(2)-Na(1)	67.42(8)	N(1)-C(8)-C(9)	119.4(3)
C(9)-Na(2)-Na(1)	66.68(8)	C(7)-C(8)-C(9)	128.5(4)
C(17)-O(1)-C(20)	109.1(3)	N(1)-C(8)-Na(2)	62.41(17)

C(7)-C(8)-Na(2)	133.2(2)	O(2)-C(21)-H(21A)	102.2(17)
C(9)-C(8)-Na(2)	75.4(2)	C(22)-C(21)-H(21A)	117.6(17)
C(10)-C(9)-N(2)	111.9(3)	O(2)-C(21)-H(21B)	107.7(18)
C(10)-C(9)-C(8)	129.5(4)	C(22)-C(21)-H(21B)	106.5(19)
N(2)-C(9)-C(8)	118.6(3)	H(21A)-C(21)-H(21B)	117(3)
C(10)-C(9)-Na(2)	129.1(2)	C(21)-C(22)-C(23)	104.4(4)
N(2)-C(9)-Na(2)	65.15(17)	C(21)-C(22)-H(22A)	116(2)
C(8)-C(9)-Na(2)	74.1(2)	C(23)-C(22)-H(22A)	109(2)
C(9)-C(10)-C(11)	107.3(3)	C(21)-C(22)-H(22B)	107(2)
C(9)-C(10)-H(10)	126(2)	C(23)-C(22)-H(22B)	115(2)
C(11)-C(10)-H(10)	126(2)	H(22A)-C(22)-H(22B)	105(3)
C(12)-C(11)-C(10)	135.8(4)	C(24)-C(23)-C(22)	103.6(4)
C(12)-C(11)-C(16)	119.4(3)	C(24)-C(23)-H(23A)	113.6(18)
C(10)-C(11)-C(16)	104.8(3)	C(22)-C(23)-H(23A)	113.5(17)
C(11)-C(12)-C(13)	119.6(4)	C(24)-C(23)-H(23B)	111(3)
C(11)-C(12)-H(12)	119.3(19)	C(22)-C(23)-H(23B)	115(3)
C(13)-C(12)-H(12)	121.0(19)	H(23A)-C(23)-H(23B)	100(3)
C(14)-C(13)-C(12)	119.9(4)	O(2)-C(24)-C(23)	106.7(4)
C(14)-C(13)-H(13)	119.4(18)	O(2)-C(24)-H(24A)	119(2)
C(12)-C(13)-H(13)	120.7(17)	C(23)-C(24)-H(24A)	110(2)
C(15)-C(14)-C(13)	121.4(4)	O(2)-C(24)-H(24B)	105.6(19)
C(15)-C(14)-H(14)	122(2)	C(23)-C(24)-H(24B)	118(2)
C(13)-C(14)-H(14)	117(2)	H(24A)-C(24)-H(24B)	98(3)
C(14)-C(15)-C(16)	119.8(4)	O(3)-C(25)-C(26)	105.3(3)
C(14)-C(15)-H(15)	126.4(19)	O(3)-C(25)-H(25A)	105.3(18)
C(16)-C(15)-H(15)	113.8(19)	C(26)-C(25)-H(25A)	110.6(17)
N(2)-C(16)-C(15)	128.1(3)	O(3)-C(25)-H(25B)	104.2(17)
N(2)-C(16)-C(11)	112.0(3)	C(26)-C(25)-H(25B)	117.5(19)
C(15)-C(16)-C(11)	119.8(4)	H(25A)-C(25)-H(25B)	113(3)
O(1)-C(17)-C(18)	106.7(3)	C(25)-C(26)-C(27)	100.7(4)
O(1)-C(17)-H(17A)	107(2)	C(25)-C(26)-H(26A)	116.3(17)
C(18)-C(17)-H(17A)	111(2)	C(27)-C(26)-H(26A)	115.1(18)
O(1)-C(17)-H(17B)	108.8(19)	C(25)-C(26)-H(26B)	102.0(16)
C(18)-C(17)-H(17B)	112.4(19)	C(27)-C(26)-H(26B)	117.9(17)
H(17A)-C(17)-H(17B)	111(3)	H(26A)-C(26)-H(26B)	105(2)
C(19)-C(18)-C(17)	102.9(4)	C(28)-C(27)-C(26)	102.0(3)
C(19)-C(18)-H(18A)	107(3)	C(28)-C(27)-H(27A)	113(2)
C(17)-C(18)-H(18A)	106(2)	C(26)-C(27)-H(27A)	112(3)
C(19)-C(18)-H(18B)	107.1(17)	C(28)-C(27)-H(27B)	112.7(19)
C(17)-C(18)-H(18B)	109.6(17)	C(26)-C(27)-H(27B)	114.4(19)
H(18A)-C(18)-H(18B)	122(3)	H(27A)-C(27)-H(27B)	103(3)
C(20)-C(19)-C(18)	103.6(4)	O(3)-C(28)-C(27)	105.7(3)
C(20)-C(19)-H(19A)	115.4(19)	O(3)-C(28)-H(28A)	106.6(17)
C(18)-C(19)-H(19A)	114.0(19)	C(27)-C(28)-H(28A)	112.6(17)
C(20)-C(19)-H(19B)	105(2)	O(3)-C(28)-H(28B)	112(2)
C(18)-C(19)-H(19B)	114(2)	C(27)-C(28)-H(28B)	107(2)
H(19A)-C(19)-H(19B)	105(3)	H(28A)-C(28)-H(28B)	113(3)
O(1)-C(20)-C(19)	105.1(3)	O(4)-C(29)-C(30)	104.1(3)
O(1)-C(20)-H(20A)	109.9(18)	O(4)-C(29)-H(29A)	110.6(18)
C(19)-C(20)-H(20A)	107.8(19)	C(30)-C(29)-H(29A)	106.2(19)
O(1)-C(20)-H(20B)	106.5(16)	O(4)-C(29)-H(29B)	105.3(17)
C(19)-C(20)-H(20B)	113.4(16)	C(30)-C(29)-H(29B)	105.8(18)
H(20A)-C(20)-H(20B)	114(3)	H(29A)-C(29)-H(29B)	123(2)
O(2)-C(21)-C(22)	104.9(4)	C(29)-C(30)-C(31)	103.2(4)

C(29)-C(30)-H(30A)	108(2)	C(34)-C(33)-H(33B)	110(2)
C(31)-C(30)-H(30A)	114.4(18)	H(33A)-C(33)-H(33B)	110(3)
C(29)-C(30)-H(30B)	106.7(19)	C(35)-C(34)-C(33)	102.4(4)
C(31)-C(30)-H(30B)	116.5(18)	C(35)-C(34)-H(34A)	110(3)
H(30A)-C(30)-H(30B)	107(3)	C(33)-C(34)-H(34A)	121(3)
C(32)-C(31)-C(30)	104.4(4)	C(35)-C(34)-H(34B)	109(2)
C(32)-C(31)-H(31A)	117(3)	C(33)-C(34)-H(34B)	112(2)
C(30)-C(31)-H(31A)	102(3)	H(34A)-C(34)-H(34B)	103(4)
C(32)-C(31)-H(31B)	111.3(19)	C(34)-C(35)-C(36)	102.9(4)
C(30)-C(31)-H(31B)	106.7(17)	C(34)-C(35)-H(35A)	92(3)
H(31A)-C(31)-H(31B)	114(3)	C(36)-C(35)-H(35A)	114(3)
O(4)-C(32)-C(31)	105.7(3)	C(34)-C(35)-H(35B)	119(2)
O(4)-C(32)-H(32A)	109(2)	C(36)-C(35)-H(35B)	115(2)
C(31)-C(32)-H(32A)	107(2)	H(35A)-C(35)-H(35B)	111(4)
O(4)-C(32)-H(32B)	111.5(19)	O(5)-C(36)-C(35)	106.2(3)
C(31)-C(32)-H(32B)	116(2)	O(5)-C(36)-H(36A)	108.9(19)
H(32A)-C(32)-H(32B)	107(3)	C(35)-C(36)-H(36A)	109.2(19)
O(5)-C(33)-C(34)	104.6(4)	O(5)-C(36)-H(36B)	103(2)
O(5)-C(33)-H(33A)	112.7(18)	C(35)-C(36)-H(36B)	120(2)
C(34)-C(33)-H(33A)	110(2)	H(36A)-C(36)-H(36B)	109(3)
O(5)-C(33)-H(33B)	109(3)		

Table 4. Anisotropic displacement parameters ($\text{\AA}^2 \times 10^4$) for the disodium salt of 2,2'-biindolyl (CCDC 737620). The anisotropic displacement factor exponent takes the form: $-2\pi^2 [h^2 a^{*2} U^{11} + \dots + 2 h k a^* b^* U^{12}]$.

	U ¹¹	U ²²	U ³³	U ²³	U ¹³	U ¹²
Na(1)	218(8)	267(9)	291(9)	37(7)	-22(6)	61(7)
Na(2)	181(8)	306(10)	304(9)	15(8)	18(7)	58(7)
O(1)	177(15)	299(18)	397(16)	-25(14)	-15(12)	76(12)
O(2)	321(17)	321(17)	367(16)	111(14)	14(13)	46(14)
O(3)	359(16)	368(17)	275(16)	19(14)	-75(13)	162(14)
O(4)	236(15)	548(19)	224(14)	-39(13)	-4(12)	138(14)
O(5)	325(16)	346(18)	262(15)	23(14)	-9(13)	26(13)
N(1)	188(18)	270(20)	252(19)	14(16)	0(15)	40(17)
N(2)	169(17)	260(20)	212(18)	37(16)	17(14)	70(16)
C(1)	170(20)	250(30)	190(20)	-1(19)	57(18)	10(20)
C(2)	250(30)	320(30)	260(20)	50(20)	20(20)	80(20)
C(3)	280(30)	310(30)	300(30)	-10(20)	20(20)	30(20)
C(4)	170(20)	430(30)	320(30)	-50(20)	-40(20)	-50(20)
C(5)	260(30)	390(30)	240(20)	70(20)	0(20)	50(20)
C(6)	200(20)	310(30)	200(20)	20(20)	46(19)	80(20)
C(7)	190(20)	240(30)	300(20)	50(20)	26(19)	50(20)
C(8)	170(20)	270(30)	180(20)	50(20)	63(18)	40(20)
C(9)	200(20)	300(30)	210(20)	30(20)	36(19)	70(20)
C(10)	250(20)	260(30)	270(20)	100(20)	51(19)	130(20)
C(11)	130(20)	190(30)	250(20)	30(19)	60(18)	-10(20)
C(12)	300(30)	270(30)	350(30)	120(20)	80(20)	110(20)
C(13)	260(30)	260(30)	330(30)	-30(20)	30(20)	-10(20)
C(14)	250(20)	300(30)	270(20)	20(20)	-10(20)	80(20)
C(15)	260(30)	250(30)	300(30)	0(20)	-50(20)	80(20)
C(16)	190(20)	230(30)	250(20)	20(20)	19(18)	60(20)
C(17)	310(30)	300(30)	400(30)	60(30)	-50(30)	50(20)
C(18)	300(30)	380(30)	600(40)	10(30)	60(30)	90(30)
C(19)	280(30)	400(30)	420(30)	120(30)	110(20)	110(20)
C(20)	190(20)	380(30)	450(30)	90(30)	20(20)	-10(20)
C(21)	290(30)	310(30)	320(30)	40(20)	50(20)	-30(20)
C(22)	480(30)	430(40)	480(30)	40(30)	100(30)	-100(30)
C(23)	500(30)	240(30)	510(30)	90(30)	200(30)	110(30)
C(24)	250(30)	390(30)	460(30)	160(30)	70(20)	50(20)
C(25)	300(30)	380(30)	270(30)	90(20)	10(20)	110(20)
C(26)	340(30)	390(30)	210(30)	40(20)	20(20)	50(20)
C(27)	310(30)	450(30)	340(30)	160(20)	-20(20)	160(30)
C(28)	300(30)	340(30)	440(30)	70(30)	-20(20)	130(30)
C(29)	200(20)	530(30)	210(20)	10(20)	10(20)	20(20)
C(30)	310(30)	420(30)	430(30)	50(30)	-50(20)	-20(20)
C(31)	450(30)	390(30)	460(30)	-30(30)	0(20)	180(30)
C(32)	220(30)	530(30)	370(30)	20(30)	20(20)	190(30)
C(33)	330(30)	640(40)	430(30)	200(30)	-20(30)	10(30)
C(34)	450(40)	480(40)	670(40)	220(30)	-20(30)	-80(30)
C(35)	380(30)	360(30)	690(40)	100(30)	-70(30)	0(30)
C(36)	250(30)	290(30)	460(30)	40(20)	-50(20)	50(20)

Table 5. Hydrogen coordinates ($\times 10^4$) and isotropic displacement parameters ($\text{\AA}^2 \times 10^3$) for the disodium salt of 2,2'-biindolyl (CCDC 737620)

	x	y	z	U_{iso}
H(2)	3200(30)	1170(30)	1610(20)	39(12)
H(3)	1210(30)	270(30)	684(17)	15(9)
H(4)	-130(30)	1640(20)	194(15)	-1(7)
H(5)	570(30)	3940(30)	602(19)	30(11)
H(7)	2660(30)	6000(30)	1712(17)	17(9)
H(10)	4590(30)	7840(30)	2490(20)	41(11)
H(12)	6740(30)	9880(30)	3437(17)	21(9)
H(13)	8820(30)	10220(30)	4327(19)	24(10)
H(14)	9580(30)	8450(30)	4731(19)	33(11)
H(15)	8330(30)	6290(30)	4216(17)	19(10)
H(17A)	6240(30)	1430(30)	1540(20)	24(12)
H(17B)	6000(30)	920(30)	2350(20)	40(11)
H(18A)	7660(40)	-180(40)	1960(20)	64(16)
H(18B)	8220(30)	750(30)	1252(19)	21(10)
H(19A)	10010(40)	1290(30)	2320(20)	50(12)
H(19B)	8930(30)	1210(30)	2990(20)	35(12)
H(20A)	9060(40)	3270(40)	3160(20)	50(12)
H(20B)	9120(30)	3280(30)	2070(20)	42(11)
H(21A)	2580(30)	2180(30)	3040(20)	34(11)
H(21B)	2140(30)	2050(30)	3982(17)	5(9)
H(22A)	1450(40)	-90(40)	3540(20)	60(14)
H(22B)	2500(30)	0(30)	2890(20)	38(12)
H(23A)	3010(30)	-460(30)	4509(19)	34(11)
H(23B)	3930(40)	-520(40)	3870(20)	52(15)
H(24A)	4130(40)	1610(40)	5070(30)	80(15)
H(24B)	5300(40)	1370(30)	4503(19)	37(11)
H(25A)	5810(30)	4320(30)	5495(18)	30(10)
H(25B)	6620(30)	5560(30)	5107(18)	24(10)
H(26A)	7680(30)	5190(30)	6542(19)	17(9)
H(26B)	8630(30)	5580(30)	5833(18)	33(10)
H(27A)	8950(40)	3400(40)	6060(20)	50(13)
H(27B)	7440(40)	2820(40)	6090(20)	59(13)
H(28A)	9010(30)	3440(30)	4650(19)	45(11)
H(28B)	7750(40)	2270(40)	4760(20)	43(14)
H(29A)	5080(30)	3790(30)	-590(20)	43(11)
H(29B)	4120(30)	3190(30)	224(18)	27(10)
H(30A)	4480(30)	1700(30)	-1090(20)	32(11)
H(30B)	4380(30)	1230(40)	-190(20)	55(12)
H(31A)	6550(40)	1020(40)	-370(20)	69(17)
H(31B)	6740(30)	1740(30)	-1117(18)	20(10)
H(32A)	7810(30)	2790(30)	370(20)	31(12)
H(32B)	7780(40)	3720(40)	-280(20)	63(14)
H(33A)	7540(40)	7190(30)	1590(20)	48(12)
H(33B)	8080(40)	6470(40)	760(20)	37(13)
H(34A)	10370(50)	7420(50)	1120(30)	100(20)
H(34B)	9600(30)	8500(40)	1510(20)	46(12)
H(35A)	9470(50)	8070(50)	2610(30)	130(20)
H(35B)	11090(40)	7630(30)	2500(20)	44(12)

H(36A)	10270(30)	5470(30)	2144(17)	21(10)
H(36B)	9100(40)	5690(40)	2780(20)	60(13)
